University of Naples Federico II

Department of Chemical Sciences

PhD in Chemical Sciences

AMPs: Rational Design, Synthesis and Biophysical Studies of the Interaction Process with Model Membranes

Rosario Oliva

Tutors: Prof. Luigi Petraccone

Prof. Pompea Del Vecchio

Advisor: Prof. Flavia Nastri

XXXI Cycle – 2015/2018

Contents

List of Abbreviations

2Nal = 2-naphthyl-L-alanine

AFM = Atomic Force Microscopy

AMPs = Antimicrobial Peptides

CD = Circular Dichroism

CDs = Cyclodextrins

Chol = Cholesterol

CL = Cardiolipin

cmc = Critical Micellar Concentration

Cys(S^{t}Bu) = S-(tert-butylthio)-L-cysteine

Cys(^{t}Bu) = S-(tert-butyl)-L-cysteine

DLS = Dynamic Light Scattering

DMPC = 1,2-dimyristoyl-*sn*-glycero-3-phosphocholine

DOPC = 1,2-dioleoyl-*sn*-glycero-3-phosphocholine

DPH = 1,6-diphenyl-1,3,5-hexatriene

DPPC = 1,2-dipalmitoyl-*sn*-glycero-3-phosphocholine

DPPE = 1,2-dipalmitoyl-*sn*-glycero-3-phosphoethanolamine

DPPG = 1,2-dipalmitoyl-*sn*-glycero-3-phospho-1′-*rac*-glycerol

DSC = Differential Scanning Calorimetry

εAhx = 6-aminohexanoic acid

FRET = Fluorescence Resonance Energy Transfer

GP = Generalized Polarization

GUVs = Giant Unilamellar Vesicles

H_{II} = Inverted Hexagonal Phase

HP-β-CD = Hydroxypropyl-β-cyclodextrin

ITC = Isothermal Titration Calorimetry

Laurdan = 6-dodecanoyl-2-dimethylaminonaphtalene

L_α = Lamellar Liquid Crystalline Phase

L_o = Lamellar Liquid Ordered Phase

L_β = Lamellar Gel Phase

$L_{\beta'}$ = Lamellar Gel Phase with Tilted Hydrocarbon Chains

LPS = Lipopolysaccharide

LTA = Lipoteichoic acid

LUVs = Large Unilamellar Vesicles

L/P = Lipid-to-peptide Ratio

MIC = Minimum Inhibitory Concentration

MLVs = Multilamellar Vesicles

N-Rh-DHPE = N-(Lissamine rhodamine B sulfonyl) phosphatidylethanolamine

PA = Phosphatidic Acids

PC = Phosphatidylcholine

PE = Phosphatidylethanolamine

PG = Phosphatidylglycerol

PI = Phosphatidylinositol

POPC = 1-palmitoyl-2-oleoyl-*sn*-glycero-3-phosphocholine

POPG = 1-palmitoyl-2-oleoyl-*sn*-glycero-3-phospho-1′-*rac*-glycerol

PS = Phosphatidylserine

SBE-β-CD = Sulfobutylether-β-cyclodextrin

SM = Sphingomyelin

SUVs = Small Unilamellar Vesicles

TA = Teichoic acid

Preface

The emergence of resistance from bacteria to the conventional antibiotics has become a serious global problem during the last years. The onset of resistance is mainly due to the massive and out-of-control use of these drugs in our community. In fact, microorganisms have developed a series of mechanism which render antibiotics ineffective. Therefore, seeking for new anti-infective agents is becoming increasingly necessary. Among these antimicrobial peptides (AMPs) have been proposed.

AMPs are a class of peptides with a broad spectrum of activity against different pathogenic organisms (e.g. bacteria, fungi, viruses and cancer cells) and they are part of the innate immune system of virtually all forms of life. Usually, they are composed by 10-50 amino acids and are enriched of positively charged (e.g. lysine and arginine) and hydrophobic residues. Even if the exact action mechanism is still under debate, it is widely accepted that the primary target is represented by the lipid matrix of the pathogens' membranes. Thus, AMPs interact with them in a non-specific way, inducing membrane destabilization and finally cell death. It is believed that, due to the unique mode of action, AMPs could overcome the problem of resistance to conventional antibiotics in multi-drug resistant bacteria and even to currently used anticancer drugs for the treatment of tumor cells. For these reasons, AMPs have attracted great attention as drugs of the future. Thus, the final goal in studying AMPs is their use as drugs. However, AMPs pharmacological application is not straightforward. Many aspects must be considered. A good AMP should interact selectively with the bacterial membrane, should not be toxic to eukaryotic cells and should be resistant to proteases degradation. To develop AMPs with these improved features it is of fundamental importance to understand the role played by lipid composition and peptide physico-chemical properties in determining peptides activity. To this aim, in my PhD thesis I studied the molecular details, at level of peptide-lipid interaction, of the action mechanism of several antimicrobial peptides by a series of biophysical techniques. In particular, I characterized the interaction of natural amino acids-containing peptide as well as of synthetic peptides composed by unnatural amino acids with model biomembranes.

In the first part of the project, I carried out the synthesis of the 9-residue peptide P9Nal(SS) which contains unnatural amino acids. It was designed in order to obtain a peptide with a good antimicrobial activity, low cytotoxicity and high resistance to proteases. Then, biophysical studies of its interaction with eukaryotic and bacterial model membranes were carried out. The obtained information can be very useful in

developing antimicrobial agents for biomedical applications. This study is described in detail in the chapter 3.
In the chapter 4 is reported the biophysical characterization of the interaction of two P9Nal(SS)-derived peptides, named P9Nal(SR) and P9Trp(SS), with liposomes mimicking bacterial membrane. The two peptides were obtained by replacing some residues in the primary sequence of P9Nal(SS). As shown in chapter 4, the peptides are less hydrophobic than the parent peptide. The obtained data reveal how these substitutions can modulate the membranotropic activity of peptides.
In the second part of the project, I faced the problem to understand the molecular details of the action mechanism of (P)GKY20, a natural amino acids-containing peptide modelled on the C-terminus region of the human thrombin. Its good antimicrobial activity and low cytotoxicity is well known. However, its action mechanism has never been studied before. Thus, I performed an extensive biophysical characterization of the interaction of the (P)GKY20 with model membranes. The obtained results elucidated its mechanism of action against bacterial model membrane and, at the same time, allow to understand its low cytotoxicity. All the results concerning this AMP are presented in the chapter 5.
The last part of this thesis is devoted to an idea developed during the third year: the encapsulation of AMPs with cyclodextrins (CDs) as a way to protect the peptides from degradation and improve their pharmacological properties. Indeed, antimicrobial peptides containing natural L amino acids are, unfortunately, prone to degradation which limits seriously AMPs applications as drugs. To verify the ability of CDs to encapsulate AMPs without altering their antimicrobial properties, I studied the interaction of (P)GKY20 peptide with sulfobutylether-β-CD and of the obtained complex with bacterial-like liposomes.
These preliminary results reveal that (P)GKY20 form a 1:1 stable complex with sulfobutylether-β-CD. Further, the obtained complex is able to perturb the stability of bacterial-like liposomes. Thus, the sulfobutylether CD could represent a suitable encapsulating agent for (P)GKY20 peptide which could improve its pharmacological profile. The obtained results are presented in the chapter 6.

Since the peptide interaction with model membranes is quite complex being composed by many steps, a strategy which involves different biophysical techniques was adopted to study a particular aspect of the interaction process. Calorimetric, spectroscopic and microscopic techniques were applied (where possible) and by combining the data, it was possible to depict a possible action mechanism highlighting the key steps. **Differential Scanning Calorimetry** (DSC) was employed to study the effect of peptide interaction on the liposomes thermotropic properties. Moreover, using an appropriate lipid system, information about lipid self-organization (e.g. lipid domains formation) can be obtained. **Steady-State**

Fluorescence Spectroscopy and **Fluorescence Anisotropy** were extensively employed to obtain information on both AMPs (e.g. determination of binding constants, degree of insertion into the lipid bilayer) and lipids (e.g. changes in membrane viscosity due to changes in lipid packing). Liposomes morphological changes were monitored by **Dynamic Light Scattering** (DLS). Instead, changes in peptide secondary structure upon binding were followed by means of **Circular Dichroism** (CD) and an estimation of secondary structure content was obtained by the spectra deconvolution. **Atomic Force Microscopy** (AFM) and **Confocal Fluorescence Microscopy** instruments were employed to directly visualize the effect of peptides on bacterial model membranes.

Chapter 1

Antimicrobial Peptides (AMPs)

1.1 Introduction

The increasing spread of bacteria resistant to conventional antibiotics has become a worldwide emergence [1,2]. In fact, due to massive and out-of-control use of these drugs in humans and animals, bacteria have developed a series of mechanisms [3] which render antibiotics ineffective. For example, about 80% of bacterial strains of *Staphylococcus aureus* are immune to the penicillin [4]. Moreover, the number of new discovered (or synthetized) antibiotics is decreasing [5]. Thus, there is an urgent need of a new class of antimicrobial agents.

Antimicrobial peptides (AMPs) are an interesting class of small peptides which can overcome this problem. It is believed that, due their unique and non-specific action mechanisms which involve a direct interaction with the lipid matrix of pathogens' membranes, they could help in fighting infections caused by multidrug-resistant (MDR) bacteria [6,7]. For this reason, AMPs represent serious candidates as alternative to conventional antibiotics and have attracted much attention in the scientific community.

AMPs are primary known for their antibacterial activity, but they are also active against other microorganisms such as fungi (antifungal peptides), viruses (antiviral peptides), parasites (anti-parasite peptides) and even cancer cells (anticancer peptides) [8–10]. AMPs are part of the defense system of virtually of form of life, from prokaryotic bacteria to eukaryotic mammals and plants [11]. Some of them may be expressed constitutively. Others are inducible and are expressed only in response to the presence of a foreign microorganism [12]. AMPs can be modified after their expression (post-translational modification). The most common modifications are: amidation, glycosylation, acylation and halogenation [13,14]. They represent the first defense line against invading microorganisms. In fact, they are particularly abundant in all tissues that are in some way in contact with external world. For example, in humans AMPs are found in the skin, intestinal and oral mucosa [15].

The era of amino-acids based antimicrobials started in 1922, when Fleming discovered lysozyme [16]. This small globular protein can hydrolyze the glycosidic bond between the N-acetylglucosamine and N-acetylmuramic acid residues in the peptidoglycan, the constituent of the bacterial cell wall [17]. This discovery was overshadowed when the same scientist discovered penicillin in 1928 [18] starting the antibiotic era. Due to this important discovery, the interest on AMPs drastically diminished. In the 1960s, the development of multi-drug resistant bacteria brought

the attention again to AMPs as alternative to antibiotics. The first antimicrobial agent discovered was the gramicidin in 1939 in Bacillus strains [19,20]. Despite, its cytotoxicity, gramicidin was found effective for topical treatments of wounds and ulcers. Probably, the first eukaryotic AMPs was found in plants. From the plant *Triticumaestivum,* an AMP named purothionin was isolated. Purothionin showed a good activity against some bacterial strains [21]. In the 1960s, the first AMP from animals was reported. It was the brombinin from frogs [22]. In the following years, a series of new AMPs were reported thus increaseing our knowledge on the subject. Just to cite two important studies, it is possible to report the discovery of two well studied peptides: cecropins and magainins (a brief and comprehensive review about history of AMPs can be found in [23]). In the 1980s, Boman reported the discovery of the potent AMPs cecropins in *Hyalophora cecropia* after bacteria injection in the insect. It was the first report of an α-helix antimicrobial peptide [24,25]. In 1987, Zasloff reported the isolation and characterization of cationic AMPs magainins from the African frog *Xenopus laevis,* pointing out its defensive role in the organism [26]. Today, more than 3000 antimicrobial peptides are known. Information about them can be found in an online database [27] at http://aps.unmc.edu/AP/main.php which is constantly update. It is probably that this database represents only a small fraction of existing AMPs and others will be discovered in the future.

1.2 AMPs Properties

Antimicrobial peptides are a heterogeneous class of small peptides composed by 10-50 amino acids [12]. The primary target of AMPs is represented by the lipid matrix of the cytoplasmic bacterial membrane that they destabilize leading to the pathogen death [28]. As stated in the previous section, more than 3000 different peptide sequences are known. Despite this, all AMPs share common physico-chemical properties which are fundamental for their biological activity. The general features that must be considered are:

- Sequence;
- Conformation;
- Amphipathicity;
- Hydrophobicity;
- Charge;
- Polar angle.

Sequence. AMPs can be composed by any combinations of amino acids. Essentially, they are enriched of hydrophobic and cationic residues. Usually the ratio between

the number of hydrophobic and charged residues varies from 1:1 to 2:1 [29]. At physiological pH, lysine and arginine residues are positively charge which render AMPs cationic leading to the class of cationic antimicrobial peptides (cAMPs). There are also anionic AMPs [30] which represent a small fraction of known AMPs [8] and will not be discussed here. Although there is a low sequence homology among AMPs, two features are frequently observed. The first one regards the presence of a glycine residue at the N-terminus, that is highly conserved. The glycine serves as capping residue providing resistance to aminopeptidases [31]. The second one is the amidation (a post-translational modification) at the C-terminus which provides resistance to carboxypeptidases [31].
Finally, the presence of aromatic residues such as tryptophan and tyrosine could favor the localization of peptide at the membrane-water interface [32] due to the contemporary presence of polar groups (amide in Trp and OH in Tyr) and hydrophobic aromatic rings in the side chains which render the residues nor too much hydrophilic nor too much hydrophobic.

Conformation. Despite the low sequence homology and the wide variety of primary structures, AMPs tend to adopt similar conformation upon interaction with membranes. AMPs can adopt three different conformations: α-helix, β-sheet and random structure.
The most common secondary structure is the α-helix. Usually, AMPs have a random structure in solution and adopt an α-helix structure upon interaction with membrane. An example of helical peptide is represented by magainin [33]. The conformational change has a profound impact on the peptides' activity. In fact, the peptides' ability to adopt a helical structure is related to its ability to perturb the membrane integrity. Moreover, the lack of the secondary structure upon binding to eukaryotic membrane represents a way through which the peptides' cytotoxicity could be minimized [34]. Peptides that adopt β-sheet conformation are quite different from α-helical ones. Usually, they adopt a more ordered structure in solution due to presence of cysteine residues that can form disulfide bridges thus stabilizing the three-dimensional structure. Upon interaction with the membrane, their conformation does not change. A good example is tachyplesin that possess two disulfide bonds [35]. In Fig. 1.1 are reported the structures of magainin 2 [36] and tachyplesin I [37] as examples of α-helix and β-sheet peptides, respectively.

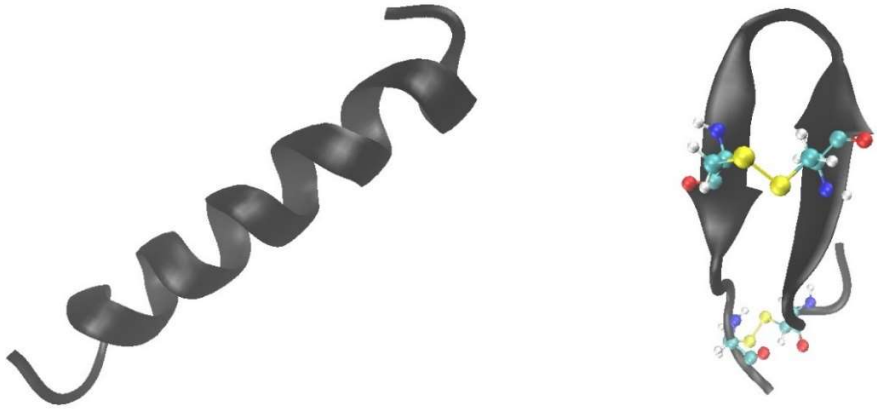

Fig. 1.1 Cartoon representations of (left) magainin 2 (pdb: 2MAG) and (right) tachyplesin I (pdb: 1MA2). In tachyplesin I the two disulfide bridges are represented as yellow spheres. The picture was made with VMD (Visual Molecular Dynamics) software.

Amphipathicity. This property is directly linked to the conformation of AMPs. The α-helix or β-sheet structure adopted by AMPs are amphipathic structures. This means that they have a hydrophobic face on one side and a polar face on the other side (Fig. 1.2) where the respective residues are clustered.

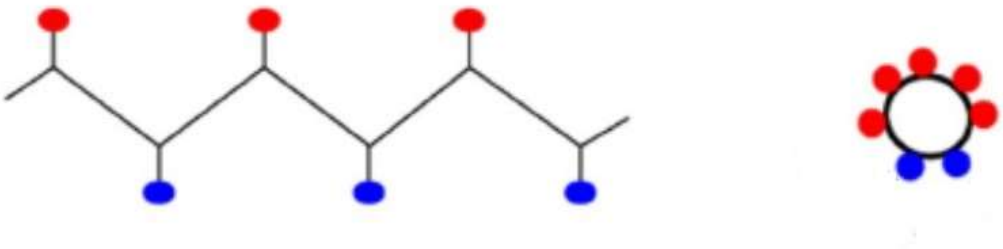

Fig. 1.2 Schematic representations of amphipathic structures. (Left) β-sheet and (right) α-helix. Blue and red circles correspond to polar and non-polar residues, respectively. Adapted from [29].

This structure facilitates the peptide interaction with the membrane: the hydrophilic side interacts with the polar head groups of lipids and, at the same time, the hydrophobic side interact with the hydrophobic acyl chains. Thus, it plays an important role in the interaction with microbial membrane [38].

The peptides' amphipathicity is quantitatively measured by the mean helical hydrophobic moment ($<\mu_H>$) [39]. It is defined as the vector sum of the single amino acids hydrophobicities, normalized to that of an ideal α-helix. High values of the hydrophobic moment mean high amphipathicity. It is possible to calculate the hydrophobic moment by using online tools, such as Heliquest at

http://heliquest.ipmc.cnrs.fr/cgi-bin/ComputParams.py [40]. The best way to represent the amphipathicity is by means of the helical wheel projections. An example is reported in Fig 1.3 for the designed AMP "peptide 8" [41]. From this projection, the peptide amphipathic structure is quite clear.

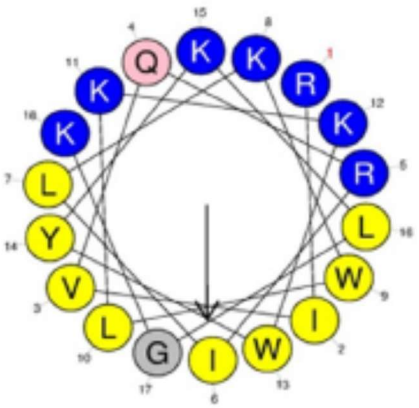

Fig. 1.3 The helical wheel projection of the AMP named peptide 8. Yellow circles are hydrophobic residues. Blue circles represent hydrophilic residues. The arrow represents the calculated hydrophobic moment (0.741). Adapted from [41].

The effect of amphipathicity on the AMPs activity is not completely clear. For example, it was reported no correlation between amphipathicity and biological activity in a series of L-V13K analogs antimicrobial peptides [42]. Another study on a series of 20 synthetic peptides demonstrated that the increase of amphipathicity is correlated with hemolytic activity but in a minor extent with antimicrobial activity [43]. On the other hand, a study with magainin 2 analogs demonstrated that both bacterial and hemolytic activities increase with an increase of amphipathicity [44]. Thus, it seems that the amphipathicity plays a role in determining the antibacterial and hemolytic activities and it is peculiar of the peptide sequence.

Hydrophobicity. Peptide hydrophobicity is related to the primary structure and is defined as the percentage of hydrophobic residues within a peptide [12]. For most antimicrobial peptides it reaches 50%, meaning that half of the residues in the sequence are hydrophobic [31]. Hydrophobicity is an important parameter for the peptides' biology activity since it determines the degree of partition inside the hydrophobic core of the membrane [45]. Several studies evidenced that an increase of hydrophobicity is related to a hemolytic activity increase but a decrease of selectivity against bacterial strains [12]. For example, a study on the peptide L-V13 K showed that the substitution of Ala with the more hydrophobic Leu residue, increases the hemolytic activity of about 62 times. At the same time, the

antimicrobial activity against *Pseudomonas aeruginosa* does not change [46]. In another study (in which the effects of different parameters on a series of 20 AMPs were explored) is reported that an increase of hydrophobicity increases the hemolytic activity slighting affecting the antimicrobial activity [43].

Charge. Antimicrobial peptides exhibit a selective interaction towards the bacterial membrane. It is believed that electrostatic interaction between the positively charged peptide and negatively charged membrane is the first step in the interaction process and it is responsible for the selectivity. For this reason, the global charge on the peptide plays an important role in the antimicrobial activity [12].
Most cationic antimicrobial peptides possess a net positive charge ranging from +2 to +9. They are enriched of lysine and arginine residues positively charged at physiological pH. At acidic conditions histidine residues can be positively charged contributing to the overall charge.
There is a relation between charge and biological activity. As general rule, an increase of the net positive charge causes an increase of the antimicrobial activity [29]. In fact, a study on a series of peptides demonstrated that an increase of the positive charge increases the peptide potency against bacteria [47]. However, it seems that the charge cannot be increased indiscriminately. In fact, for some peptides there is a threshold value above which a decrease of the antimicrobial activity was observed. For example, in a study carried out on a series on magainin 2 analogs it was shown that an increase of the charge above the threshold value of +5 leads to a decrease of antimicrobial activity [48]. The observed decrease could be due to the strong electrostatic repulsions in the packed structure of the peptide upon interaction with the membrane. Even if the increase of positive charge seems a straightforward way to improve the antimicrobial activity, the possible rise of the hemolytic activity should be considered. In fact, the hemolytic activity also depends on the net charge. There is a threshold charge value (depending on the peptide sequence), above which the undesirable hemolytic activity increases [29]. This aspect was well demonstrated in a study carried out on series of peptides analogs where the positive charge of a peptide was varied holding constant the other peptide features [47].

Polar angle. This parameter measures the relative spatial proportion of polar and apolar face in amphipathic peptides [49]. In a perfect amphipathic α-helix, where one face is composed by hydrophobic residues and one face by only polar residues, the polar angle is 180°. An increase of the hydrophobic side will reduce the polar side leading to a decrease of the polar angle and vice versa. Changes in the primary sequence can alter the polar angle. Several studies have found a correlation between the polar angle and the permeabilization of the membrane. It seems that a decrease of the polar angle leads to an increase of the membrane permeabilization [49]. In a

study on two model peptides which only have different polar angle (100° and 180°), it was shown that the peptide with the lower polar angle induces greater permeabilization, translocation and rate of pores formation [50].

Even just from this brief description of antimicrobial peptides general features, it becomes clear that the fine interplay among these parameters defines the peptides' activity. Moreover, they are not independent to each other. A modification of one parameter can change others. This demonstrates that the inter-relationships among these parameters are the key factors in determining the biological activity of antimicrobial peptides.

1.3 Classification of AMPs

Antimicrobial peptides are a heterogeneous class of molecules. It's very hard to categorize them in specific classes. However, a possible classification can be attempted according to their secondary structures (adopted upon interaction with the membrane) and amino acids composition [8,51,52]:

- Linear α-helical peptides;
- β-sheet peptides;
- mixed α/β peptides
- peptides enriched of a specific amino acid.

Linear α-helical peptides represent the most characterized group. These peptides adopt a random structure in solution but an amphipathic α-helix structure when interact with the membrane. Examples of AMPs belonging to this class are: magainins (Fig. 1.1), pexiganan and cecropins [53,54].
The second class is composed by peptides with a β-sheet structure. These peptides are usually enriched of cysteine residues. In solution, they can adopt a β-sheet conformation stabilized by disulfide bridges. Upon interaction with membranes, the conformation only slightly changes. β-sheet peptides can contain two or more cysteine residues. An example of AMPs with two Cys residues is tachyplesin (reported above, in Fig. 1.1). Another good example is represented by human defensins (both α- and β-defensins) which are characterized by the presence of three disulfide bridges [55].
Peptides with a mixed structure of α and β are also described. As an example, the drosomycin from the insect *Phormia terranovae* has a β-sheet composed by three strands and a small segment which adopts a α-helical structure. The whole structure is stabilized by the presence of four disulfide bridges [56]. From the same insect, it

was isolated the peptide defensin A with a β-sheet formed by two antiparallel strands and a segment in α-helix. The structure is stabilized by two disulfide bridges [56].
Finally, there are some AMPs in which a specific amino acid is overrepresented. These peptides can adopt different structures apart from the ones reported above. They can be enriched of proline, glycine, arginine, tryptophan and histidine residues. The peptide formaecin from the ant *Myrmecia gulosa* is a proline-rich peptide. It is composed by 16 residues: 5 of which are proline residues [57]. Plasticins are examples of glycine-enriched AMPs which adopt a β structure in solution [58]. PR-39 is an arginine enriched AMPs of 39 residues, 11 of which are arginines [59]. It is effective against both gram -negative and -positive bacteria and even cancer cells. Its action mechanism probably involves a direct bind to DNA [60] rather than the common membrane destabilization. In fact, it is thought that arginine-enriched peptides can translocate across the membrane interacting with intracellular components. This class of AMPs are called cell penetrating peptides (CCPs) and will not be considered here [61,62]. As an example of Trp enriched AMPs it should be cited indolicidin [63]. This 13-residues peptide with 5 Trp adopts a unique extended structure with two half turns in the presence of dodecylphosphocholine micelles [64]. Finally, the antimicrobial peptide clavanin A is an example of histidine-enriched peptide [65]. It is composed by 23 amino acids, 4 of which are histidine residues. Upon interaction with liposomes mimicking bacterial membrane, it adopts a curved helical structure [66].

1.4 AMPs Action Mechanisms

Antimicrobial peptides are a class of active molecules. They are involved in a wide variety of functions such as epithelial cell proliferation, wound healing and stimulation of the production of chemokines [52]. However, they are best known for their antimicrobial activity, which is the subject of this thesis. How do they carry out this important biological activity? It is widely accepted that the final target of AMPs is the lipid matrix of the membrane [6,12,28]. In fact, AMPs can interact with the cytoplasmic membrane of bacteria leading to its permeabilization and, finally, cell death. It is important to note that this interaction is non-specific with no receptor involved. In fact, it has been reported that the replacement of all L- amino acids in the sequence with the corresponding D- enantiomers does not affect antimicrobial activity [67]. The first step of the interaction process between peptides and the pathogens' cell is represented by electrostatic interactions. At physiological pH, AMPs are positively charged (section 1.2) and bacterial membranes are enriched of negatively charged lipids (section 2.4) [68]. Once peptides are in contact with the cell surface, they must cross the cell wall for gram-positive bacteria, and outer (cytosolic) membrane and cell wall for gram-negative bacteria before to interact with

the cytoplasmic membrane, the target of AMPs [69]. For gram-negative bacteria, it was proposed that peptides displace divalent ions associated with lipopolysaccharides (LPS) in the cytosolic membrane [70]. In this way, a destabilization of the membrane occurs, and peptides can gain access to the inner membrane. The way through which AMPs cross the thick cell wall of gram-positive bacteria is not fully understood. It seems that the presence of peptidoglycan is not important in gaining the access to the cytoplasmic membrane. On the contrary, teichoic acids are involved in the translocation across the cell wall, since they could limit peptides' availability at the surface of the cytoplasmic membrane [71,72]. Moreover, the peptides' ability to cross the cell wall seems to depend on their secondary structures and oligomerization state. In some way, peptides reach the cytoplasmic membrane of bacteria and are adsorbed on the membrane surface where they change the conformation. The most common conformational change is from random-coil to α-helix (for linear AMPs). Together, these three steps constitute "the binding steps" of peptides to the membrane (Fig. 1.4) and is common to all AMPs.

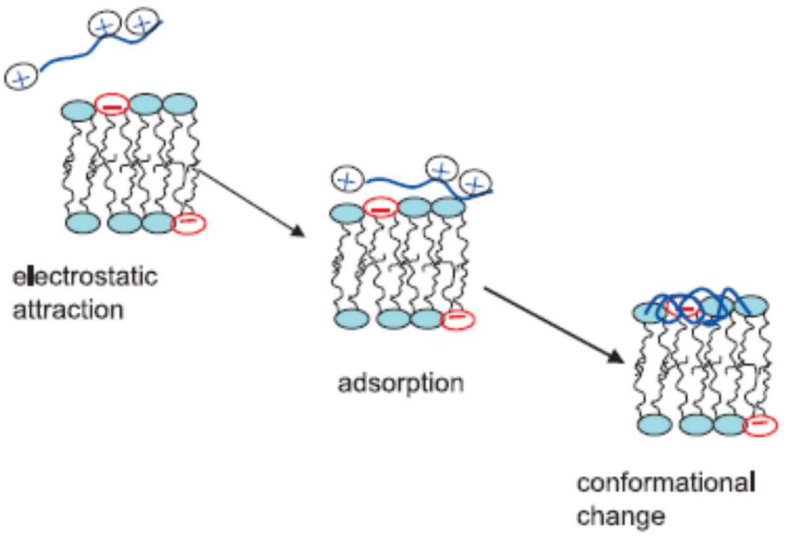

Fig. 1.4 The three steps involved in the binding of linear AMPs to the negatively charged membrane. Adapted from [73].

After this stage, the peptide molecules remain associated on the surface of the negatively charged membrane. To exert their activity, peptides must be locally concentrated. Thus, they must reach a critical concentration called the threshold concentration [28]. This parameter is defined as the minimum peptide concentration (or lipid-to-peptide ratio, L/P, in an experiment) required to exert the biological effect [28]. Melo et al. [28] established that to observe a biological effect a very high

membrane coverage, close to the membrane saturation, is required [12]. Thus, it appears clear that the binding affinity of a peptide for a membrane with a specific composition is fundamental in determining how much peptide is required to kill the bacteria. A correlation between Minimum Inhibitory Concentration (MIC), the lipid to peptide ratio, L/P at saturation and the partition constants exists. The minimum inhibitory concentration is the microbiological parameter indicating the minimum peptide concentration at which bacterial growth is inhibited). As an example, in the case of melittin a partition constant of $6 \cdot 10^4$ was determined for the interaction with liposomes composed by phosphatidylcholines (PCs) and phosphatidylglycerols (PGs) [74]. From this partition constant a lipid-to-peptide ratio at saturation of about 2.5/1 is estimated. From these two parameters, the MIC value can be determined which reproduce the experimental value for *E. coli*. Thus, there is a link between membrane coverage (threshold) and effect *in vivo* [28].
As a consequence of membrane coverage (threshold concentration), the peptide can destabilize the membrane, but how does it take place? This is a very difficult task to address. The mechanism by which a peptide destabilizes a membrane depends on several parameters, such as lipid composition and all the physico-chemical properties of both the membrane (e.g. physical state) and peptide (charge, length, amphipathicity, hydrophobicity, conformation). However, to explain the AMPs action mechanism, different models have been proposed. Three of them are the most common invoked and are schematically represented in Fig. 1.5:

- barrel-stave model;
- toroidal model;
- carpet model.

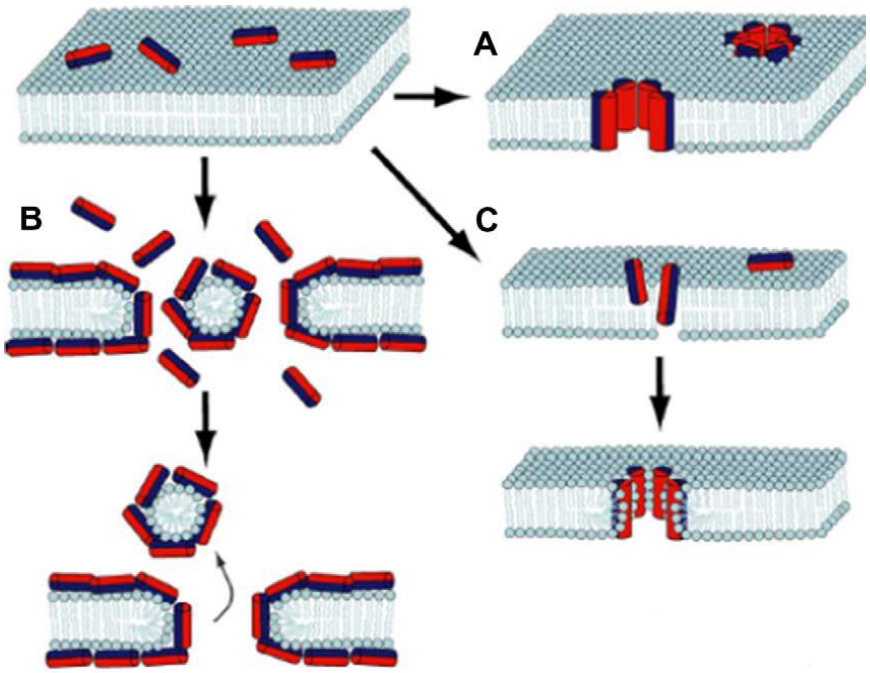

Fig. 1.5 The three most common invoked AMPs action mechanisms. (A) Barrel-stave model; (B) Carpet model; (C) Toroidal model. The amphipathic peptides are represented as cylinders: the red portion are polar residues, the blue one represents hydrophobic residues. Adapted from [12].

In the so-called barrel-stave model (Fig. 1.5, A), AMPs induce the permeabilization by forming pores in the membrane. These pores are formed by interacting trans-membrane peptides that face their apolar residues toward the hydrophobic core of the membrane and polar residues toward the center of the pores which are filled with water. In the initial step, peptides bind in their monomeric form to the surface, interacting with the polar head groups of lipids leading to a local membrane thinning. This favors the peptides insertion in the hydrophobic part of the outer leaflet of the membrane, since most of them are too short to span the membrane completely. At the threshold concentration, the peptides' monomers self-assemble and insert deep in the membrane forming pores. This mechanism is characteristic of hydrophobic peptide with a low charge density. An example of peptide which it is believed to act through this mechanism is alamethicin [75]. This peptide forms a helix bundle composed by 6 peptides which lines the pore. Its orientation respect to the bilayer depends on the membrane hydration state and the lipid-to-peptide ratios underlying the importance of threshold concentration concept [76,77].
The second mechanism is called toroidal model. As in the barrel-stave, also this model predicts the formation of pores. The main difference is that in the toroidal model, peptides are always associated with the lipid polar head groups.

In this model, peptides partition into the membrane (assuming a trans-membrane orientation) and induce a bending in the membrane leaflets which connect to each other (Fig. 1.5, B). Thus, the pore is lined by peptides and lipid head groups and filled with water. Peptides with high charge density and not particularly hydrophobic act through this mechanism. The bending of the membrane and the association of lipid polar heads with peptides stabilizes the pore. In fact, without it, the electrostatic repulsion among peptides will be too high that a pore cannot be formed. An example of peptide that acts through this mechanism is magainin [78,79].
In the carpet mechanism (Fig. 1.5, C), proposed by Shai in 1996 [80] peptides cover the membrane like a carpet. At the threshold concentration, peptides produce a detergent-like effect which solubilize the membrane. Thus, the permeabilization does not occur through the formation of pores. In this mechanism, the peptide is not necessarily inserted in the hydrophobic core, but it can remain attached to the lipid polar head groups. In addition, peptides might form transient pores that allow to peptides to translocate to the inner leaflet of the membrane favoring the solubilization process. Examples of peptides which it is believed to act through this mechanism are ovispirin [81] and cecropin [80]. Both these peptides don't penetrate inside the membrane hydrophobic core and remains attached to the lipid head groups with their helical axes perpendicular to the bilayer normal.
The three models described above are membranolytic mechanisms. It means that they predict the membrane permeabilization through its disruption (with stable pores or with a detergent-like effect).
Other mechanisms have been proposed in which a membrane disruption does not occurs [12]. The development of these models was necessary from the observation that some peptides are effective against bacteria, but they are not able to perturb the membrane [82,83].
One of these models is the aggregate channel model [84,85]. In this model, peptides insert into the membrane in form of unstructured aggregates. These aggregates are only transient and allow to the peptides to cross the membrane without causing a significant membrane disruption. Once inside, the peptides can interact with intracellular targets as DNA, RNA and proteins [68].
Another one is the molecular electroporation model, proposed for the peptide annexin V [12]. In this model, peptides with a high charge density generate an electric field. The electric field promotes the formation of transient pores which increase the membrane permeability without causing it any kind of damage.
Some peptides can perturb the membrane by promoting the formation of specific lipid-peptide domains [86]. In this mechanism, the preferential interaction of peptides with the negatively charged lipids (phosphatidylglycerols, cardiolipins) leads to a lateral phase segregation of anionic lipids from the zwitterionic ones. The formation of discrete domains induces a destabilization of the membrane since the

interface among domains act as defects which increase membrane permeability [87]. For example, it was demonstrated by means of calorimetric measurements that the small peptide Ac-RW [88] is able to induce the formation of a PE (phosphatidylethanolamine) and PG (phosphatidylglycerols) enriched domains in model membrane composed by a mixture of both lipids. It is known that PEs and PGs, in their pure forms, prefer to adopt different phases: inverted hexagonal and lamellar, respectively (see section 2.6). The interface among domains of different phases destabilizes the membrane without disrupting it. The formation of domains can have a deep impact also on the biological activity of the cell [12]. For example, it can alter the diffusion rates of lipids and membrane proteins. Moreover, the membrane curvature is also affected by the lipid segregation process. It is known that a correct curvature is required for some process such as cell division [89].

In conclusion, several peptides and membranes properties dictate the action mechanism. Often, a peptide doesn't act through a single, well defined mechanism. Sometimes, its mechanism is unique. Find a relation between peptides' structural properties and mechanism is a very difficult task.

1.5 AMPs in Clinical Trials

The efforts of the scientific community in studying AMPs are all devoted to a common final goal: the application of AMPs as drugs. These studies are important in revealing the relation between peptides' properties and biological activity. In this way the design of new AMPs with high antimicrobial activity and low cytotoxicity is possible.
AMPs as drugs offer a series of advantages [90,91] among which it is possible to cite: safety, tolerability, efficacy and selectivity. A lot of peptides are characterized by low MIC values and low hemolytic activity. This automatically means that human body well tolerates them because AMPs are selective and interact preferentially with pathogens. Unfortunately, peptides are not chemically e physically stable. They are prone to hydrolysis and oxidation reactions which can modify the biological activity. Moreover, the plasma half-life is short. In fact, once inside the human body, they are subjected to the proteases action [92] that cleave the peptide at specific residue or directly at one of the two termini. This inevitably leads to an unfavorable pharmacological profile. Thus, there are some limitations in the application as drugs and several strategies have been developed to face these problems. The introduction of unnatural amino acids, β-amino acids or D- enantiomers as well as protection of both N- and C- termini contribute increasing the peptide half-life [91,93]. The attachment of fatty acids (lipopeptides) or PEG (polyethylene glycol) can also enhance serum stability [90].

Apart from the “scientific problems”, financial problems should be considered, as the high production cost which limit AMPs applications in medicine [94]. From this very brief description, it appears clear that the development of a peptide-based drug is not simple. However, due to selectivity, low cytotoxicity, broad spectrum of activity and no resistance development, AMPs have attracted the attention of several pharmaceutical companies [95].

Today, about 60 peptide-based drugs are available on the market and many others are at different stages of clinical trials [90,91]. Examples of AMPs in clinical trials are reported.

Pexiganan is a peptide derived from magainins and is at phase III of clinical trials. It is composed by 22 amino acid and it has a broad spectrum of activity against bacteria (both gram-positive and negative) and fungi [54]. The final goal is to obtain a pexiganan-containing formulation for topical application in the treatment of infected diabetic foot [91,96]. Omiganan, is an antimicrobial peptides derived from indolicidin, a Trp-rich peptide [97]. It is in phase III of clinical trials for the evaluation of safety and efficacy in the topical treatment of rosacea. Omiganan is also in phase II for the development of a gel against acne vulgaris. Finally, another example of AMP in development is represented by PAC-113, a peptide derived from histatin 5, enriched in histidine residues. It has shown activity against the fungus *Candida albicans* [98]. It is in phase III clinical trials aimed in finding the optimal dose for the treatment of candidiasis of oral cavity [91].

These examples show that application of AMPs as drugs is possible. So, AMPs have an enormous potential as future therapeutics.

Chapter 2

Biological Membranes

2.1 Introduction

Biological membranes are fluid structures composed by lipids, proteins and carbohydrates [99]. Membranes are fundamental components of every kind of cells, from simpler prokaryotes like bacteria to the more complex higher organisms as animals [100]. Biological membranes separate the inner part (intracellular space) of a cell from the external part (extracellular space) or delimit organelles inside a cell (e.g. membrane of mitochondria). More specifically, in the first case we will refer to the membrane as "the plasma membrane" which constitute the cell boundaries. In Fig. 2.1 is reported a schematic representation of a plasma membrane highlighting its major components.

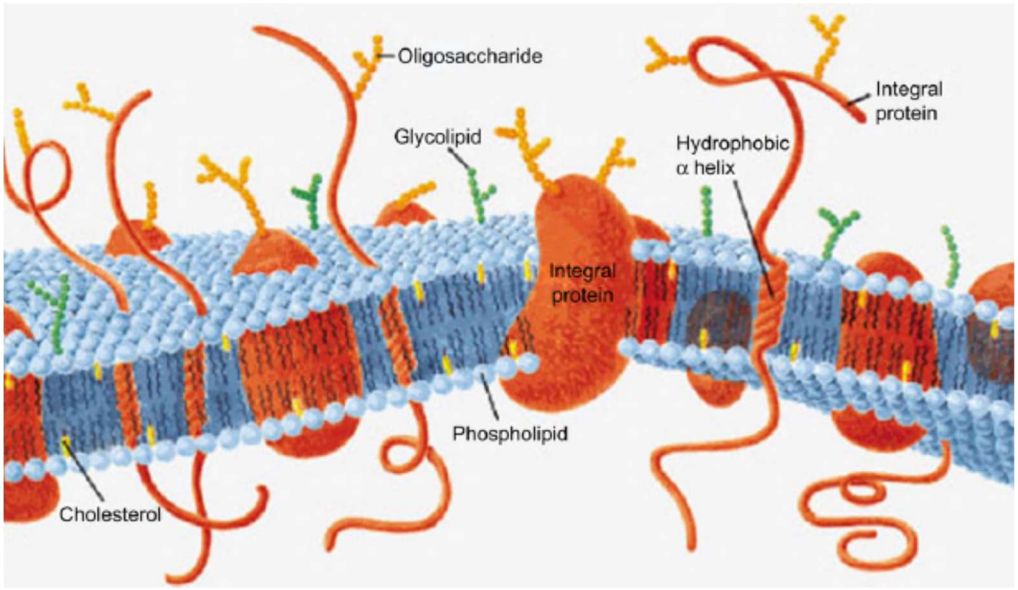

Fig. 2.1 A schematic representation of a plasma membrane. Their main constituents are lipids, proteins and carbohydrates. Adapted from [99].

The fluid mosaic model developed by Singer and Nicolson [101] is the common representation used to describe cell membrane structure and dynamics. In this model and in its update version [102] the membrane components, lipids and proteins are distributed inhomogeneously like a mosaic. But differently from a Roman mosaic in which the tesserae are fixed, the membrane tesserae (its components) are in constant motion. They can diffuse along the plane of the membrane (translational diffusion)

or can rotate around an axis perpendicular to the membrane plane. Occasionally, lipids can go from the inner leaflet to the outer and vice versa (transbilayer diffusion or flip-flop) [103]. Following, the general features of a membrane are reported:

- A membrane is composed by a lipid double layer (two leaflets) with a thickness of 5-6 nm. Lipids are amphipathic molecules (Fig. 2.2A). They present a polar head group (hydrophilic) and two lipid chains (hydrophobic). When exposed to aqueous environment, they organize themselves spontaneously by forming a structure (the bilayer) in which the hydrophobic portion of each lipids is hidden to the water, whereas the hydrophilic portion is exposed to the water (Fig. 2.2B);

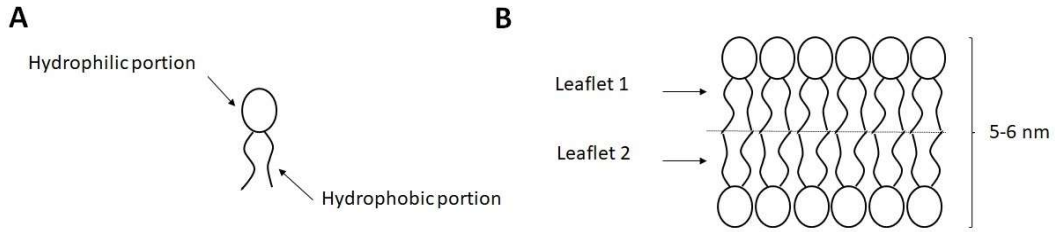

Fig. 2.2 (A) Simplified representation of a lipid molecule. The hydrophilic and hydrophobic portion of the molecule are indicated by arrows. (B) The lipid bilayer: it is formed by two lipid monolayers (or leaflets) facing their hydrophobic portions. The hydrophilic head groups are surrounded by water molecules.

- Membranes are enriched in proteins. Proteins associated with the polar head groups are called peripheral proteins. They can be found on both side of the membrane. Proteins which interact with the hydrophobic matrix of the membrane are called integral proteins. Usually, not the entire protein is embedded in the membrane, but some regions come out of the membrane (Fig. 2.1);
- All membranes contain carbohydrates. Carbohydrates do not possess a hydrophobic moiety. Consequently, they are never localized in the membrane interior. Interestingly, sugars are only found on the outer surface of the plasma membrane. Carbohydrates are always associated with lipids (glycolipids) and proteins (glycoproteins);
- The membrane is an asymmetric structure [104]. It means that the composition of the inner, cytosolic leaflet is different from the outer leaflet. For example, in the eukaryotic plasma membrane the lipid phosphatidylserine is almost found in the inner leaflet. The same holds for proteins: a peripheral protein which interact, for example, on the surface of

the outer leaflet will be found always there and never in the inner leaflet [102];

- The membrane is characterized by later heterogeneity. This means that the constituents' composition is not the same everywhere. There are small (0.1 – 1 μm in diameter) patches called "domains", enriched of specific lipids and proteins, which exhibit characteristic functional properties. The so called "lipid rafts" are a good example of domains. The rafts are enriched of sphingolipids and cholesterol. It is believed that rafts domains are the house of a series of membrane proteins involved in the cell signaling [105].

2.2 Membrane Functions: a Brief Overview

The most obvious function of a biological membrane is to separate two aqueous compartments. For a plasma membrane this involves separation between intracellular and extracellular space. Clearly the separation cannot be absolute. In fact, a cell must be able to uptake nutrients from the external environment and to remove molecules from its interior. In other words, a cell must communicate with the external environment. Thus, it acts as a selective permeable barrier which regulates the enormous traffic of molecules in and out of the cell. Essentially, molecule movements across the membrane can be divided in two big groups: passive diffusion and active transport [103,106]. In Fig. 2.3 are summarized these basic types of membrane transport.

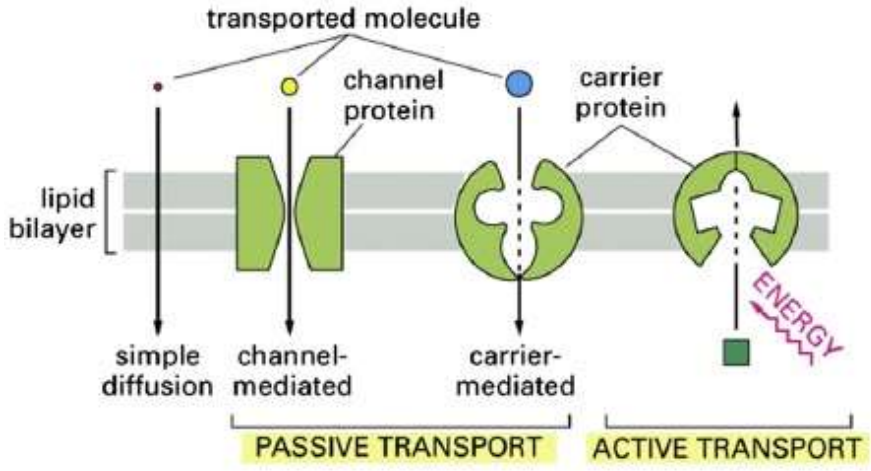

Fig. 2.3 The basic types of membrane transport: passive transport (which includes also simple diffusion) does not require energy. In contrast, active transport requires energy in form of ATP. Adapted from [99].

Passive diffusion does not require energy, but it is driven by only solutes concentration gradient. Passive diffusion can be either simple diffusion across the membrane or "assisted" diffusion, where some carriers (proteins) are involved in the process. Potassium and Sodium Channels are examples of integral membrane proteins which facilitate the diffusion of K^+ and Na^+ across the membrane. In contrast, active transport requires energy, usually in form of ATP, and it is always performed by membrane proteins. An important example of active transport is represented by Na^+/K^+ ATPase which uses ATP to pump Na^+ out of the cell and to pump in K^+ both against their concentration gradients. These mechanisms are mainly involved in the transportation of small molecules. For larger molecules (e.g. macromolecules) other ways are required. These ways include: 1) receptor mediated endocytosis (RME) also known as clathrin-dependent endocytosis where a membrane protein named clathrin favors the internalization of molecules by forming a small lipid vesicle; 2) pinocytosis, in which an invagination of the plasma membrane encapsulates external fluid materials. This leads to the formation of a vesicle which it is released inside the cell. Every kinds of fluid can be incorporated; thus, this mechanism is completely non-specific; 3) phagocytosis involves the uptake of large solid particles of macromolecules, parts of cell or even a whole microorganism. The solid particle is recognized by receptors on the membrane surface. Then, the formation of vesicles called phagosomes take place which internalize the solid particle. Finally, the particle will be transported to the lysosome for digestion.
In addition, the plasma membrane carries out other important functions:

- It contributes in protecting the structural integrity of the interior of the cell, e.g. maintaining the cytosol pH and the right osmotic pressure;
- It constitutes the point of attachment to the cytoskeleton: this helps in maintaining the cell shape;
- It is involved in the cell recognition thanks to the presence of glycolipids on its surface;
- It is involved in a series of biochemical and physiological functions: inter-cellular communication, cell adhesion [107] and energy transduction events, just to cite a few.

From this description it appears clear that membranes are involved in a great number of processes most of which are still unknown.

2.3 The Membrane Composition

The basic components of all biological membranes are lipids, proteins and carbohydrates. The composition of a plasma membrane can vary from cell to cell, depending primary on the cell function [108].
Even in a cell, the composition of plasma membrane differs from that one of organelles. For example, the myelin sheath (the plasma membrane of nervous fiber) is enriched of sphingomyelin and cholesterol and it contains only 20% by weight of proteins [109]. In contrast, the mitochondrial membrane is enriched in proteins, up to 75% by weight. This difference is primary due to the function of the membranes: the role of the myelin sheath is to insulate nerve cells (structural role), instead the mitochondrial membrane is involved in many processes such as electrons transport (active role).

2.3.1 Lipids

Lipids are fundamental components of the membrane. The principal classes of lipids found in membranes are essentially three: glycerophospholipids, sphingolipids and sterols.
For sure, glycerophospholipids are the main components of a membrane. They are composed of one glycerol molecule, a phosphate, two fatty acid chains and an alcohol. A phospholipid is an amphipathic molecule: it has a polar head group formed by glycerol, phosphate and alcohol, and a hydrophobic portion formed by the two fatty acid chains. In Fig. 2.4 is reported a representation of a glycerophospholipid.

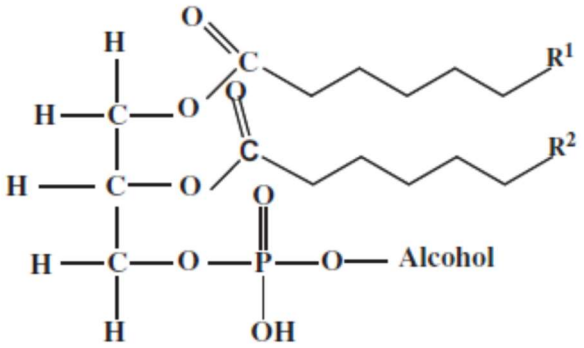

Fig. 2.4 Chemical structure of a glycerophospholipids.

The fatty acids are esterified at C1 (*sn*-1 position) and C2 (*sn*-2 position) of the glycerol. Usually the acyl chain in position *sn*-1 is saturated, instead that one in position *sn*-2 is unsaturated. Clearly this is not a rule. Both chains can be saturated or even both with multiple unsaturations. Their length can vary from 14 to 22 carbon

atoms. At the C3 of the glycerol, a phosphate group is esterified. Attached to phosphate, there is an alcohol. Based on the type of alcohol, it is possible to obtain different kinds of phospholipids (Fig.2.5): phosphatidylcholine (PC), phosphatidylethanolamine (PE), phosphatidylserine (PS), phosphatidylinositol (PI) and phosphatidylglycerol (PG). There are also phosphatidic acids (PA) in which there is no alcohol attached to the phosphate group.

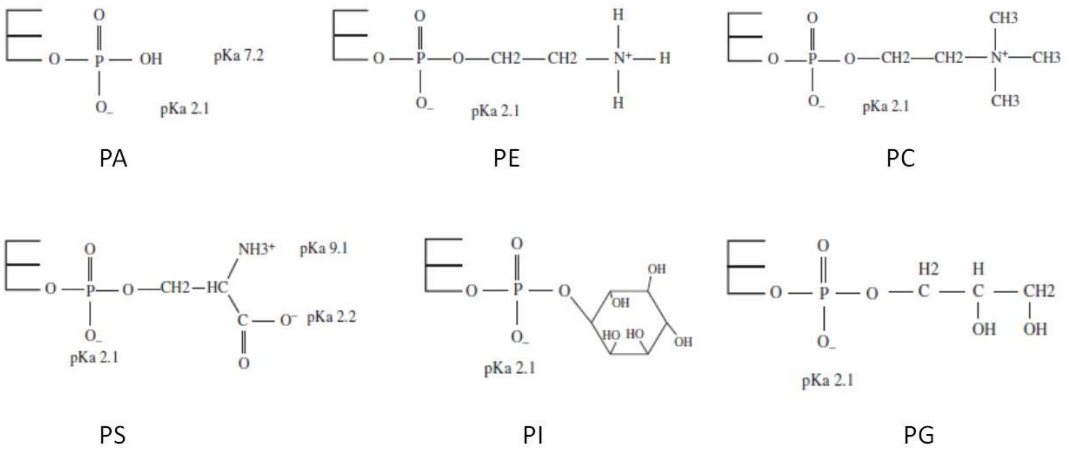

Fig. 2.5 Chemical structures of the polar head groups of glycerophospholipids. The pK_a values of the chemical groups forming the polar heads are also reported. Adapted from [99].

A particular lipid found both in eukaryotic and prokaryotic membrane [99,110] is the cardiolipin (CL). It is formed by two PAs linked together by a glycerol (Fig. 2.6). Thus, it differs from other lipids having four fatty acid chains.

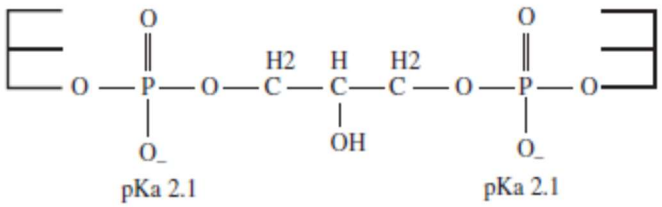

Fig. 2.6 Chemical structure of cardiolipin (CL). Adapted from [99].

All the subclasses of glycerophospholipids (Fig. 2.5 and 2.6) are amphipathic molecules. At physiological pH of 7.4 some of them are zwitterionic, and some are negatively charged. Due to the acidic character of the phosphate group, at physiological pH, it brings always a net negative charge. Thus, the net charge of a particular lipid is determined by the phosphorylated alcohol. For example, PCs have

not ionizable groups and a positive charge on the nitrogen atom. Thus, it is zwitterionic with no net charge. PEs instead, are slightly negative charged. This is because the amine group of PE has a pK_a around 8.5. CLs, instead, have a negative charge of about 2 dues to the presence of two phosphate groups which are not fully ionized [111].

Each subclass of phospholipids has a role in the membrane. PCs are the most abundant phospholipids in all the eukaryotic membranes. Basically, they have a structural role, determining many properties of the membrane, for example the fluidity. Another structural lipid is the PE. It is the second most abundant lipid in eukaryotic organisms, but it is the main lipid in the membrane of bacteria. This is because, in eukaryotes PEs are converted into PCs. This process is not possible in bacteria. PSs are negatively charged lipids which have a different role. In fact, they are involved in activating and anchoring proteins to the membrane. It is interesting to note that PSs are found almost exclusively in the inner leaflet of the membrane (bilayer asymmetry). This is accomplished by proteins named flipases [112]. With the ageing of the cell, PSs accumulate in the outer leaflet of the membrane and this is a signal that the cell should be recycled. PIs, another negatively charged lipids, play a central role in cell signaling and regulation [113]. PIs are present, more or less, in every cell type but they are particularly abundant in the cells of the brain. PGs, anionic lipids, are found in low abundance in the membrane of eukaryotes. An exception is represented by lung surfactant in which PGs constitute up to 10% of all lipids [114]. Moreover, PGs are among the main components of the bacterial membrane [115]. PAs are unique lipids involved in different processes such as membrane fission and fusion events. At physiological pH, they are negatively charged. Finally, CLs are abundant in the mitochondrial membrane where they are involved in electron transport stabilizing some electron transport proteins. CLs are also present in the bacterial membrane. They take part in some processes such as cell division, membrane transport and energy metabolism [116].

The second important class of lipids is represented by sphingolipids. All the sphingolipids are based on the sphingosine, an amino alcohol with a hydrophobic tail of 18 carbon atoms and a trans double bond at C4 (Fig. 2.7).

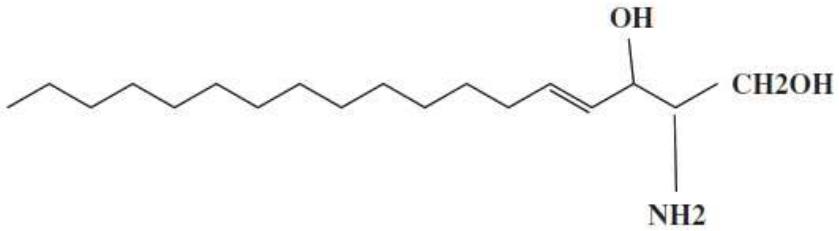

Fig. 2.7 The chemical structure of sphingosine, the precursor of all sphingolipids.

All the sphingolipids derive from the sphingosine by attaching an alcohol to the C1 and a fatty acid chain (saturated or not) to the its unique nitrogen atom. Depending on the alcohol on the C1 we can identify five different subclasses:

- Ceramide, where the attached group is a simple hydrogen atom;
- Sphingomyelin, where the attached group is a phosphatidylcholine or a phosphatidylethanolamine;
- Cerebroside, with a sugar such as glucose or galactose;
- Globoside, with up to four sugar molecules;
- Ganglioside where the attached group is a complex oligosaccharide.

The most abundant sphingolipid in humans is sphingomyelin (SM). In this lipid, the head group is a phosphocholine. Thus, like PCs, at physiological pH it is zwitterionic. The fatty acid chain can vary in length (up to 24 C atoms) and usually it is longer and more saturated respect to the hydrocarbon chains in PCs. In Fig. 2.8 is reported a chemical structure of a sphingomyelin, where the attached fatty acid has 16 C atoms and it is saturated.

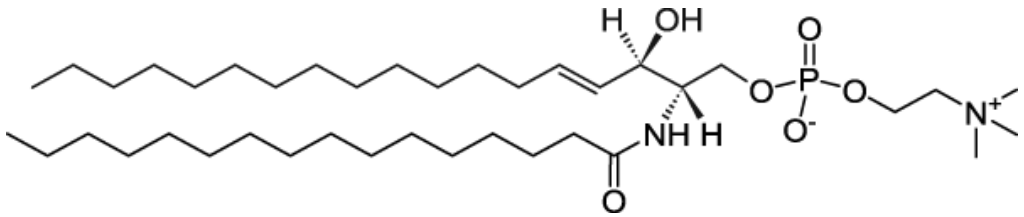

Fig. 2.8 The chemical structure of palmitoyl-sphingomyelin. Taken from https://avantilipids.com/.

Sphingomyelin is present in many mammalian cells, but it is particularly abundant in the plasma membranes of the nervous cells [117]. It has a higher affinity for cholesterol, with which forms organized microdomains termed “lipid rafts” [118,119]. These microdomains can function as signaling platforms that regulate the localization of proteins [120]. Other sphingolipids are involved in different

functions. For example, gangliosides are found in the outer leaflet of the membranes where are involved in cell-cell recognition [121].
The third class of lipids commonly found in the membranes are sterols [122]. They are components of the membrane of animals, plant and fungi but it is completely absent in prokaryotes. Sterols are very water insoluble and readily partition inside the hydrophobic core of the membrane. The basic structure is formed by four rigid rings (Fig. 2.9) where at C3 an OH group is attached which form the polar head group of this lipid.

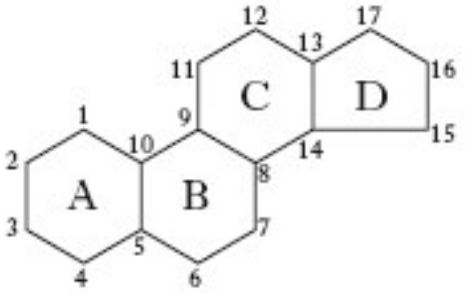

Fig. 2.9 The chemical structure of sterol which constitutes the basic structure of all sterols.

Some carbons in the rings could be also unsaturated. At the C16, a hydrocarbon tail is found. Depending on the structure of the tail, we will have different kinds of sterols. In Fig. 2.10 are reported the three main sterols found in animals (cholesterol), fungi (ergosterol) and plants (β-sitosterol).

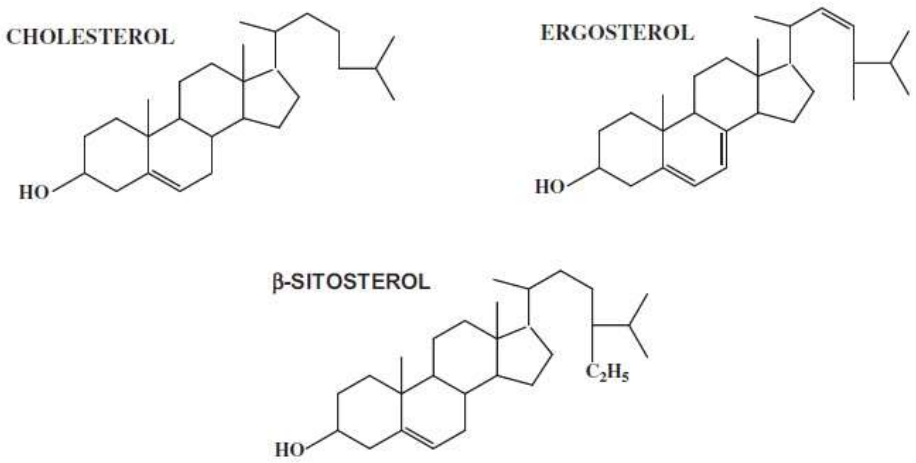

Fig. 2.10 The chemical structures of cholesterol, ergosterol and β-sitosterol.

Cholesterol (Chol) is found in many cell membranes. It constitutes up to 50% by weight of all lipids in the plasma membrane and it is particularly abundant in the brain. The main role of cholesterol in membranes is to regulate their fluidity [122] controlling the phase behavior of the bilayer (see section 2.7). This is accomplished thanks to its unique flat structure which permits its intercalation among phospholipid chains. Thus, cholesterol is important in supporting membrane lateral organization, stability and preventing the leakiness of solutes across the membrane. Moreover, cholesterol is a precursor of a series of steroid hormones (e.g. testosterone), vitamin D and bile salts. In conclusion, cholesterol has two functions: it has a structural role and a biochemical role as a precursor of important molecules.

2.3.2 Membrane Proteins

Proteins are an important component of the membrane. Differently from lipids, all proteins have an active role. They can serve as enzymes which catalyze some reaction at the water/membrane interface, they are involved in the active transport of solutes and they can function as receptor in the surface of the membrane. Basically, all the membranes have proteins. Their percentage by weight can vary from 20% up to 75%, depending on the function of the membrane. If the membrane has only a structural role, the % of proteins will be very low. Conversely, if a membrane must catalyze a series of reactions, its protein content will be very high.
Membrane proteins can be classified in two big groups: peripheral and integral proteins [123].
Essentially, a peripheral protein is a water-soluble protein which interact with the membrane surface through electrostatic interaction or hydrogen bonds. Some of them interact directly with the anionic lipids, others interact on the surface of integral proteins. Since the weak forces involved in this interaction, peripheral proteins can be easily removed by changing the pH or the ionic strength of the medium.

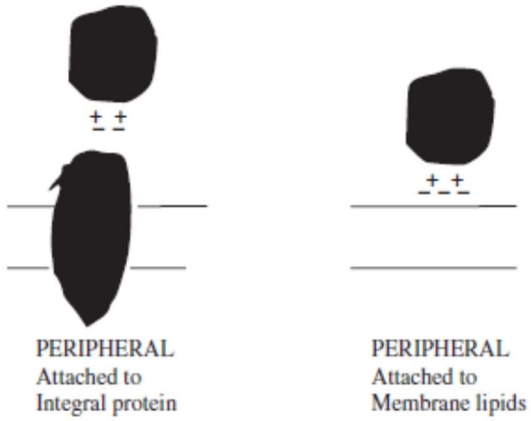

Fig. 2.11 A schematic representation of the two kinds of peripheral proteins found in membranes. Adapted from [99].

A good example of peripheral protein which interact directly with lipid head groups is myelin basic protein [124] whose malfunctions are involved in multiple sclerosis. Cytochrome c, instead, is an example of peripheral protein which interacts with an integral protein. In fact, cytochrome c is weakly bound to cyctchrome c oxidase that is localized in the inner membrane of mitochondria [125].
Integral proteins penetrate inside the membrane and interact directly with the hydrophobic core. Usually, these proteins span the entire membrane (they are trans-membrane protein) with some segments exposed on both side of the membrane (as well represented in Fig. 2.1). The residues which interact with the lipid chains are clearly hydrophobic. Instead, the portions out of the membrane are enriched in polar amino acids. A general feature of integral proteins is that they have aromatic residues as tryptophan and tyrosine localized at membrane/water interface [32,126]. The portion of integral protein, which is embedded in the membrane hydrophobic core, adopts a specific motif. On this basis we can divide integral proteins in several classes (Fig. 2.12):

1. Single trans-membrane α-helix proteins;
2. Multiple trans-membrane α-helices proteins;
3. β-barrel proteins.

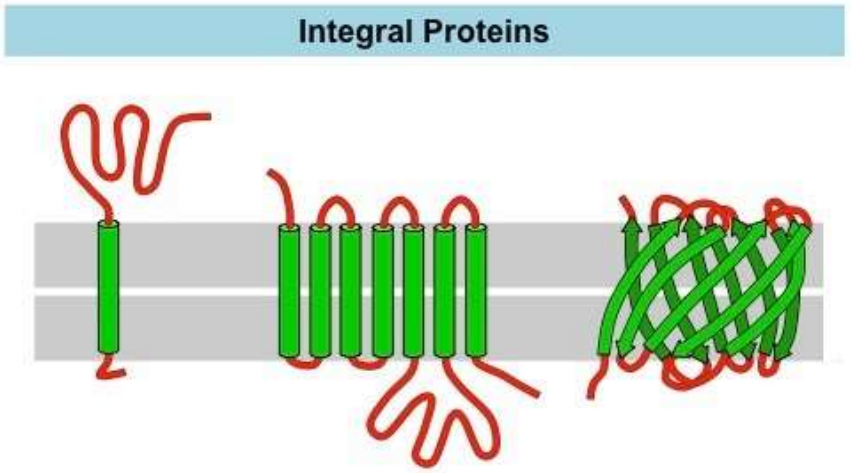

Fig. 2.12 The three kinds of integral proteins. From left to right: single trans-membrane α-helix, multiple trans-membrane α-helices proteins and β-barrel.

Single trans-membrane α-helix proteins have a single helix which span the entire membrane. Since the average thickness of a membrane is about 5-6 nm, a trans-membrane α-helix should have 20 amino acids. An example of this kind of integral protein is represented by glycophorin [127]. Multiple trans-membrane α-helices proteins, instead, are composed by several helical structures embedded in the membrane. An example is represented by the 7 α-helix trans membrane protein bacteriorhodopsin [128]. The last type of structure adopted by integral proteins is the β-barrel. It is composed by 16 or more anti-parallel β-strands arranged like a cylinder (the barrel) inside the membrane. β-barrels are very common in the outer membrane of gram-negative bacteria. The bacterial porins are an example [129]. They are composed by 18 strands connected by turns on cytoplasmic side and loops on the extracellular side.
Many integral proteins are also attached to the membrane through lipid anchors. The most important lipid chains involved are: myristic acid, palmitic acid, prenylated hydrophobic chains and glycosylphosphatidylinositol (GPI).

2.3.3 Membrane Carbohydrates

Carbohydrates (or sugars) are the third component found in biological membranes. Being water-soluble molecules, they do not partition inside the hydrophobic core of the membrane. Sugars are exclusively found on the outer surface of the membrane and always attached to lipids (glycolipids) or proteins (glycoproteins). This aspect suggest that sugars are involved in the interaction of the cell with the external environment. Among carbohydrates diverse function, it is possible to mention: cell-

cell recognition, membrane receptors, membrane proteins protection from degradation, chaperones, proteins stability [99]. Carbohydrates have also a protecting role in protein-derived antimicrobial peptides. Moreover, sugars are fundamentals for the activity of some AMPs [130]. Carbohydrates can also contribute to the membrane physical state, modulating its fluidity [131]. Commonly, in membranes are found about nine different sugars: α-D-glucose, α-D-mannose, α-D-galactose, α-L-fucose, α-D-xylose, α-L-arabinose, N-acetylglucosamine, N-acetylgalactosamine and sialic acid. It is possible to find attached to proteins and/or lipids a single sugar molecule or more, up to 15.
In glycolipids, carbohydrates can be covalently linked (through a glycosidic bond) directly to a fatty acid (simple glycolipids) or to the glycerol of the lipid head group of glycerolipids, forming the class of glycerol-glycolipids. On the other hand, carbohydrates linked to the oxygen atom on C1 of sphingolipids form the class of sphingo-glycolipids (Fig. 2.13).

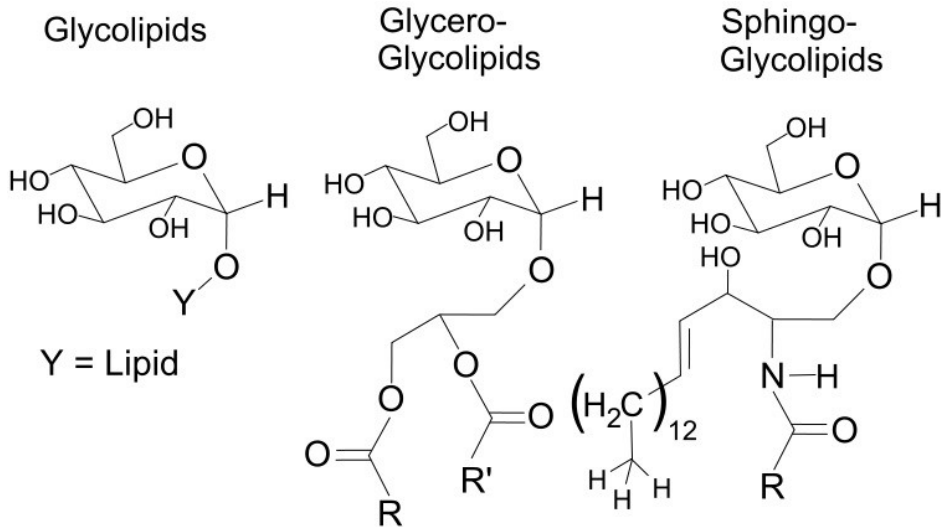

Fig. 2.13 The chemical structure of glycolipids (left), glycero-glycolipids (middle) and sphingo-glycolipids (right). Adapted from https://en.wikipedia.org/wiki/Glycolipid.

In animals, the major glycolipids are sphingo-glycolipids. They can accumulate into lipid rafts where they are involved in the cell signaling. Cerebrosides are sphingo-glycolipids with only one sugar molecules (usually a glucose or a galactose). Globosides can have two, three or four sugar molecules (in the form of di-, tri- or tetra-saccharide) linked to the sphingolipid. Finally, gangliosides have a complex oligosaccharide. A special mention merits a class of glycolipid localized in the outer membrane of gram-negative bacteria: the lipopolysaccharide (LPS) [132]. Briefly, it is composed by a disaccharide of N-acetylglucosaimne with multiple fatty acid

chains. The hydrophobic tails can be linked to the disaccharide free OH group or to the acetyl group. Attached to the disaccharide moiety, there is a complex polysaccharide whose composition varies from bacterium to bacterium.
Carbohydrates can also be found attached to membrane proteins. The combination of proteins and sugars forms glycoproteins. The process through which sugars are added to proteins is known as glycosylation. There are two types of glycoproteins: N-glycosylated and O-glycosylated (Fig. 2.14). Intuitively, in the case of N-glycosylated proteins, the glycosylation occurs at the nitrogen atom of asparagine. The first sugar attached is always a N-acetylglucosamine. From this unit, other sugars can be attached. In O-glycosylated proteins, carbohydrates are linked to the oxygen atom of serine and threonine residues.

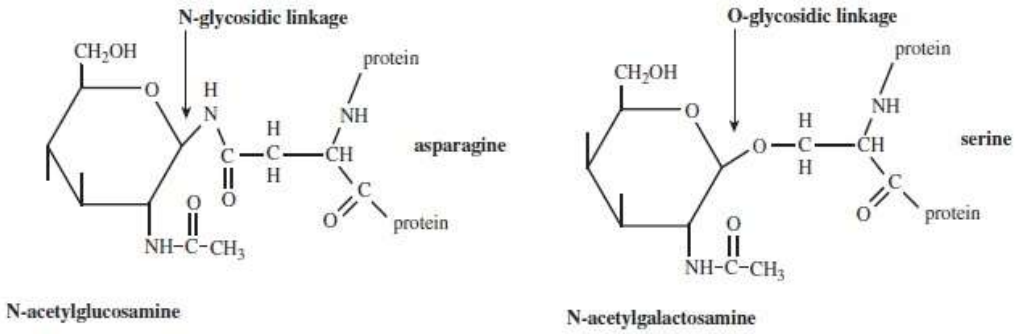

Fig. 2.14 The two types of proteins glycosylation. (Left) N-glycosylation always starts with a N-acetylglucosamine. (Right) O-glycosylation involving a residue of serine. Adapted from [99].

Usually, the sugar chain of O-glycosylated proteins is shorter respect to N-glycosylated proteins. Moreover, the N-glycosylation is common for all the membrane proteins which have an active role (enzymatic), whereas O-sugars are predominant in structural proteins. For example, in the plasma membrane (a very active membrane) about 90% of protein are glycosylated. The number of N-linked sugars is more than the O-linked ones [99].

2.4 A Comparison between Eukaryotic and Prokaryotic (Bacterial) Membranes

All the living organisms are formed by cells [100]. Essentially, there are two cell types: prokaryotic cells and the more complex eukaryotic ones. They differ in a wide variety of aspects which can be found in every biology text. Here we focus our attention to a specific part of the cell: the membrane. Eukaryotic and prokaryotic membranes are both formed by a lipid bilayer. However, there are some important differences between them, both structurally and compositionally.

The main constituent of the eukaryotic plasma membrane is represented by phosphatidylcholines (PCs). Other constituents are phosphatidylethanolamines (PEs), sphingomyelins (SMs), cholesterol (Chol), phosphatidylinositols (PIs) and phosphatitdyserines (PSs) [108]. As example, the average lipid composition of mammalian liver cells is (in mol %): 45-55% PCs, 15-25% PEs, 10-15% PIs, 5-10% PSs, 5-10% SMs and 10-20% Chol. Clearly, the abundance of these lipids varies from cell to cell [133]. Moreover, the lipid composition of the inner leaflet is different from that one of the outer leaflet [134]. The zwitterion lipids, PCs and SMs, are mainly found in the outer leaflet. On the contrary, PEs and anionic lipids (PSs and PIs) are localized in the inner leaflet. Thus, from the point of view of an external observer, the plasma membrane of a eukaryotic cell appears with no net charge.
Bacterial membranes are enriched of the zwitterionic lipids as PEs, and anionic lipids PGs and CLs [87,135]. The exact composition and the ratio between zwitterionic and anionic lipids depend on the type of bacterium and even on the environment surrounding the microorganism [136].
Bacterial cells do not have only membranes, but they have also a cell wall formed by sugars [137]. Together, cell wall and membrane form a complex structure which separate the cytosolic space from the external environment. There are two classes of bacteria: gram-negative and gram-positive (Fig. 2.15).

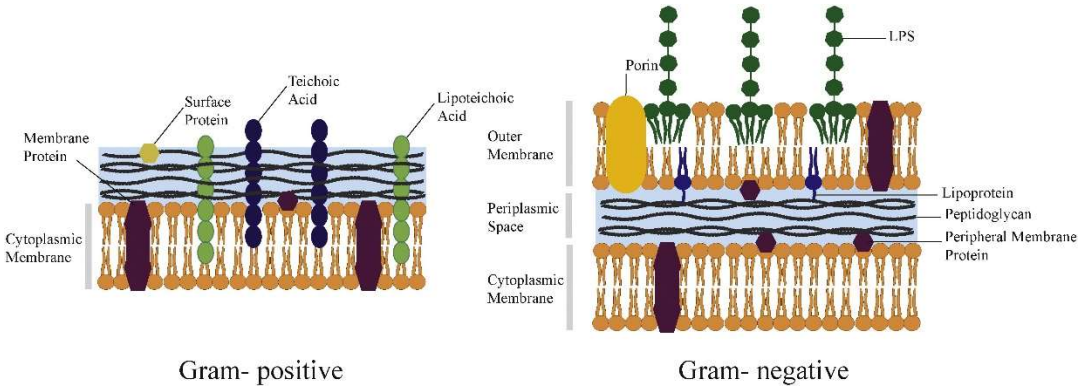

Fig. 2.15 Schematic representations of the gram-positive (left) and gram-negative (right) bacterial membranes. Taken from [87].

Gram-positive bacteria have a lipid double composed by PEs, PGs and CLs. The bilayer is surrounded by a thick cell wall of about 40-80 nm [138] composed by a polymer of N-acetylglucosamine and N-acetylmuramic acid linked through a β-(1,4) glycosidic bond, i.e. peptidoglycan. In addition, peptidoglycan is cross-linked by a pentapeptide which links together the sugar layers. Attached to the peptidoglycan, there are polyanionic molecules named teichoic acids (TAs). TAs can also be directly embedded in the membrane through a lipid anchor, forming lipoteichoic acids

(LTAs) [71]. In contrast, gram-negative bacteria possess two distinct membranes (the outer and the inner or cytoplasmic membrane) separated by a thin layer of peptidoglycan of about 7-8 nm [138] without TAs.
Both the leaflets of the cytoplasmic membrane and the inner monolayer of the outer membrane in gram-negative bacteria are composed by zwitterionic lipids PEs and anionic ones, PGs and CLs. Instead, the external leaflet of the outer membrane is enriched by lipopolysaccharides (LPS), briefly described in the section 2.3.3. Clearly, attached to the membranes, there are also proteins, both peripherals and integrals involved in numerous functions.
In bacterial membranes, the anionic lipids are not only localized in the inner leaflet but are exposed to the surface. This confer to the membrane a net negative charge. This is the main difference with the eukaryotic membrane which is fundamental in the interaction with antimicrobial peptides, described in chapter 1.

2.5 Lipids Self-Assembly

Lipids are amphipathic molecules. When exposed to the aqueous medium, they tend to self-assemble into aggregates. The main force which drives the aggregation of lipid molecules, and the formation of membranes and model membranes as liposomes (see section 2.8), is the hydrophobic effect [139,140]. In aqueous medium, a lipid molecule is surrounded by water molecules. Water does not interact in the same way with all the portions of the lipid molecules. There are some favorable interactions with the polar head group. There are also unfavorable interactions of waters with the lipid hydrocarbon chains. This brings to the formation of an ice-like structure (the water cage) around the acyl chains because water molecules prefer to interact to each other through hydrogen bonds. In this cage, water molecules are not free to move: their motion is restricted. From a thermodynamic point of view, we will say that water molecules around hydrocarbon chains are characterized by low entropy. When a second lipid molecule is added, it immediately interacts with the first lipid molecule. This leads to the release of water molecules from the cage. Now the water molecules are free to move in the bulk. This release increases the entropy of water. It is this increase of entropy that is the main responsible for the aggregation of lipids.
In addition, there are other minor forces that contribute to the bilayer stability: head group-water interactions, head group-head group interactions, entropy of caged lipid chains and van der Waals interactions [99].
Lipids have a polar head group (often charged) which can interact favorably with water molecules, contributing to the stabilization of the membrane. For example, water molecule can from a hydrogen bond with the oxygen atom of the phosphate group. Additional stabilizing forces come from head group-head group interactions

between neighbouring lipids. These interactions are mainly ionic in nature. Another stabilizing force comes from the increase in entropy of lipid chains when are buried to the water. In fact, the formation of the water cage around hydrocarbon chains restrict their motion (low entropy). When the aggregate is formed, the acyl chains are segregated in the bilayer hydrophobic core which results in an increase of chains motion (high entropy). The last forces involved in the stabilization of the membrane are the van der Waals interactions. These are very weak forces which involve the hydrocarbon chains. van der Waals interactions are the result of the interaction among induced dipoles that form instantaneously between two close acyl chains.
In Fig. 2.16 are summarized all the forces involved in the bilayer formation, keeping in mind that the main responsible is the hydrophobic effect.

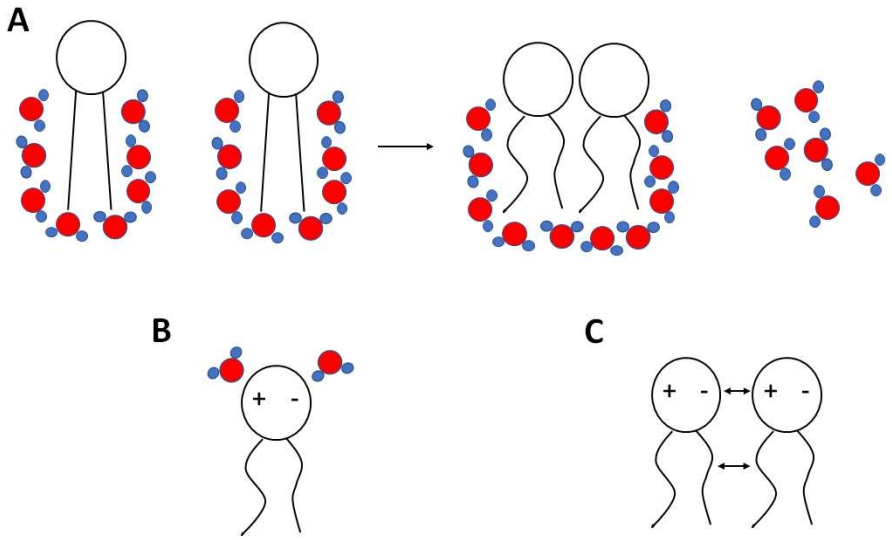

Fig. 2.16 The main forces involved in membranes' formation. (A) Hydrophobic effect and entropy of caged lipid chains; (B) head group-water interactions; (C) head group-head group and van der Waals interactions.

The tendency to aggregate depends on several factors. It depends on the lipid concentration in solution, their chemical structure and the ionic strength of the medium [141]. The concentration at which amphipathic molecules start to aggregate is defined critical micellar concentration (cmc). In solution, the cmc for bilayer-forming lipids is in the range 10^{-10}-10^{-6} M [142]. For example, the cmc value in water for dimyristoylphosphatidylcholine (DMPC) is 6 nM, and for dipalmitoylphosphatidylcholine (DPPC) is about 0.4 nM. Thus, the cmc value decreases as the acyl chains length increases. The effect of the ionic strength is important in lipids with a net charge. The cmc value of dioctanoyl-

phosphatidylserine in water is about 2.2 mM. In the presence of 5 mM Ca^{2+}, the cmc decreases to 0.4 mM.

2.6 Lipid Structures: Lamellar and Non-Lamellar Structures (Phases)

In the previous section, we stated that lipids tend to interact to each other forming an aggregate. But, which kind of structure do they form? Looking at the biological membrane, we can think that all lipids form a bilayer having a flat structure, named lamellar phase. Depending on the lipid chemical structure and the environmental conditions (pH, temperature, ionic strength, water content), lipids can self-assemble in different structures. At high water concentration, three stable phases exist [99,141]:

- Lamellar;
- Inverted Hexagonal;
- Cubic.

It is possible to predict in which kind of structure a lipid self-assembles by considering the lipid shape. Membrane lipids can be divided into three basic geometrical shapes: truncated cone, cylinder and inverted cone (Fig. 2.17).

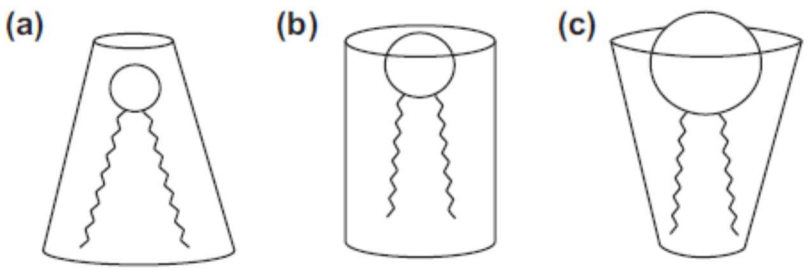

Fig. 2.17 Membrane lipids shapes: (a) truncated cone, (b) cylinder and (c) inverted cone. Adapted from [99].

Bringing close to each other these geometrical shapes, we can have an idea on which kind of structure will be formed. For example, if we put together all cylindrical shape lipids, we will obtain a lamellar structure. It is more convenient to define a geometrical parameter, the packing parameter S, through which is possible to predict the final form of the assembly. The packing parameter is defined as $S = v/a_0l$ where v is the hydrocarbon volume, a_0 is the optimal head group area and l is the length of fully extended lipid chain [143]. When $S < 1$, the lipid shape is inverted cone. These lipids will self-assemble forming spherical or non-spherical micelles with a positive curvature. A good example is represented by the class of Lyso PCs (e.g. 1-palmitoyl-

2-hydroxy-*sn*-glycero-3-phosphocholine) that form micellar structures. For cylindrical lipids, S = 1 and they will form lamellar structures (the bilayer). PCs are cylindrical lipids and they prefer to adopt lamellar phase with no curvature. When S > 1, the lipid shape is truncated cone. In this case, lipids can form inverted, non-lamellar structures with a negative curvature. PEs and Chol are truncated cone shaped and they adopt non-lamellar phase (e.g. hexagonal) [144]. Unfortunately, this scheme works only for one-component aggregate. When two or more lipids form the aggregate, other factors (as electrostatic and van der Waals interactions, hydrogen bonds) should be considered which render the prediction impossible.
The lamellar phase is the most common structure. The lipid bilayer as described by the fluid mosaic model is a lamellar structure. The lamellar phase can exist in a variety of states, depending on how the lipid molecules interact to each other (see section 2.7 for a detailed description). The second most important structure is the non-lamellar phase named inverted hexagonal (H_{II}). It is composed by six parallel lipid tubes of indefinite length. Each tube is formed by truncated cone lipids: the polar head groups point towards the tube cores (which are filled with water), instead lipid chains outside. The tubes are taken together by means of hydrophobic interactions and are arranged like a hexagon (Fig. 2.18).

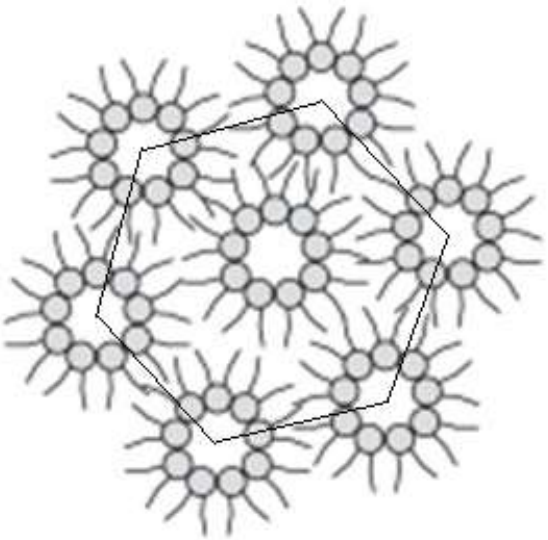

Fig. 2.18 A representation of the inverted hexagonal (H_{II}) phase.

Lipids as PEs can adopt this phase. Since a great amount of truncated cone lipids are required to have a full hexagonal phase, their existence in membranes is still under debate. However, PEs propensity to adopt H_{II} phase may have a role in membrane fusion. In fact, PEs can help in achieving highly curved intermediate structures

during fusion [145]. The last category of possible phases is represented by cubic phases [146,147]. It is composed by a single continuous or discontinuous curved bilayer which is folded in a three-dimensional structure. The cubic phases can exist in three different morphology, reported in Fig. 2.19.

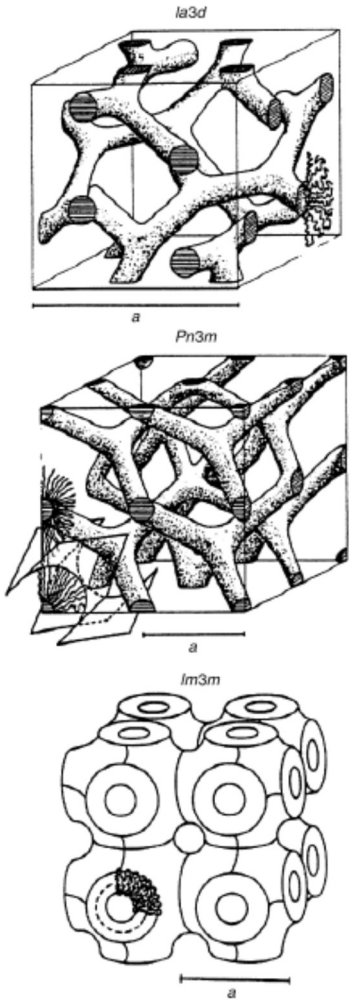

Fig. 2.19 Schematic representations of three different morphologies of the cubic phases. Taken from [146].

Without entering in the details of these quite complex structures, it seems that they exist in the membrane. For example, cubic phase was observed in the plasma membrane of archaebacteria and in the membranes of mitochondria of mammals [141].

It is important to note that these "exotic" structures are rarely observed in membranes. They are reported in model membranes (liposomes) composed by one or two components. Usually, real membranes adopt the lamellar phase. This is a very

important point because the majority of lipids are not cylindrical. Thus, it seems that cylindrical lipids have a strong influence on the final structure adopted by membranes. A clear example is the inner membrane of bacteria. As stated in the section 2.4, it is composed by PEs, PGs and CLs [12]. The major component (up to 80%) is the truncated cone PE, instead the cylindrical lipid PG is the minor constituent. Despite of this, the membrane of bacteria adopts a lamellar structure.

2.7 Lamellar States and Phase Transitions

As stated in the previous section, membranes exist in the so-called lamellar phase. Inside this phase, different physical states can be adopted depending on the chemical structure, temperature and medium conditions (pH and ionic strength). These parameters determine how lipids interact to each other.
Basically, the membrane can exist in two distinct lamellar phases: the gel phase and the liquid crystalline phase (L_α). In the gel phase, the hydrocarbon chains are in their extended conformation (all-trans). The acyl chains can be tilted ($L_{\beta'}$) or not (L_β) respect to the bilayer plane. In this way they tightly interact to each other forming a compact bilayer. The gel phase is characterized by:

- Low fluidity;
- High degree of order;
- Relative impermeability;
- High bilayer thickness.

In the L_α phase, the hydrocarbon chains are not in the all-trans conformation, but they assume a gauche conformation. This leads to a less packed bilayer. Thus, the liquid phase is characterized by:

- High fluidity;
- Low degree of order;
- Relative permeability;
- Low bilayer thickness.

It is important to give an exact definition of terms fluidity and order. The term “fluidity” refers to the motion of lipid in the bilayer plane. The term “order” refers to the relative amount of trans/gauche conformers in the acyl chains [102]. The amount of trans conformers is higher in an ordered bilayer. In Fig. 2.20 are reported a schematic representation of the gel and liquid phases.

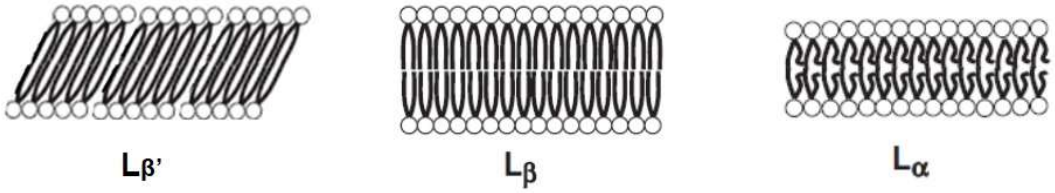

Fig. 2.20 Schematic representation of a lipid bilayer in the gel phase with tilted hydrocarbon chains ($L_{\beta'}$), gel phase with no tilted chains (L_{β}) and liquid crystalline phase (L_{α}). Adapted from [102].

Other phases are possible. One of these is the rippled gel phase ($P_{\beta'}$) in which the bilayer surface is not flat, but it is undulated [148]. The lipid chains are in the all-trans conformation, as in the gel phase. The $P_{\beta'}$ does not exist for all lipids, but it is characteristic of some saturated lipids, as DPPC and DMPC [148]. A schematic representation of the rippled gel phase is reported in Fig. 2.21.

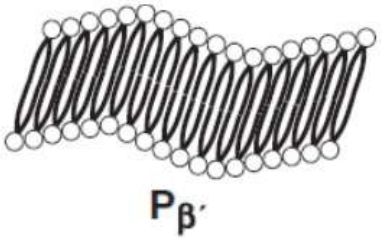

Fig. 2.21 The rippled gel phase ($P_{\beta'}$). Adapted from [102].

It is not known if $P_{\beta'}$ phase has a biological role. This is because the addition of other lipids eliminates it. Thus, it is difficult to detect in real membranes. Another important lamellar phase is represented by the liquid ordered phase (L_o) [149,150]. This phase is observed in the presence of Chol (e.g. lipid rafts). The L_o phase has property in between the gel and liquid crystalline phases. In particular, it is characterized by:

- A bilayer thicker than the L_{α} and thinner than the L_{β} phases;
- Higher degree of order compared to L_{α}, and lower degree or order compared to L_{β};
- Higher mobility (fluidity) of lipids respect to the L_{β} and lower mobility respect to the L_{α};
- Less permeable and more permeable than the L_{α} and L_{β}, respectively.

All lipid bilayers are characterized by definite melting temperatures at which the transition to one phase to another one occurs. The most important melting temperature is the temperature at which a bilayer goes from the gel to liquid phase

(T_m). As an example, we can consider the thermotropic behavior of liposomes composed by only DPPC [102,151]. In Fig. 2.22 are reported the phase transitions for this lipid bilayer.

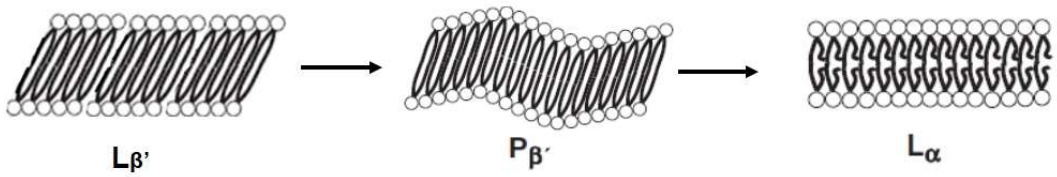

Fig. 2.22 The phase transitions in model membranes composed by only DPPC. $L_{\beta'}$: gel phase with tilted hydrocarbon chains, $P_{\beta'}$: rippled gel phase, L_α: liquid crystalline phase.

In DPPC liposomes, there are two transitions. The first one from the $L_{\beta'}$ to $P_{\beta'}$, named pre-transition, occurs at about 36 °C. We indicate this temperature as T_p (pre-transition temperature). As represented in the Fig. 2.22 it is mainly due to the rearrangement of polar head groups of lipids. A second transition, from the $P_{\beta'}$ to L_α, occurs in between 41 and 42 °C and it is termed main-transition. This transition is the gel-to-liquid phase transition and occurs at the main-transition temperature (T_m). It is due to acyl chains melting which go from an all-trans conformation to a gauche conformation.

The temperature at which a bilayer transits from one phase to another is strictly dependent on the lipids chemical structure. To be more precisely, it depends on length of acyl chains, the nature of polar head group and the presence of unsaturation. The melting temperature increases as the acyl chains length increases. This is because as the number of C atoms increases, the number of van der Waals interactions also increases. For example, DPPC with two acyl chains of 16 C atoms has a T_m around 42°C, instead DMPC with two acyl chains of 14 C atoms has a T_m about 23 °C [152,153].

The melting temperature is inversely related to the number of unsaturation in the hydrocarbon chains. More unsaturated a lipid is, lower the T_m is. For example, the lipid DSPC (distearoylphosphatidylcholine) with two saturated chains of 18 C atoms has a T_m around 58 °C. Conversely, its analog DOPC (dioleoylphosphatidylcholine) with two mono unsaturated chains of the same length has a T_m of -22 °C [152,153]. This strong temperature decrease is due to the fact that in natural lipids all the unsaturations are cis [154]. The cis unsaturation bends the lipid chains that cannot pack efficiently.

Finally, the head group has also an influence on the T_m. As reported above, model membranes composed by DPPC have a transition temperature about 42 °C. DPPE (dipalmitoylphosphatidylethanolamine), with the same two saturated lipid chains, has a transition temperature (for the lamellar gel-to-liquid transition) at 62 °C [155].

Probably this is due to the ability of phosphatidylethanolamine to form intermolecular hydrogen bonds that are not possible in cholines.
It is important to note that transition between lamellar and non-lamellar phases are also possible. These can be induced by temperature, pH and ionic strength changes. An example of temperature-induced change is represented by saturated PEs (e.g. DPPE). Model membranes of DPPE adopt a lamellar gel phase (L_β) at low temperature. On the contrary, at high temperature (about 120 °C) they adopt the inverted hexagonal phase (H_{II}) [155].
PSs are cylindrical shaped lipids. At pH = 7 they tend to adopt a lamellar phase. When the pH is less than 4, they transit to the inverted hexagonal phase [99]. This phenomenon is due to the protonation of the carboxyl in the head group which reduces its apparent area without affecting the acyl chains. Thus, it seems that reducing the pH, PSs become truncated cone lipids.
An example of ionic strength-induced transition is represented by the case of cardiolipins (CLs). When TOLC (1',3'-bis[1,2-dioleoyl-*sn*-glycero-3-phospho]-glycerol) molecules are dispersed in water, they form a lamellar structure in the liquid crystalline phase. After the addition of NaCl at the concentration of about 3 M, TOLCs transit to the inverted hexagonal phase [156].

2.8 Model Membranes: Liposomes

As showed in the previous sections, biological membranes are very complex structures. For this reason, a variety of simple model membranes have been developed. There are many model membranes such as lipid monolayers [157], micelles, bicelles [158] and supported bilayers [159]. One of the most common used models are liposomes. Liposomes, or lipid vesicles, are colloidal particles formed by one or more sphere-shaped lipid bilayer [160]. The lipid bilayer surrounds an aqueous core and separate it from the external aqueous space (Fig. 2.23).

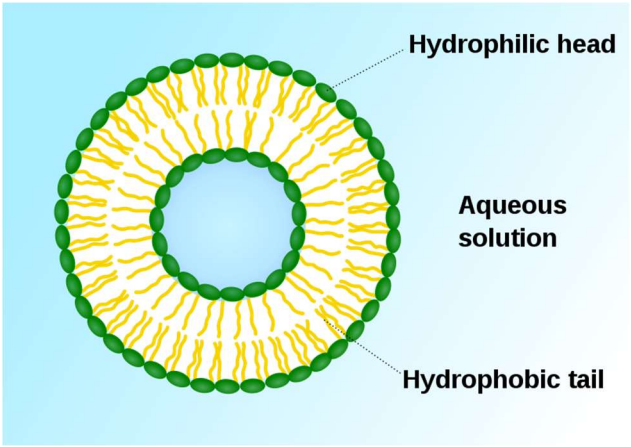

Fig. 2.23 A representation of a liposome formed by one sphere-shaped bilayer (unilamellar liposome).

Alec Bangham discovered liposomes in 1964 and thus, he can be considered the "father of liposomes" [161]. To be more exact, Bangham reported the observation of what we call now multilamellar vesicles: liposomes formed by two or more concentric lipid bilayer (like an onion).
Liposomes are multipurpose structures. The most obvious application is as model membrane systems. They are very useful in studying:

- the general physical and chemical properties of a bilayer;
- how two lipids interact to each other in the bilayer (lipids miscibility);
- the interaction of proteins, peptides and drugs with membranes, highlighting the involvement of a particular lipid.

During this PhD thesis, liposomes were employed as a model of eukaryotic and bacterial membrane.
Another important application is as drug delivery systems. Liposomes can incapsulate drugs in their inner aqueous core. Moreover, insoluble drugs can be dissolved in the hydrophobic core of the membrane. In this way, drugs can reach a particular target in the body. The general properties of liposomes such as biodegradability, biocompatibility, small size, amphipathic character and low toxicity have permitted their application in medicine [162].
Liposomes are classified according to their dimensions and lamellarity. Basically, there are four different liposome types (Fig.2.24):

- SUVs: Small Unilamellar Vesicles. These liposomes are formed by a single lipid bilayer with a diameter smaller than 100 nm;

- LUVs: Large Unilamellar Vesicles. Liposomes composed by a single bilayer with a diameter ranging from 100 nm to 200 nm;
- GUVs: Giant Unilamellar Vesicles. Liposomes with a single bilayer of 1-100 μm;
- MLVs: MultiLamellar Vesicles. Liposomes composed by two or more concentric bilayer with a diameter up to 5000 nm.

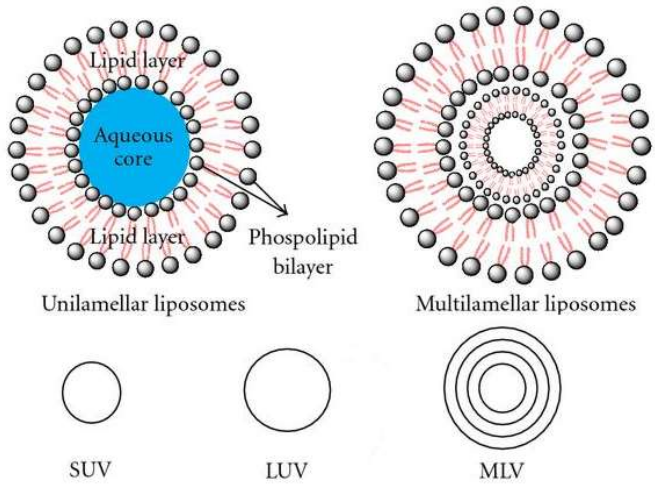

Fig. 2.24 The different kinds of liposomes.

The preparation of liposomes is a very easy procedure. Lipids are dissolved in organic solvent (usually a mixture of chloroform and methanol) and placed in a round-bottom flask. The organic solvent is then evaporated under a gentle nitrogen gas (to avoid lipid oxidation). During this procedure a thin lipid film is produced. The flask is placed under vacuum over night to remove the final traces of organic solvent. Finally, the dried lipid film is hydrated with water or buffer at the temperature above the T_m. During the hydration, lipid molecules spontaneously assembly forming liposomes (see section 2.5 for a description of forces involved in lipid self-assembly). What it is produced by this simple protocol are MLVs. Unfortunately, MLVs have some disadvantages. They are not uniform in size and are formed by concentric bilayers which render them not a perfect membrane model. For these reasons, various methodologies were developed to obtain liposomes uniform in size and with a single lipid bilayer.
Small unilamellar vesicles (SUVs) are produced by sonicating a suspension of MLVs with a tip sonicator. During this procedure multilamellar aggregates are broken. Lipids spontaneously re-assembly producing unilamellar vesicles of the smallest diameter (which depends on the lipid composition) [160].

Large unilamellar vesicles (LUVs) are produced again starting from MLVs. But in this case, the lipid suspension is forced to pass thorough a polycarbonate filter with a specific cut-off (usually 100 nm and 200 nm). This technique is named extrusion [163].
Finally, giant unilamellar vesicles (GUVs) are produced in a wide variety of procedures. The most common one is the electroformation method [164]. In this method a deposit of lipids on a metallic plaque is rehydrated and exposed to an AC electric field.
The choice of what kind of liposomes must be used depends on what we are looking for and the employed technique. For example, in differential scanning calorimetry measurements almost exclusively MLVs are used. This is because, MLVs ensure a better peak resolution compared to SUVs and LUVs. In confocal fluorescence microscopy, GUVs must be used. SUVs and LUVs are to small and cannot see in the microscope.

Chapter 3

Synthesis, Biological and Biophysical Studies of Unnatural Amino Acids Containing Peptides

3.1 Introduction

The final goal in studying AMPs is their utilization as drugs to fight infections caused by bacteria. To accomplish this issue, it is fundamental to develop a peptide with selective toxicity against bacteria, low toxicity towards mammalian cells and resistance to proteolysis to increase its half-life [92,165]. The design and synthesis on new AMPs could represent a way to overcome these problems. In this frame, the introduction of unnatural amino acids in the primary sequence of peptides represents a very good strategy rendering AMPs less prone to proteases action, enhancing their half-life in serum. Further, the physico-chemical properties of the unnatural amino acids can play an important role in determining the peptide selectivity. Usually, an optimization procedure is followed, where some residues are replaced by others in order to obtain a new selective and resistant peptide. In this context, the physico-chemical characterization of the new AMPs with model membranes can help in revealing the key factors which modulate the antibacterial activity and the cytotoxicity. The knowledge of the main factors involved in these aspects represent important information which can be used in the peptide optimization process.

Here, it is reported the design and synthesis of the P9Nal(SS) peptide, and two analogs, P9Trp(SS) and P9Nal(SR). Biological assays were performed in order to evaluate their antimicrobial activities on bacteria, cytotoxicity and resistance to proteolysis. Overall, these data show that the synthetic peptides have a broad spectrum of antibacterial activity and that the introduction of unnatural amino acids effectively increase their stability in serum. Moreover, low selectivity between bacterial and eukaryotic cells was observed. In order to explore the origin of the low selectivity, a detailed biophysical characterization of the interaction of P9Nal(SS) with liposomes mimicking eukaryotic and cytoplasmic bacterial membrane was also carried out. P9Nal(SS) was chosen, among the three peptides, as it possesses the broader spectrum of antibacterial activity, higher stability in serum but low selectivity.

The results of biophysical studies on P9Nal(SS) reveal that there is a divergence in the action mechanism against the two cell types. In fact, using DPPC/DPPG vesicles as a simplified model of the bacterial membrane, P9Nal(SS) peptide interact superficially inducing domains formation. Above a threshold concentration, it is able to penetrate in the hydrophobic core of the membrane disrupting the lipid packing.

On the contrary, for DPPC liposomes mimicking the eukaryotic membrane, only surface binding was observed. Thus, the action mechanism responsible for the antimicrobial activity could be different to that for the undesired cytotoxicity.
A further physico-chemical characterization of the interaction of P9Trp(SS) and P9Nal(SR) peptides with bacterial model membrane is reported in the chapter 4. A comparison among the results obtained for the three peptides revealed important differences in their membrane perturbation activities.

3.2 Peptides' Design

The three new synthetic peptides were designed in collaboration with Prof. E. Notomista of the Department of Biology of the University of Naples Federico II and synthetized in collaboration with the research group of Prof. A. Lombardi and F. Nastri of the Department of Chemical Sciences, University of Naples Federico II.
All of them contain cationic and hydrophobic residues. The sequence of the three peptides are:

1. P9Nal(SS): H-εAhx-Cys(S^{t}Bu)-Lys-(2Nal)$_2$-Lys-Lys-Cys(S^{t}Bu)-εAhx-NH$_2$;
2. P9Trp(SS): H-εAhx-Cys(S^{t}Bu)-Lys-(Trp)$_2$-Lys-Lys-Cys(S^{t}Bu)-εAhx-NH$_2$;
3. P9Nal(SR): H-εAhx-Cys(^{t}Bu)-Lys-(2Nal)$_2$-Lys-Lys-Cys(^{t}Bu)-εAhx-NH$_2$.

where εAhx is 6-aminohexanoic acid, Cys(S^{t}Bu) is a cysteine with a disulphide and a tert-butyl group, Cys(^{t}Bu) is a cysteine with a tert-butyl moiety, 2Nal is 2-naphthyl-L-alanine, Lys is a lysine and Trp is tryptophan residue. All the three peptides are composed by 9 residues and own a net positive charge of 4 at the physiological pH of 7.4. The molecular weights of the three peptides are 1405 g/mol, 1382 g/mol and 1340 g/mol for P9Nal(SS), P9Trp(SS) and P9Nal(SR), respectively. The chemical structures of the three peptides are reported in Fig. 3.1.

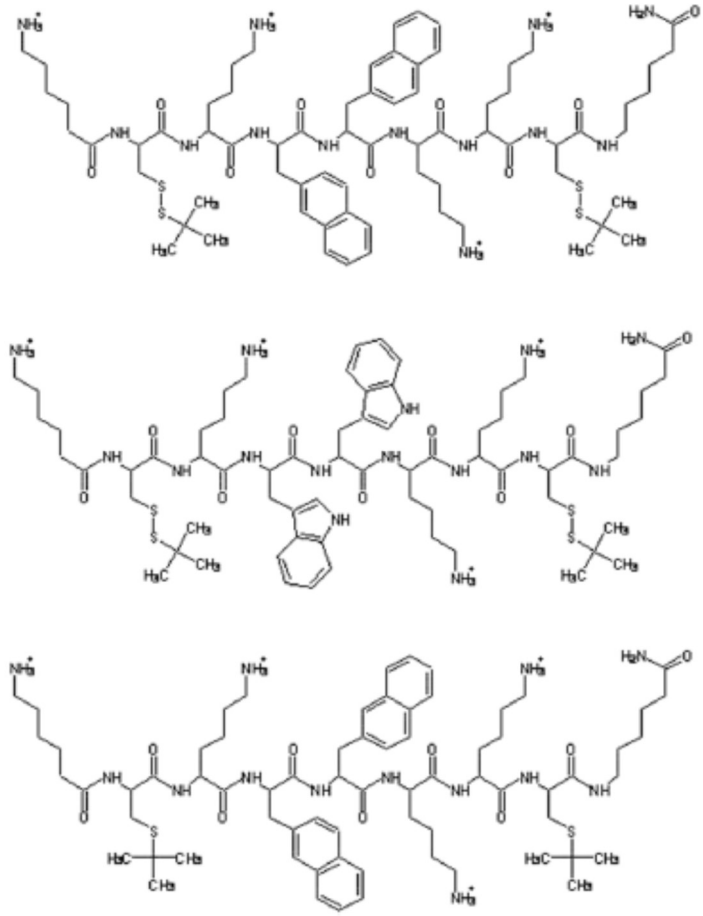

Fig. 3.1 The chemical structure of (top) P9Nal(SS) peptide, (middle) P9Trp(SS) and (bottom) P9Nal(SR) peptides. Taken from [93].

At both the C- and N- termini, εAhx residues were introduced to protect the peptides from the action of exopeptidases. Moreover, due to their hydrophobic tail, εAhx residues contribute to the overall hydrophobicity. The residue at the C-terminus is amidated. Instead, the amino group of the N-terminus of εAhx is not modified and provides an additional positive charge. Thus, the three Lys residues and the N-terminus εAhx account for the peptides' positive charge. The aromatic residues (2Nal and Trp) were introduced to modulate the hydrophobicity. They are in the middle of the primary sequences, close to each other in position 4 and 5. It was shown that the introduction of these residues increases the antibacterial activity of several peptide sequences [166,167]. Finally, modified Cys residues were introduced as it was shown [168]. that some AMPs increase their antimicrobial activity upon disulphide reduction. To explore the eventual role of disulphide reduction, Cys(S^{t}Bu) and Cys(^{t}Bu) residues were introduced in P9Nal(SS) and P9Nal(SR), respectively.

3.3 Materials and Methods

Materials. Fmoc protected amino acid and coupling reagents were purchased from NovaBiochem and used without further purification. H-PAL Chemmatrix resin was from Sigma Aldrich. Peptide synthesis and purification solvents were from Romil (Biopure grade). Piperidine and N,N'-diisopropyl ethylamine were from NovaBiochem. The fluorescent probe DPH (1,6-Diphenyl-1,3,5-hexatriene) and acrylamide solution (40% w/v) were purchased from Sigma Aldrich Chemical. The lipids 1,2-dipalmitoyl-*sn*-glycero-3-phosphocholine (DPPC), 1,2-dipalmitoyl-*sn*-glycero-3-phospho-1′-rac-glycerol (DPPG) and 1-palmitoyl-2-oleoyl-*sn*-glycero-3-phospho-1′-rac-glycerol (POPG) were purchased from Avanti Polar Lipids Inc. (Alabaster, AL, USA) and used without further purifications.
Deionized water was used for the phosphate buffer and all sample preparations.

Peptide Synthesis. Peptides were synthesized by standard Fastmoc protocols on an ABI 433 A automatic peptide synthesizer. Dry H-PAL Chemmatrix resin (0.31 mmol g^{-1} substitution) was weighed to get a 0.25 mmol scale, and manually swelled in N-Methyl-2-pyrrolidone (NMP). Double coupling steps were performed for the two bulky aromatic residues. After the final deprotection step, the resin was washed with 2-propanol and with methanol and then dried. Cleavage and deprotection was performed with 25 mL of a 95:2.5:2.5 trifluoroacetic acid (TFA): tri-isopropyl silane (TIS):H_2O solution. Cleavage reaction was performed for two hours, the first at 0 °C and the second at room temperature under gentle magnetic stirring. The exhaust resin was washed three times with fresh TFA and then discarded by filtration. The combined filtrates were concentrated in vacuo and the crude peptide precipitated with five volumes of diethyl ether. Crude peptide was washed three times with diethyl ether to remove the scavenged groups and then dried to get a 44% final yield.

Peptide Purification. Crude peptides were purified by preparative HPLC on a Shimadzu LC-8A system. A Vydac C18 column (22 mm × 250 mm; 10 μm) was used, eluted with a H_2O 0.1% TFA, (eluent A) and CH_3CN 0.1% TFA (eluent B) linear gradient at 22 mL min^{-1} flow rate. Fractions were separated according to their absorbance at 210 nm by an online UV detector (Shimadzu). Peptide fractions were then checked for their purity by analytical LCMS. Peptide identities were confirmed by LCMS analysis on a Shimadzu 20ADxr coupled with a Shimadzu ESI-IT-TOF mass detector (probe voltage 4.5 kV; probe temperature 25 °C; desolvation temperature 250 °C; detector voltage 1.5 kV). All analyses were performed with a Vydac C18 column (2.1 mm × 100 mm; 5 μm), eluted with a H_2O 0.05% TFA, (eluent A) and CH_3CN 0.05% TFA (eluent B) linear gradient, from 5% to 95% (solvent B), over 30 minutes, at 0.2 ml min−1 flow rate. Pure fractions were pooled

and lyophilized as TFA salts (purity >95%). Peptide samples for biological assays were further subjected to counter ion exchange on a DEAE-Sephadex weak acidic resin. Briefly, peptide solutions in water were loaded on a 0.5 mL syringe column, and then eluted by decreasing the pH with an acetate buffer at pH 4.3 to obtain the desired peptide acetate salt. Further, the relative hydrophobicities of P9 peptides were evaluated through their retention in reverse phase HPLC.

Biological Assays.

Antimicrobial activity assay (standard condition). The antimicrobial activity of the three designed peptides was tested against *Escherichia coli* (ATCC® 25922™), *Pseudomonas aeruginosa* (ATCC® 27853™), *Pseudomonas aeruginosa* PAO1 wild type strain, *Bacillus subtilis* subsp. *spizizenii* (ATCC® 6633™), *Staphylococcus aureus* (ATCC® 6538 P™) and *Staphylococcus aureus* MRSA (methicillin-resistant *Staphylococcus aureus*) WKZ-2 (kindly provided by collection of Prof. Edwin Veldhuizen, University of Utrecht, Holland). MIC assays were performed by broth microdilution method [169] using Nutrient Broth (Becton Dickinson Difco, Franklin Lakes, NJ) as bacterial growth medium. Recombinant (P)GKY20 peptide [170] was used as control antimicrobial peptide. MIC values were measured as the lowest concentration at which no visible growth was observed at the end of the incubation time. Experiments were performed three times for each peptide.

Antimicrobial activity of peptide pre-incubated in 10% serum. In addition to the antimicrobial activity assays, MIC values of the three designed peptides were determined against *Escherichia coli* ATCC 25922, also upon peptides incubation in 10% serum (fetal bovine serum, Microgem Lab, Cat. S1860, Italy) for 1 hour or 16 hours at 37 °C (water bath). Following the incubation time, MIC assays were carried out as previously described. Recombinant peptides (P)GKY20 and ApoE(133–150) and synthetic peptide Ac-ApoE(133–150)-NH_2 with acetylated N-terminus and amidated C-terminus [170,171] were treated as the three designed peptides and used as control antimicrobial peptides. Experiments were performed five times for each peptide.

Cytotoxicity Assay. Cytotoxic effects of the three peptides on human epithelial colorectal adenocarcinoma cells (CaCo-2) and on aneuploid immortal keratinocyte cells line from adult human skin (HaCaT) were assessed by performing the (3-(4,5-dimethylthiazol-2-yl)-2,5-diphenyltetrazolium bromide (MTT) reduction inhibition assay [172]. Both human cell lines were obtained from the American Type Culture Collection (ATCC, Manassas, VA, USA) and grown at 37 °C in a humidified incubator containing 5% CO_2 in Dulbecco's modified Eagle's medium (DMEM) supplemented with 10% fetal bovine serum, 4 mM glutamine, 400 units/mL

penicillin, and 0.1 mg mL^{-1} streptomycin. Cells were plated on 96-well plates at a density of 5 × 103 per well in 100 µL of medium and incubated at 37 °C with 5% CO_2. Medium was then replaced with 100 µl of fresh media containing peptide solution to a final concentration ranging from 0.1–10 µM/well. After a time of incubation ranging from 18 to 48 hours at 37 °C, the peptide-containing medium was removed, and 10 µL of a 5 mg mL^{-1} MTT stock solution in DMEM without red phenol, corresponding to a final concentration of 0.5 mg L^{-1} in DMEM (final volume of 100 µL), was added to the cells. After 4 h of incubation, the MTT solution was removed and the MTT formazan salts were dissolved in 100 µL of 0.1 N HCl in anhydrous isopropanol. Cell survival was reported as the relative absorbance, with respect to control, of blue formazan measured at 570 nm with a Synergy Multi Plate Reader. Cytotoxicity experiments were performed at least three times independently. Standard deviations were always <10% for each experiment.

Liposome Preparation. Lipids were weighted in a glass vial and dissolved in a chloroform/methanol mixture (2/1 v/v). A thin film was produced by evaporating the organic solvent by gentle dry nitrogen gas. The sample was placed in a vacuum for at least 3 h. The dried lipids were then hydrated, in the liquid-crystalline phase at the temperature of 50 °C, with an appropriate amount of 20 mM phosphate buffer pH 7.4, and vigorously vortexed obtaining a suspension of multilamellar vesicles (MLVs). Small unilamellar vesicles (SUVs) were obtained using a Sonics VCX130 tip sonicator until the suspension became transparent (about 20 min, at room temperature). Dynamic light scattering (DLS) measurements were used to check the size of lipid vesicles after sonication. The obtained average of the hydrodynamic radii of SUVs (~90 nm) are consistent with the formation of unilamellar vesicles. SUVs containing the fluorescent probe DPH (1,6-Diphenyl- 1,3,5-hexatriene) were obtained by adding to the lipids dissolved in the organic mixture a definite amount of a solution of DPH in chloroform at the lipids/DPH mole ratio of 200. Liposomes with different composition were prepared: i) DPPC, as a model of eukaryotic membrane; ii) DPPC/DPPG (8/2 mol/mol) and DPPC/POPG (8/2 mol/mol) as simplified models of bacterial membrane. Samples of liposomes in the presence of peptide were prepared by mixing appropriate volumes of peptide in solution and liposomes suspension to get the desired lipid-to- peptide (L/P) ratio.

Circular Dichroism (CD). CD spectra of P9Nal(SS) were recorded by using a JASCO J-715 spectropolarimeter, from Jasco Corporation (Tokyo, Japan), in a 0.1 cm path length quartz cuvette as an average of 3 scans. In order to obtain CD spectra with the highest signal-to-noise ratio, the following instrument parameters were set as suggested in [173]: scan speed of 20 nm/min, 4 s response time and 2 nm bandwidth. The temperature was set to 25 °C. Peptide samples were prepared in 20

mM phosphate buffer pH 7.4 at the concentration of 35 μM in absence and in the presence of SUVs at total lipid concentration of 0.35 mM, 1.75 mM and 3.5 mM. For each sample, a background blank (buffer or lipid suspension alone) was subtracted.

Differential Scanning Calorimetry (DSC). DSC measurements were performed using a nano-DSC from TA Instruments (New Castle, DE, USA). MLVs were used for all DSC experiments since they provide the better resolution of the peak [174]. A volume of 300 μL of 0.5 mM vesicles suspension (DPPC, DPPC/DPPG or DPPC/POPG) in the absence or in the presence of peptide was placed in the calorimetry vessel, and successive heating and cooling scans were performed at 1 °C/min over the temperature range of 20–55 °C. The excess heat capacity function (<ΔCp>) was obtained after baseline subtraction. A buffer-buffer scan was subtracted from the sample scan. The samples composed by lipid suspension and peptide were prepared before the DSC experiments, by adding the appropriate amount of peptide to the lipid suspension and waiting at least 30 min to ensure that the equilibrium has been reached. The results presented here all refer to the second heating scan. The obtained data were analyzed by means of NanoAnalyze software supplied with the instrument and plotted using the Origin software package (OriginLab, Northampton, MA, USA).

Steady-state Fluorescence. All the fluorescence experiments were performed using a Fluoromax-4 spectrofluorometer (Horiba, Edison, NJ, USA) operating in the steady-state mode at the temperature of 25 °C.

Fluorescence anisotropy. Fluorescence anisotropy measurements were carried out for the probe DPH embedded into SUVs at total lipid concentration of 150 μM. The excitation wavelength was set to 355 nm and the emission was monitored at 427 nm. The slits were set to 4 nm for both the excitation and emission monochromators. The experiments were performed using a 1 cm path length quartz cuvette. Fluorescence anisotropies (r) were determined according to the equation:

$$r = \frac{I_{VV} - GI_{VH}}{I_{VV} + 2GI_{VH}}$$

where I_{VV} is the fluorescence intensity obtained by setting both the excitation and emission polarizers vertically, I_{VH} is the fluorescence intensity obtained by setting the excitation polarizer vertically and the emission polarizer horizontally and G is the instrument-specific correction factor, which accounts for the difference in the

polarizers transmission efficiency of vertically and horizontally polarized light [175,176].

Fluorescence Resonance Energy Transfer (FRET). In the FRET experiments, the P9Nal(SS) peptide in solution was excited in the presence of SUVs labeled with DPH. The excitation wavelength was set to 277 nm and emission spectra were recorded in the range 300–510 nm, using a 1 cm path length quartz cuvette. The slits for the excitation and emission monochromators were set to 3 nm and 6 nm, respectively. As references the spectra of peptide in buffer or in the presence of vesicles without DPH were also collected. From each sample, a blank (vesicles in the absence of the peptide or buffer solution) measurement was subtracted. The concentration of peptide was fixed at 5 μM and spectra at L/P ratio of 50 were recorded.

Fluorescence quenching. For fluorescence quenching experiments, a 7 μM solution of peptide, in the absence or in the presence of SUVs at lipid-to-peptide mole ratio (L/P) of 100, was placed in a quartz cuvette with a path length of 1 cm and titrated with acrylamide solution (40% w/v). The titrations were performed at fixed peptide concentration in the absence and presence of acrylamide concentrations up to ~50 mM. The excitation wavelength was set to 277 nm, and the emission spectra were collected from 290 nm to 500 nm. The obtained data were analyzed using the Stern-Volmer equation [175,176]:

$$\frac{F_0}{F} = 1 + K_{SV}[Q]$$

where F_0 is the fluorescence intensity in the absence of the quencher, F is the fluorescence intensity at each step of titration in the presence of the quencher, [Q] is the concentration of acrylamide. Due to acrylamide absorption at the excitation wavelength, the fluorescence intensities were corrected using the formula $F_{obs} = F_{corr} \cdot 10^{\frac{-Aex \cdot d}{2}}$ where F_{obs} is the observed intensity, F_{corr} is the corrected intensity, A_{ex} is the absorbance of acrylamide at the excitation wavelength and d is the cuvette path length [177].

3.4 Results: Biological Study

In order to verify the antimicrobial activity, serum stability and toxicity towards eukaryotic cells of the three synthetic peptides, biological assays were performed. These experiments were carried out in collaboration with the research groups of Prof.

E. Notomista and Prof. E. Pizzo of the Department of Biology at the University of Naples Federico II.

3.4.1 Evaluation of Antimicrobial Activity, Serum Stability and Cytotoxicity

The antimicrobial activities were evaluated by determining the MIC values (minimum inhibitory concentration, a microbiological parameter that indicate the minimum peptide concentration at which bacterial growth is inhibited) against gram-negative and gram-positive bacterial strains and are collected in Table 1.

Table 1 The antibacterial activity of the three peptides against gram-negative and -positive bacteria. The activities are expressed as minimum inhibitory concentration (MIC, in μM).

Peptide	**Gram-negative**			**Gram-positive**		
	E. coli ATCC25922	*P. aeruginosa* ATCC27853	PAO1 Wt	*B. spizizenii* ATCC6633	*S. aureus* MRSA	*S. aureus* ATCC6358P
(P)GKY20	10	20	20	20	80	5
P9Nal(SS)	10	2.5	10	10	20	10
P9Trp(SS)	10	2.5	10	40	40	20
P9Nal(SR)	10	1.25	10	40	40	40

As control, (P)GKY20 peptide, derived from the C-terminal region of human thrombin was used [178]. This peptide is composed only by natural amino acids and the termini are not protected. As demonstrated in Table 1, the three peptides are active against both kinds of bacteria, showing activities similar to those of the control peptide. The MIC values are in the range 1.25-10 μM for gram-negative bacteria, instead are in the range of 10-40 μM for gram-positive bacteria. Thus, the peptides are a little bit more effective against gram-negative bacteria. Among the three peptides, P9Nal(SS) has a broader spectrum of activity. In fact, for gram-positive bacteria, its MIC values are lower compared to those obtained for P9Trp(SS) and P9Nal(SR).
In P9Nal(SS) and P9Nal(SR), the residues Cys(S^{t}Bu) and Cys(^{t}Bu) were introduced, respectively, in order to explore the eventual role of disulphide reduction [168]. Since the two peptides exhibit the same activity against gram-negative bacteria, it seems that the disulphide reduction process does not play a significant role in determining their antimicrobial activity.
In Table 2 are reported the MIC values obtained for peptides pre-incubated in 10% fetal bovine serum (FBS) for 1 hour or 16 hours against *Escherichia coli* ATCC 25922.

Table 2 The antibacterial activity of the three peptides against *Escherichia coli* ATCC 25922 after pre-incubation in 10% serum for 1 hour and 16 hours. The activities are expressed as minimum inhibitory concentration (MIC, in μM).

Peptide	**No P.I.[a]**	**1h P.I.[a]**	**16h P.I.[a]**	**Fold Change (1h)[b]**	**Fold Change (16h)[c]**
(P)GKY20	10	10	>80	1	>8
ApoE(133-150)	5	>80	>80	>16	>16
Ac-ApoE(133-150)-NH_2	5	20	>80	4	>16
P9Nal(SS)	10	10	40	1	4
P9Trp(SS)	10	10	80	1	8
P9Nal(SR)	10	10	>80	1	>8

[a] P.I. = pre-incubation; [b,c] the fold change is the ratio between the MIC value obtained after pre-incubation for 1 hour (or 16 hours) and the MIC value for the not incubated peptide.

As control, (P)GKY20 and ApoE(133-150) with free termini were used. In addition a version of ApoE(133-150), named Ac-ApoE(133-150)-NH_2, with acetylated N-terminus and amidated C-terminus was employed. ApoE(133-150) is a natural-containing amino acids peptide derived from the receptor binding region of the human apolipoprotein E. The data reported in Table 2 indicated that the three synthetic peptide and (P)GKY20 did not change their potency after 1-hour incubation in 10% serum, i.e. no change in MICs. On the contrary, the unprotected termini ApoE peptide completely lost its antimicrobial activity (MIC > 80 μM) and the Ac-ApoE(133-150)-NH_2 showed a fourfold increase in its MIC value. After 16 hours of incubation in 10% serum, all the control peptides and P9Nal(SR) lost their antimicrobial activities. On the other hand, P9Nal(SS) and P9Trp(SS) showed a fourfold and eightfold increase in their MIC values, respectively. These important results revealed that the contemporary presence of 2Nal and Cys(S^tBu) contribute to the resistance to proteases present in the serum.

In Fig. 3.2 are summarized the results obtained for the evaluation of toxicity of the three peptides towards two eukaryotic cell lines: human epithelial colorectal adenocarcinoma cells (CaCo-2) and aneuploid immortal keratinocyte cells (HaCaT). The experiments were performed by increasing peptides concentration from 0.1 μM to 10 μM and at four different times: 18,24,36 and 48 hours.

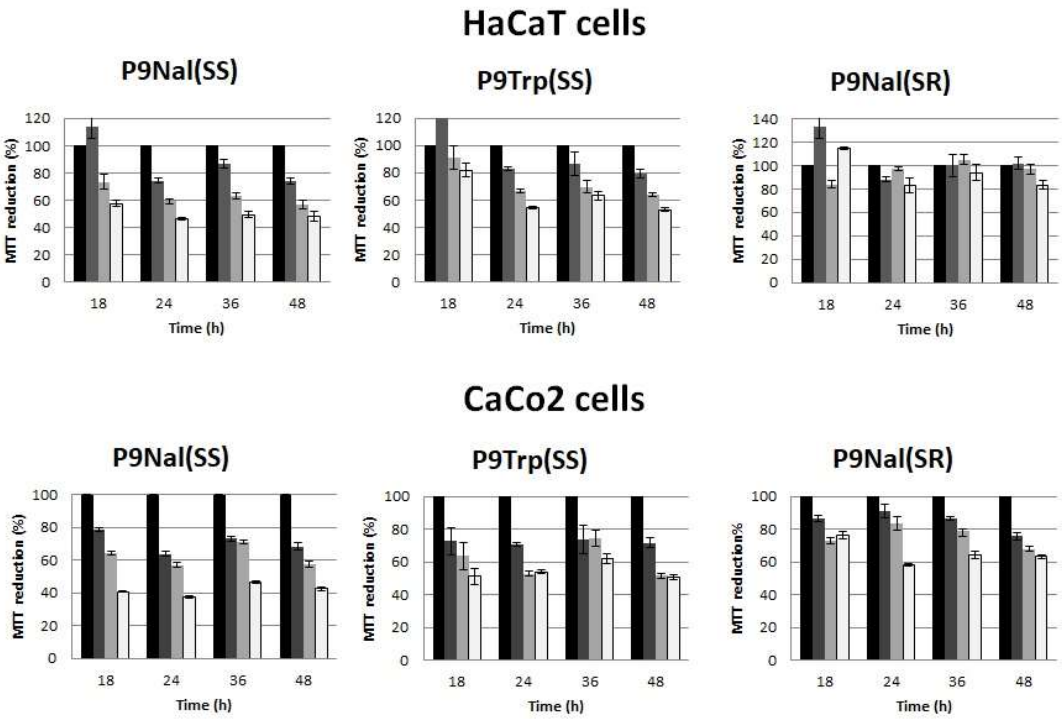

Fig. 3.2 Toxicity MTT assay for the three synthetic peptides on HaCaT and CaCo-2 cells. Color legend: black = control, dark grey = 0.1 μM peptide, grey = 1 μM peptide, white = 10 μM peptide.

The obtained results showed that both P9Nal(SS) and P9Trp(SS) have an effect on both cell lines and that this effect is dose-dependent. In fact, by increasing their concentration a higher cell mortality was observed. Moreover, it seems that P9Nal(SS) is slightly more toxic than P9Trp(SS). In contrast, P9Nal(SR) has no toxic effects on HaCaT cells at low doses (0.1 and 1 μM). On the contrary, its effect is slightly higher on CaCo-2 cells at the same doses. Its effect on CaCo-2 further increases at 10 μM.

As described in the section 1.2, several factors modulate the AMPs biological activity. One of these parameters is represented by hydrophobicity [12]. Thus, the relative hydrophobicities of the three peptides were evaluated through their retention in reverse phase HPLC (Fig. 3.3)

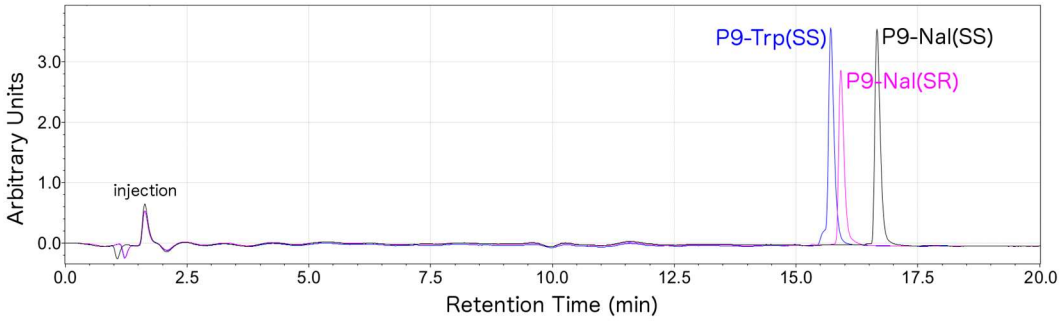

Fig. 3.3 Analytical RP-HPLC chromatograms collected at 280 nm upon injections of P9-Nal(SS) (black line), P9-Nal(SR) (pink line) and P9-Trp(SS) (blue line).

As evidenced in Fig. 3.3, among the three peptides, P9Nal(SS) is the most hydrophobic. P9Nal(SR) seems a little bit more hydrophobic than P9Trp(SS). However, they have comparable hydrophobicities. These results well correlate with the observed higher cytotoxicity (section 1.2) and higher activity of P9Nal(SS) against gram-positive bacteria. In fact, it was demonstrated that an increase of hydrophobicity increases the activity against gram-positive bacteria but has only limited effect against gram-negative bacteria [179].

3.5 Results: Biophysical Study of the Interaction of the P9Nal(SS) Peptide with Model Membranes

In order to clarify the action mechanism underlying the antimicrobial and cytotoxic activity of P9Nal(SS), a physico-chemical characterization of the interaction of this peptide with model membranes mimicking eukaryotic and bacterial membranes was carried out. Particularly, DPPC and DPPC/DPPG (8/2 mol/mol) vesicles were used as simplified models of eukaryotic and bacterial cytoplasmic membrane, respectively. P9Nal(SS) was chosen, among the three peptides, as it possesses the broader spectrum of antibacterial activity, higher stability in serum and it's toxic to both eukaryotic cell lines. A further physico-chemical characterization of the interaction of the other two peptides (P9Trp(SS) and P9Nal(SS) peptides) with bacterial model membrane is reported in chapter 4.

3.5.1 The Conformation of P9Nal(SS) Peptide

Circular dichroism (CD) spectroscopy is a powerful technique that can give information about the secondary structure of peptide and proteins [173]. Thus, CD spectroscopy in the far-UV region of the spectrum was employed to characterize the conformational behavior of P9Nal(SS). In Fig. 3.4 are reported the CD spectra of

peptide in solution and in the presence of small unilamellar vesicles (SUVs) of DPPC and DPPC/DPPG at L/P of 10, 50 and 100.

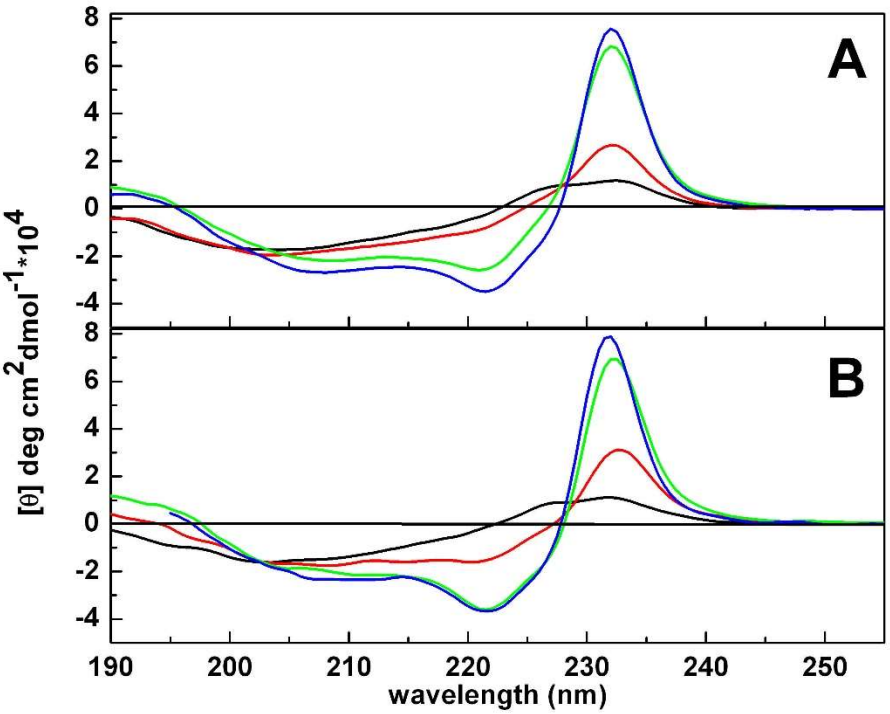

Fig. 3.4 CD spectra of P9Nal(SS) in 20 mM phosphate buffer, pH 7.4 (black line) and in the presence of (A) DPPC and (B) DPPC/DPPG small unilamellar vesicles at L/P of 10 (red), 50 (green) and 100 (blue).

In solution, the spectrum of peptide is characterized by the presence of a positive band at about 230 nm and a negative band at about 203 nm, indicating that P9Nal(SS) adopts a random structure. In the presence of SUVs, both DPPC and DPPC/DPPG, P9Nal(SS) changes significantly its conformation, demonstrating that the peptide can bind to both model membranes. In fact, it was observed an intensity increase of the positive band around 230 nm coupled with the appearance of two minima at about 222 nm and 207 nm. Moreover, at L/P 50 and 100 a positive band at about 190 nm also appears. These observations suggest that the peptide approaches a helix-like conformation in the presence of both model membranes.

It is known that in the region 220-240 nm, aromatic residues contribute to the recorded spectrum [180,181]. Thus, the positive band is probably due to contribution of aromatic residues (2Nal) in the primary sequence. This is confirmed by the comparison of CD spectra of P9Nal(SS) to those of P9Trp(SS) and P9Nal(SR) (Fig. 3.5). In fact, the positive band is present in 2Nal containing peptides and it is absent in the spectrum of P9Trp(SS).

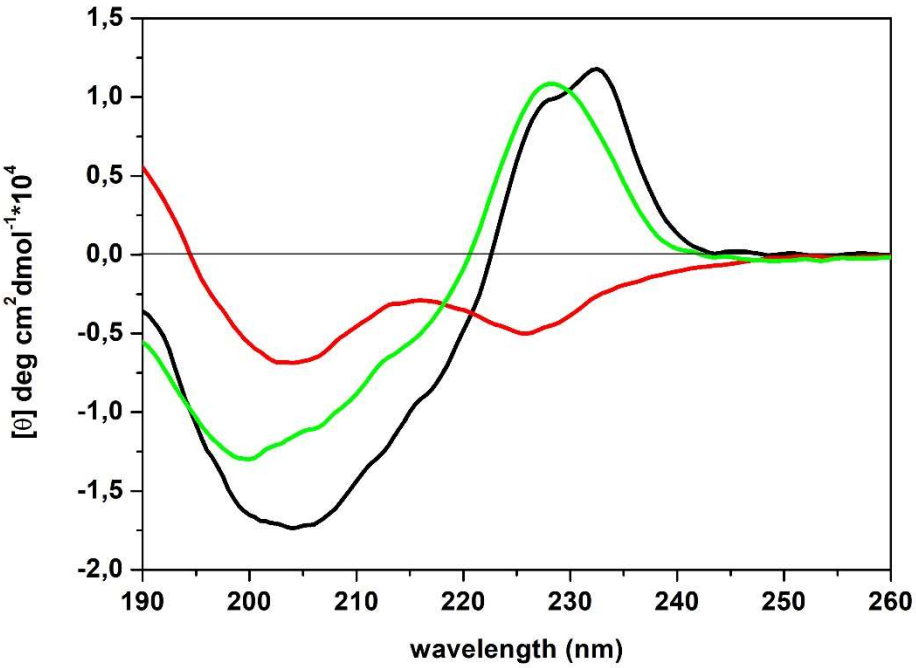

Fig. 3.5 The CD spectra of (black line) P9Nal(SS), (red line) P9Trp(SS) and (green line) P9Nal(SR) in 20 mM phosphate buffer, pH 7.4. The temperature was set to 25 °C.

The positive band at 230 nm and its increase in the presence of lipid vesicles could be attributed to the exciton effect. Since the 2Nal residues are very close to each other (position 4 and 5), an interaction between their excited states contribute to the observed spectrum [182,183]. Upon binding to lipid vesicles, the interaction between 2Nal residues is stronger than in the absence of liposomes, which account for the observed intensity increase of the positive band. This effect leads to the splitting of the excited state in two components opposite in signs. In this case, a positive band at 230 nm and a negative one at around 220 nm (positive couplet) was observed. Thus, upon the interaction with lipid vesicles, the peptide adopts a helical conformation where the negative band, typical of the α-helix at around 222 nm sums to negative band due to positive couplet. The result is that the minimum at around 220 nm is more intense than the minimum at 207 nm.

3.5.2 The Effect of P9Nal(SS) on Bilayer Stability

Since many AMPs carry out their activity through a destabilization of the lipid bilayer, differential scanning calorimetry (DSC) measurements on DPPC and

DPPC/DPPG multilamellar vesicles were performed. The DSC thermograms of DPPC and DPPC/DPPG (Fig. 3.6) vesicles in absence of peptide are very similar and characterized by two well defined transition [151,184]. The first one is the transition from the lamellar gel phase to rippled gel phase which occurs at about 36 °C. It is named pre-transition and it is due to a rearrangement of polar head groups. The second one is a transition from the rippled gel phase to liquid phase at about 42 °C. It is named main transition and it is due to the melting of hydrocarbon chains of lipids. Thus, DSC offers the opportunity to investigate the thermotropic properties of two distinct regions of lipid bilayer (surface and hydrophobic core) and the effect of peptide on them. In Fig. 3.6 are reported the DSC curves of DPPC and DPPC/DPPG vesicles on increasing peptide concentration.

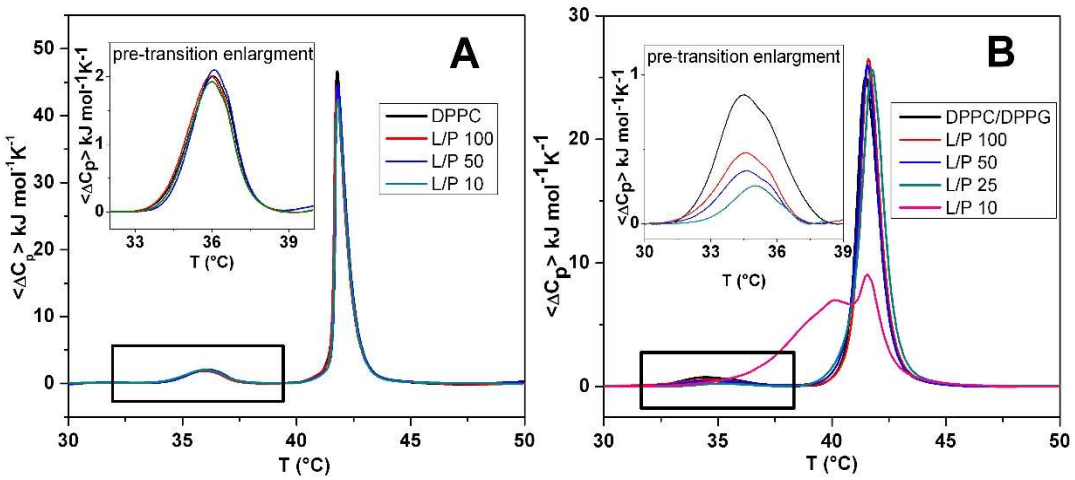

Fig. 3.6 The DSC thermograms of (A) DPPC and (B) DPPC/DPPG MLVs at the reported lipid-to-peptide (L/P) ratio. The inserts show an enlargement of the pretransition peaks.

As Fig. 3.6(A) shows, P9Nal(SS) has a very small effect on the thermotropic properties of DPPC liposomes suggesting that the peptide interacts with the DPPC bilayer only at the surface level and does not perturb significantly the lipid organization in the membrane. On the contrary, the peptide shows a strong effect on DPPC/DPPG liposomes, as indicated by modifications of both pre-transition and main transition peaks reported in Fig. 3.6(B). In particular, the peptide is able to modify the pre-transition peak even at low concentration (high L/P). By increasing peptide concentration, the enthalpy change for the pre-transition decreases and the peak is shifted at higher temperature. For the main transition, a different result was obtained. The peptide doesn't affect this transition until L/P = 50, at L/P = 25 a slight a modification of the peak was observed and at L/P = 10 a drastic change occurred. These observations suggest that the P9Nal(SS) activity on DPPC/DPPG liposomes

depends on its concentration. In fact, at low peptide concentration, the interaction takes place at the membrane surface, as demonstrated by the perturbation of pre-transition only. At high peptide concentration, the peptide penetrates inside the hydrophobic core disrupting the regular packing of lipid acyl chains (as demonstrated by the dramatic change in the main transition). At L/P = 10, the peptide is able also to perturb the lipid distribution inducing the formation of domains with different lipid compositions. This is well demonstrated by the multicomponent DSC thermogram [185] obtained at this lipid-to-peptide ratio (see section 3.5.3).

To get further insight into the effect of peptide on the stability of lipid bilayer, fluorescence anisotropy measurements were performed on vesicles labeled with diphenylhexatriene (DPH) [186,187]. DPH is a very poor-soluble water fluorescent molecule that preferentially partitioning inside the hydrophobic core of lipid bilayer [175]. Measuring its anisotropy values can give information about the micro-viscosity of the membrane (that in turn, depends on lipid acyl chains packing) and the effect of the peptide on it. In Fig. 3.7 the anisotropy values (r) of DPH embedded in DPPC and DPPC/DPPG SUVs are reported as function of peptide concentration. For DPPC liposomes, the anisotropy values do not change upon addition of peptide, even at high concentration. These results suggest that no penetration in the hydrophobic core occurs, in good agreement with DSC results. For DPPC/DPPG vesicles, the anisotropy remains roughly constant up to L/P = 50 and decreases by increasing peptide concentration (L/P < 50). These results support the idea that P9Nal(SS) is able to penetrate inside the membrane perturbing the lipid acyl chains packing in a concentration-dependent fashion.

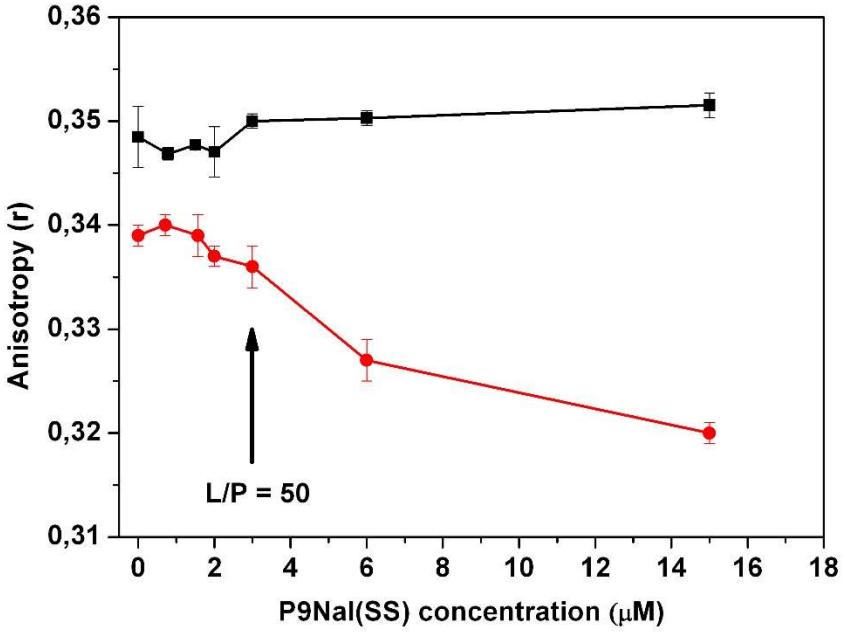

Fig. 3.7 Fluorescence anisotropy for DPH embedded in DPPC (black squares) and DPPC/DPPG (red circles) unilamellar vesicles as a function of P9Nal(SS) concentration. The experiments were carried out in 20 mM phosphate buffer, pH 7.4 at the temperature of 25 °C.

3.5.3 P9Nal(SS) Induces the Formation of Lipid Domains

As stated in the previous section, the DSC thermogram of DPPC/DPPG vesicles at L/P = 10 is composed by a multicomponent peak which indicates a possible formation of domains promoted by the peptide. Most likely, the domain formation is triggered by the preferential interaction of positively charged peptide with the anionic (DPPG) component of the membrane. However, this preferential interaction cannot unambiguously proved by using DPPC/DPPG mixture. This is because, bilayer composed by pure DPPC and pure DPPG have similar transition temperatures [153]. Consequentially, to verify the domains formation hypothesis, a strategy which involves the utilization of two lipids with very different melting temperatures was followed [188]. Thus, the DSC experiment was repeated by replacing DPPG with POPG producing model membrane composed by DPPC/POPG (8/2 mol/mol). This replacement has several advantages: i) at the mole fraction used, the two lipids are completely miscible [189]; ii) the melting temperature of pure POPG vesicles is below 0 °C and, thus, it can affect the observed phase transition of DPPC indirectly, by changing its local distribution. If the added peptide preferentially interacts with the low-melting component of the membrane (POPG),

it will promote its segregation leaving the rest of the membrane enriched in the high-melting component (DPPC), which melts at higher temperature. The DSC thermogram of DPPC/POPG multilamellar vesicles has the gel-to-liquid phase transition temperature centered at about 35.9 °C (Fig. 3.8). Upon the addition of P9Nal(SS) at L/P = 50, the DSC peak appears sharper than in the absence of the peptide (i.e. the transition is more cooperative) and the transition temperature shifts to higher values (at about 36.5 °C). This result strongly suggests that the peptide preferentially interacts with POPG molecules inducing a lipid segregation that leads to the formation of a more DPPC-rich domain, which melts at higher temperature.

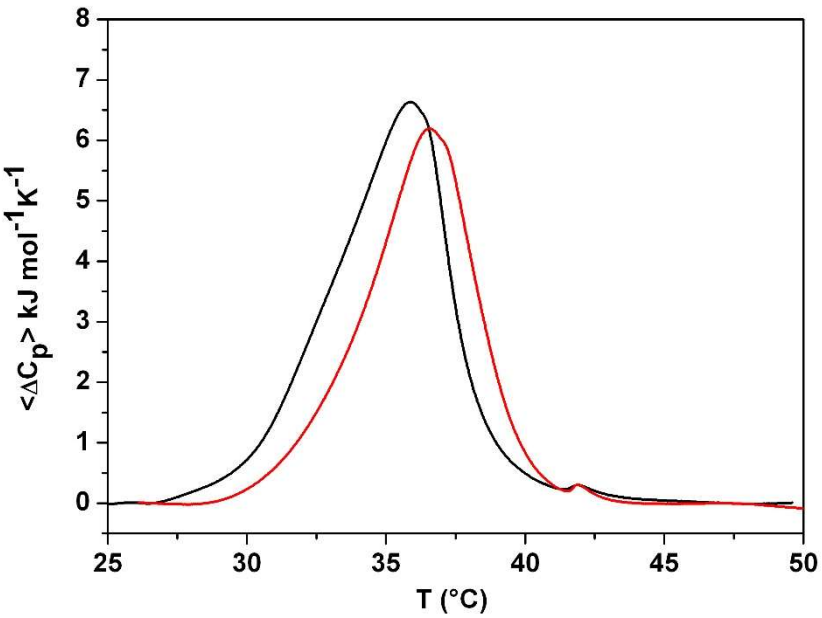

Fig. 3.8 The DSC thermogram of DPPC/POPG vesicles in the absence (black line) and in the presence of P9Nal(SS) (red line) at L/P = 50.

3.5.4 P9Nal(SS) Inserts in the Hydrophobic Core of Bacterial-like Membranes but not in the Eukaryotic Model Membranes

The fluorescence emission spectrum of P9Nal(SS) peptide, due to the two aromatic 2-naphthyl-L-alanine residues, is superimposable to the absorption spectrum of DPH in the liposomes. Thus, peptide and DPH can act as donor-acceptor pair in a fluorescence resonance energy transfer (FRET) experiment and they can be used to further characterize the peptide-lipid interaction process [187]. FRET experiment was carried out by exciting the peptide at λ_{ex} = 277 nm and recording the fluorescence

emission up to 510 nm, including the region of emission of DPH probe. In Fig. 3.9 are reported the emission spectra of peptide and DPH embedded in DPPC and DPPC/DPPG vesicles, at the lipid-to-peptide ratio of 50. As a reference, the emission spectra of peptide in buffer and in the presence of vesicles without DPH have been reported.

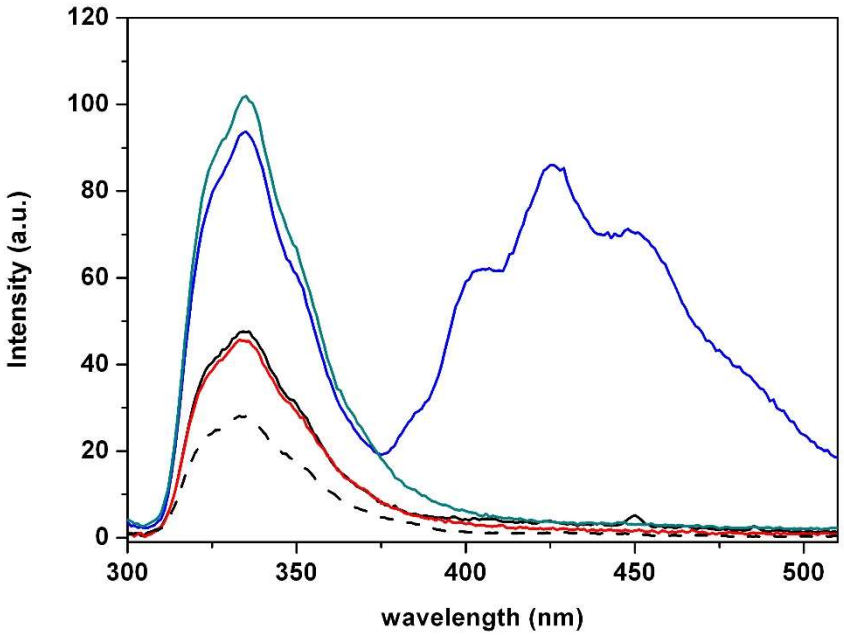

Fig. 3.9 Fluorescence emission spectra of P9Nal(SS) and DPH embedded in DPPC (black line) and DPPC/DPPG (blue line) SUVs at L/P = 50. As references, the emission spectra of the peptide in buffer (black dashed line) and in the presence of DPPC (red line) and DPPC/DPPG (green line) without DPH are also reported.

The fluorescence emission spectrum of P9Nal(SS) peptide has a maximum centered at about 337 nm. Upon the addition of lipid vesicles without DPH, the fluorescence intensity increases, confirming that the peptide is able to interact with both the membranes. The fluorescence increase observed in the presence of DPPC/DPPG is about twofold higher respect to the increase observed with DPPC vesicles. Finally, the shift of the λ_{max} observed for many fluorophores (e.g. Trp) going from to polar to a more apolar environment was not detected for 2Nal. This is because, being a apolar probe, its spectrum is insensitive to the environment polarity. Surprisingly, when DPH was added to lipid vesicles, FRET emission in the range 400-510 nm, coupled with a decrease of emission from the peptide, was observed only for DPPC/DPPG liposomes. These results can be rationalize considering the factors affecting FRET [175]. Briefly, the occurrence of FRET between a donor (D) and an

acceptor (A) depends on three parameters: i) the overlap integral, J(λ), i.e. superposition of the emission spectrum of D and absorption spectrum of A; ii) distance (d) between D and A and iii) the relative orientation (κ^2) between them. For the two lipid systems, factors i) and ii) should be very similar. Thus, the observed difference could be mainly attributed to the relative orientation between peptide fluorophores and DPH. For DPPC, the lack of FRET suggests that the orientation factor approaches zero, indicating that the 2Nal residues are perpendicular to DPH. This view is consistent with a binding of the peptide on the membrane surface, resulting in the 2Nal residues parallel to the vesicles surface. For DPPC/DPPG, the orientation factor is not zero. This result is consistent for a peptide insertion into the bilayer where the 2Nal residues assume an orientation not perpendicular to the DPH molecules.

To get further insight on the degree of insertion of peptide inside the lipid bilayer, fluorescence quenching experiment were performed. Fluorescence emission spectra of peptide in buffer or in the presence of DPPC or DPPC/DPPG at L/P = 100 were recorded at different acrylamide concentrations. According to the equation reported in "Fluorescence quenching" section, a plot of F_0/F versus acrylamide concentration gives a straight line whose slope is the Stern-Volmer constant, indicated as K_{SV}. The value of K_{SV} is an index of the degree of exposure to the aqueous solvent of the two fluorophores in the primary sequence of the peptide [175,190]. A more exposed residue will be more quenched respect to a less exposed one. In the first case, the value of K_{SV} will be greater than the value obtained in the second case. The Stern-Volmer plots obtained from the acrylamide quenching of P9Nal(SS) peptide in buffer or in the presence of lipid vesicles are reported in Fig. 3.10.

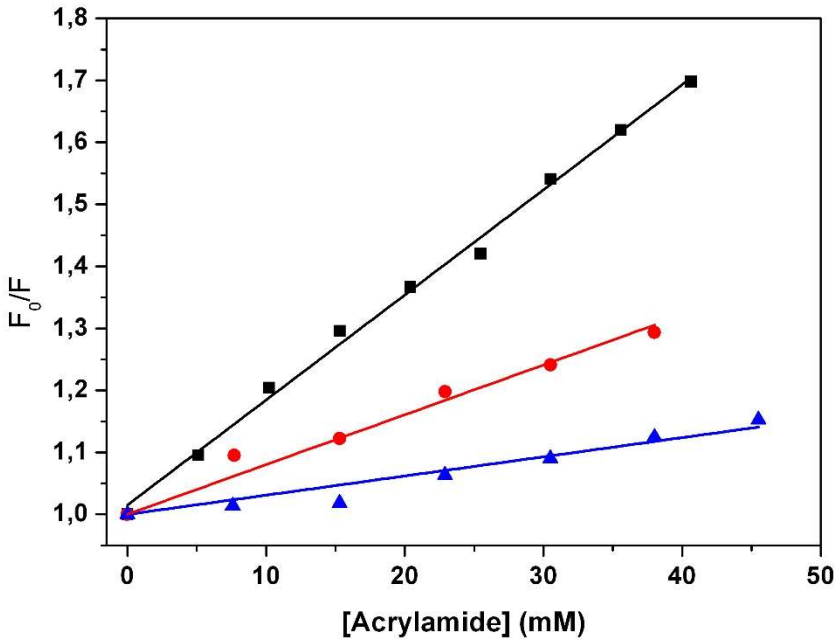

Fig. 3.10 Stern-Volmer plots for acrylamide-induced fluorescence quenching of a solution of P9Nal(SS) peptide in buffer (black squares), in the presence of SUVs at L/P = 100 composed by DPPC (red circles) and DPPC/DPPG (blue triangles). The experiments were carried out in 20 mM phosphate buffer, pH 7.4 at the temperature of 25 °C.

For the peptide in buffer, it was obtained the highest value of K_{SV} (16.9±0.4 M^{-1}). This is because of the complete exposure of 2Nal residues to the aqueous solvent. In the presence of DPPC liposomes, a value of K_{SV} of 8.0±0.5 M^{-1} was obtained. This result suggests that a reduced exposure to the solvent occurred upon interaction with the membrane. Finally, in the presence of DPPC/DPPG liposomes, a further decrease of K_{SV} was observed (3.1±0.4 M^{-1}) suggesting that the peptide is inserted inside the membrane. These results are in good agreement with the FRET data, and support the idea of different action mechanisms of P9Nal(SS) with the two model membranes.

3.6 Discussion

Antimicrobial peptides are a class of peptide-based antibiotics. They are promising candidates as drugs of the future that can face the problem of antibiotic resistance in bacteria [191]. In order to obtain antimicrobial sequences suitable for medical applications, it's mandatory to develop peptides with a selective toxicity and resistance to proteolysis [165]. In fact, AMPs applications are seriously limited by their sensitivity to proteases which leads to a reduced peptides' half-life [92]. Several

strategies can be followed, as protecting the N- and C- termini or introducing D- and unnatural amino acids [179,192]. The three peptides, here reported, were designed in order to mimic the antibacterial activity of natural AMPs. Unnatural amino acids in the primary sequence were introduced to increase peptides stability towards proteases. In this way, pharmacologically improved drugs with increased activity and half-life can be obtained.

The performed biological assays clearly showed that the synthetic peptides are more stable respect to the control peptides, which contain natural amino acids. Among the three P9 peptides, P9Nal(SR) lost completely its activity after 16 hours of incubation in serum. On the other hand, after 16 hours of incubation in serum, P9Nal(SS) and P9Trp(SS) were still active, with a MIC values of 40μM and 80 μM, respectively. These results suggest that the combination of 2Nal and Cys(S^{t}Bu) residues are more effective in protecting against proteases respect to Trp and Cys(^{t}Bu). Several other factors as hydrophobicity modulate AMPs selectivity and consequentially toxicity [12,193]. For this reason, the relative hydrophobicities of the three peptides were evaluated (Fig. 3.3). Among the three peptides, P9Nal(SS) is the most hydrophobic. P9Nal(SR) seems a little bit more hydrophobic than P9Trp(SS). However, they have comparable hydrophobicities. These results well correlate with the observed higher activity of P9Nal(SS) against gram-positive bacteria (Table 1). In fact, previous studies [179] reported that an increase of hydrophobicity increases the activity against gram-positive bacteria but has only limited effect against gram-negative bacteria. Moreover, P9Nal(SS) showed the highest activity after 16 hours of incubation in serum (Table 2). Therefore, the higher antimicrobial activity of P9Nal(SS) could be related to its lower sensitivity to proteases action and higher hydrophobicity. The MTT assays, employed to evaluate the cytotoxic effect, showed that the three peptides exert significant dose dependent effects on two human cell lines (Fig. 3.2). In particular, P9Nal(SS) showed the highest toxicity. On the contrary, P9Nal(SR) showed a lower toxicity respect to the other two peptides, especially against HaCaT cells. The higher cytotoxicity of P9Nal(SS) could be attributed to its higher hydrophobicity and good resistance to proteases. The P9Nal(SR) is less toxic than the P9Trp(SS), despite the similar hydrophobicities. This observation could be attributed to the faster degradation of P9Nal(SR) respect to P9Trp(SS) when incubated in serum (Table 2).

Collectively, the biological results indicated that the design of these new peptides have been partially successful. In fact, the peptides are effectively stable but, unfortunately, they are not selective. Hence, they are not suited for a pharmacological application. However, it remains open the possibility in the future to slightly modify the peptides to improve their selectivity. In the literature, there are several examples where cytotoxic peptides were converted in selective AMPs [194–196]. For example, it was demonstrated that the introduction of positively charged residues at

polar/apolar interface in piscidins may control the peptide insertion in the eukaryotic membrane and hence the cytotoxicity [197]. Thus, a toxic peptide can be a good starting point for a further design for obtaining a less cytotoxic sequence. To more rationally plan future modifications, biophysical studies on the peptide-lipid interaction mechanism were carried out. In particular, P9Nal(SS) peptide was chosen, since it possess the broader spectrum of activity, higher stability in serum and it's toxic against both eukaryotic cell lines. The interaction process of this peptide was performed with DPPC and DPPC/DPPG (8/2 mol/mol) vesicles, as simplified models of eukaryotic and bacterial membrane, respectively. The final intent was to clarify the action mechanisms underlying its antimicrobial and cytotoxic activity.

The CD spectra reported in Fig. 3.4 clearly indicate that P9Nal(SS) changes its conformation upon binding to both model membranes, approaching a helix-like conformation. It is known that the membrane perturbation activity of some AMPs is related to the ability to adopt a helical conformation [29]. In this regard, these results well correlate with the observed low selectivity. However, the effect of the P9Nal(SS) on the thermotropic properties of the two membranes, as measured by DSC, is completely different. Particularly, the P9Nal(SS) is not able to perturb the lipid packing of the DPPC bilayer and cannot penetrate in the membrane hydrophobic core. In contrast, DSC experiments reveal that P9Nal(SS) strongly perturbs DPPC/DPPG liposomes in a concentration dependent manner. In fact, at low L/P only the pre-transition is affected suggesting that the peptide binding at the lipid head groups/water interface. Increasing its concentration, the peptide is able to penetrate inside the membrane disrupting the regular lipids packing. Moreover, as evidenced by the multicomponent DSC peak at L/P = 10 (Fig. 3.6,B) P9Nal(SS) perturbs the lipid distribution in the membrane inducing the formation of domains of different lipid compositions. Most likely, the lipid segregation is due to the preferential interaction of the cationic peptide with negatively charged lipids. This phenomenon was already observed for other AMPs [12,86,88,198]. To strongly support this hypothesis, the DSC experiment was repeated by replacing DPPG with POPG in the mixed vesicles (Fig. 3.8). The obtained result supports the idea that the peptide prefers to interact with POPG lipids inducing a lipid segregation that leads to the formation of DPPC-rich domains that melts more cooperatively and at higher temperature. This aspect could be crucial since the interface among domains can act as defects destabilizing the bilayer [12,87,199,200] facilitating the peptide insertion in the membrane.

The ability of peptide to penetrate in DPPC/DPPG membrane but not in DPPC membrane was further demonstrated by several experiments. The results obtained in FRET (Fig. 3.9) and quenching (Fig. 3.10) experiments are compatible with a peptide localization on the surface of DPPC vesicles and a penetration of the peptide inside

DPPC/DPPG vesicles. Fluorescence anisotropy is a powerful method to follow the lipid packing perturbation upon peptide insertion in the membrane hydrophobic core. The experiments reported in Fig. 3.7 clearly demonstrated that P9Nal(SS) doesn't affect the anisotropy values for DPH embedded in DPPC vesicles. On the contrary, it drastically affects the anisotropy for DPH in DPPC/DPPG vesicles. It's interesting to note that, as for DSC results, the P9Nal(SS) affects the anisotropy values only after a threshold concentration. A threshold concentration (see also section 1.4) is always required for membrane disruption, regardless of the action mechanism [28,201] and it seems a pre-requisite for all AMPs to exert their biological activity [12].

To conclude, overall the reported data are consistent with a concentration dependent membrane perturbation mechanism for P9Nal(SS) interacting with bacterial model membrane. In particular, the peptide interacts on the membrane surface inducing anionic lipid segregation. Above a threshold L/P value, the peptide penetrates deeply in the hydrophobic core perturbing the packing among lipid acyl chains. On the other hand, the binding of peptide with DPPC liposomes is only superficially. In fact, P9Nal(SS) is not able to perturb the membrane even at low L/P ratios. Thus, the mechanisms responsible for antimicrobial activity could be different to that responsible for toxicity against eukaryotic cells.

Chapter 4

The Interaction of Two P9Nal(SS)-derived Peptides with Bacterial Model Membranes

4.1 Introduction

In this chapter, the biophysical characterization of the interaction of two P9Nal(SS)-derived peptides, named P9Trp(SS) and P9Nal(SR), with liposomes composed by DPPC/DPPG (8/2 mol/mol) as simplified model of the cytoplasmic bacterial membrane is reported.
In the previous chapter, it was shown that the P9Nal(SS) peptide is able to strongly perturb the bacterial model membrane inducing lipid domains formation and penetrating in the hydrophobic core of the membrane disrupting the regular lipid packing. As demonstrated by retention of peptides in reverse phase HPLC experiment (Fig. 3.3), the two peptides are less hydrophobic respect to P9Nal(SS) and they have comparable hydrophobicities. It is well known that the replacement of some residues with ones which decrease the total peptides' hydrophobicity can affect the biological activities [12]. Thus, the final goal of these studies was to verify the effect of the overall hydrophobicity on the peptide membranotropic activity.
Following, are reported the sequences of the three peptides, highlighting the changes compared to the parent peptide (i.e. P9Nal(SS)):

1. P9Nal(SS): H-εAhx-Cys(S^{t}Bu)-Lys-(2Nal)$_2$-Lys-Lys-Cys(S^{t}Bu)-εAhx-NH$_2$;
2. P9Trp(SS): H-εAhx-Cys(S^{t}Bu)-Lys-**(Trp)$_2$**-Lys-Lys-Cys(S^{t}Bu)-εAhx-NH$_2$;
3. P9Nal(SR): H-εAhx-**Cys(^{t}Bu)**-Lys-(2Nal)$_2$-Lys-Lys-**Cys(^{t}Bu)**-εAhx-NH$_2$.

P9Trp(SS) was obtained by replacing the two 2Nal residues with the less hydrophobic Trp residues. Instead, P9Nal(SR) was obtained from the substitution of the two Cys(S^{t}Bu), in position 2 and 8, with Cys(^{t}Bu). Cys(S^{t}Bu) residue is a cysteine with a disulphide and a tert-butyl group, while Cys(^{t}Bu) is a cysteine with a tert-butyl moiety without a disulphide.
The obtained data reveals important similarities and differences on the interaction with cytoplasmic bacterial model membrane between the two peptides and with the parent peptide P9Nal(SS). The three peptides act through the same general action mechanism which involves peptides absorption on membrane surface, conformational changes and formation of lipid domains. Upon reaching a threshold L/P value, the peptides insert in the bilayer at different levels perturbing, or not, the regular lipid packing. The collected data suggest that the penetration abilities follow

the order: P9Nal(SS) >> P9Nal(SR) ≥ P9Trp(SS) which correlate with peptides' hydrophobicity. It seems that the partition inside the membrane is not fundamental in destabilizing the membrane, since all the peptides have similar activities against gram-negative bacteria [93]. Rather, the formation of lipid domains is the key step in promoting membrane perturbation. Overall, these results could represent an important contribution in understanding the action mechanism of AMPs and for the development of new peptide-based drugs for biomedical application.

4.2 Materials and Methods

Materials. The lipids 1,2-dipalmitoyl-*sn*-glycero-3-phosphocholine (DPPC), 1,2-dipalmitoyl-*sn*-glycero-3-phospho-1′-rac-glycerol (DPPG) and 1-palmitoyl-2-oleoyl-*sn*-glycero-3-phospho-1′-rac-glycerol (POPG) were purchased from Avanti Polar Lipids Inc. (Alabaster, AL, USA) and used without further purifications. The fluorescent probe DPH (1,6-Diphenyl-1,3,5-hexatriene) and acrylamide solution (40% w/v) were purchased from Sigma Aldrich Chemical. A 20 mM phosphate buffer, pH 7.4 prepared with deionized water was used for all the reported experiments.

Liposome Preparation. Lipids were weighted in a glass vial and dissolved in a chloroform/methanol mixture (2/1 v/v). A thin film was produced by evaporating the organic solvent by gentle dry nitrogen gas. The sample was placed in a vacuum for at least 3 h. The dried lipids were then hydrated, in the liquid-crystalline phase at the temperature of 50 °C, with an appropriate amount of 20 mM phosphate buffer pH 7.4, and vigorously vortexed obtaining a suspension of multilamellar vesicles (MLVs). Small unilamellar vesicles (SUVs) were obtained using Sonics VCX130 tip sonicator until the suspension became transparent (about 20 min, at room temperature). Dynamic light scattering (DLS) measurements were used to check the size of lipid vesicles after sonication. The obtained average of the hydrodynamic radii of SUVs (∼90 nm) are consistent with the formation of unilamellar vesicles. SUVs containing the fluorescent probe DPH (1,6-Diphenyl- 1,3,5-hexatriene) were obtained by adding to the lipids dissolved in the organic mixture a definite amount of a solution of DPH in chloroform at the lipids/DPH mole ratio of 150. Liposomes composed by DPPC/DPPG (8/2 mol/mol) and DPPC/POPG (8/2 mol/mol) as simplified models of bacterial membrane were prepared. Samples of liposomes in the presence of peptides were prepared by mixing appropriate volumes of peptides' concentrated stock solution and liposomes suspension to get the desired lipid-to-peptide (L/P) ratio.

Circular Dichroism (CD). CD spectra of P9Nal(SR) and P9Trp(SS) were recorded by using a JASCO J-715 spectropolarimeter, from Jasco Corporation (Tokyo, Japan), in a 0.1 cm path length quartz cuvette as an average of 3 scans. For the acquisition of spectra, the following instrument parameters were used: scan speed of 20 nm/min, 4 s response time and 2 nm bandwidth. The temperature was set to 25 °C and controlled with a peltier system which ensures an accuracy of ±0.1 °C. Peptide samples were prepared in 20 mM phosphate buffer pH 7.4 at the concentration of 30 μM in absence and in the presence of SUVs at total lipid concentration of 0.30 mM, 1.5 mM and 3.0 mM. For each sample, a background blank (buffer or lipid suspension alone) was subtracted.

Differential Scanning Calorimetry (DSC). DSC measurements were carried out by means of a nano-DSC from TA Instruments (New Castle, DE, USA). Multilamellar vesicles (MLVs) were used for all DSC experiments since they provide the better resolution of the peak [174]. A volume of 300 μL of 0.5 mM vesicles suspension (DPPC/DPPG or DPPC/POPG) in the absence or in the presence of peptides was placed in the calorimetry vessel, and successive heating and cooling scans were performed at 1 °C/min over the temperature range of 20–55 °C. The excess heat capacity function (<ΔCp>) was obtained after baseline subtraction. A buffer-buffer scan was subtracted from the sample scan. The samples composed by lipid suspension and peptide were prepared before the DSC experiments, by adding the appropriate amount of peptide to the lipid suspension and waiting at least 30 min to ensure that the equilibrium has been reached. The results presented here all refer to the second heating scan. The obtained data were analyzed by means of NanoAnalyze software supplied with the instrument and plotted using the Origin 8.0 software package (OriginLab, Northampton, MA, USA).

Steady-state Fluorescence. All the fluorescence experiments were performed using a Fluoromax-4 spectrofluorometer (Horiba, Edison, NJ, USA) operating in the steady-state mode at the temperature of 25 °C.
Fluorescence anisotropy. Fluorescence anisotropy measurements were carried out for the probe DPH embedded into SUVs at total lipid concentration of 50 μM. The excitation wavelength was set to 355 nm and the emission was monitored at 426 nm. The slits were set to 6 nm and 10 nm for the excitation and emission monochromators, respectively. The experiments were performed using a 1 cm path length quartz cuvette. Fluorescence anisotropies (r) were determined according to the equation:

$$r = \frac{I_{VV} - GI_{VH}}{I_{VV} + 2GI_{VH}}$$

where I_{VV} is the fluorescence intensity obtained by setting both the excitation and emission polarizers vertically, I_{VH} is the fluorescence intensity obtained by setting the excitation polarizer vertically and the emission polarizer horizontally and G is the instrument-specific correction factor, which accounts for the difference in the polarizers transmission efficiency of vertically and horizontally polarized light [175,176].

Fluorescence quenching. For fluorescence quenching experiments, a 5 μM solution of peptides, in the absence or in the presence of SUVs at lipid-to-peptide mole ratio (L/P) of 100, was placed in a quartz cuvette with a path length of 1 cm and titrated with acrylamide solution (40% w/v). The titrations were performed at fixed peptide concentration in the absence and presence of acrylamide concentrations up to ~80 mM. The excitation wavelength was set to 277 nm for P9Nal(SR) and 280 nm for P9Trp(SS), and the emission spectra were collected from 290 nm to 500 nm. The obtained data were analyzed using the Stern-Volmer equation [175,176]:

$$\frac{F_0}{F} = 1 + K_{SV}[Q]$$

where F_0 is the fluorescence intensity in the absence of the quencher, F is the fluorescence intensity at each step of titration in the presence of the quencher, [Q] is the concentration of acrylamide. Due to acrylamide absorption at the excitation wavelength, the fluorescence intensities were corrected using the formula $F_{obs} = F_{corr} \cdot 10^{\frac{-Aex \cdot d}{2}}$ where F_{obs} is the observed intensity, F_{corr} is the corrected intensity, A_{ex} is the absorbance of acrylamide at the excitation wavelength and d is the cuvette path length [177].

4.3 Results

4.3.1 The Conformational Behavior of P9Nal(SR) and P9Trp(SS) Peptides

Circular dichroism (CD) spectroscopy experiments were carried out to check the ability of the two peptides to change their conformation upon binding to bacterial-like liposomes composed by DPPC/DPPG (8/2 mol/mol). Thus, in Fig. 4.1, panel A are reported the CD spectra of P9Nal(SR) in phosphate buffer and in the presence of DPPC/DPPG unilamellar vesicles at lipid-to-peptide (L/P) ratios of 10, 50 and 100. In Fig. 4.1, panel B are reported the CD spectra of P9Trp(SS) recorded in the same experimental conditions.

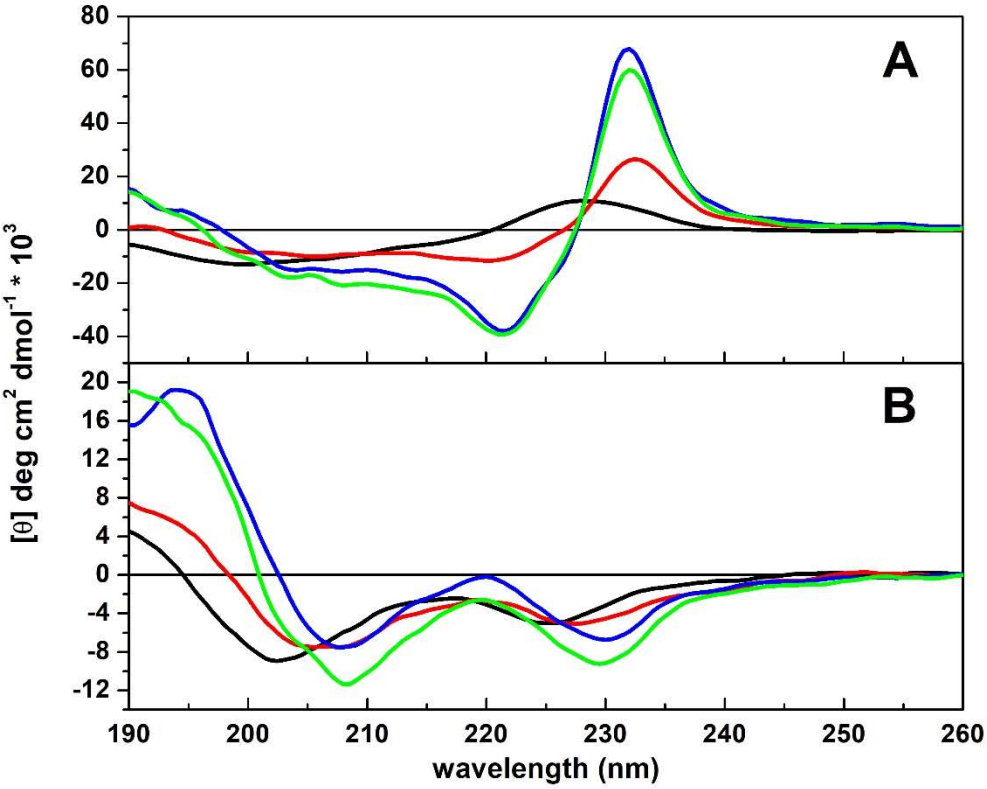

Fig. 4.1 CD spectra of (A) P9Nal(SR) and (B) P9Trp(SS) in buffer (black line) and in the presence of DPPC/DPPG unilamellar vesicles at L/P = 10 (red line), 50 (blue line) and 100 (green line). All the experiments were carried out in 20 mM phosphate buffer, pH 7.4 at 25°C.

Qualitatively, the acquired CD spectra of P9Nal(SR) are the same as the spectra obtained for the parent peptide P9Nal(SS) (section 3.5.1, Fig. 3.4). In solution, the spectrum is characterized by a positive band at about 230 nm and a negative one around 200 nm, suggesting that P9Nal(SR) adopts a random structure [173]. Upon the addition of unilamellar vesicles, the intensity of the positive band increases as the lipid concentration increases. Moreover, two minima centered at about 220 nm and 205 nm appear. At L/P = 50 and 100 a positive band rises at about 190 nm. These results indicate that P9Nal(SR) adopts a helix-like conformation in the presence of lipid vesicles. As for P9Nal(SS), the positive bands in the range 230-240 nm could be due to the excited state interactions of 2Nal residues which contribute to the observed spectra (exciton effect) [182,183]. The CD spectrum of P9Trp(SS) in phosphate buffer showed two negative bands at about 225 nm and 200 nm. The band at 225 nm could be attributed to the contribution of two Trp residues [180,181,183]. Instead, the band at about 200 nm is typical of small unstructured peptides. Thus,

P9Trp(SS) is essentially random coil in solution. In the presence of DPPC/DPPG vesicles, a band around 195 appears. Its intensity increases as the lipid concentration increases. Moreover, the band at 200 nm shifts towards longer wavelengths, reaching about 208 nm at L/P = 100. These results suggest that, as for the P9Nal(SR), also P9Trp(SS) approaches a more ordered structure in the presence of liposomes, most likely a helix-like conformation. The band at 225 nm also shifts towards longer wavelength, reaching about 230 nm at L/P = 100. The shift of this band could be attributed to changes in the local environment experienced by the two Trp residues. Similar observations are reported for others Trp-containing peptides [183,202,203].

4.3.2 The Effects on the Lipid Bilayer Stability

Differential scanning calorimetry is powerful technique to study the thermotropic properties of lipid vesicles and the effects of added peptides on them and it was successfully applied in several different studies [204–206]. Thus, in order to study the effects of P9Nal(SR) and P9Trp(SS) on bilayer stability, DSC measurements with liposomes composed by DPPC/DPPG were carried out. In Fig. 4.2 are reported the DSC thermograms of DPPC/DPPG multilamellar vesicles in the presence of P9Nal(SR) (panel A) and P9Trp(SS) (panel B) at L/P = 10, 5 and 1.

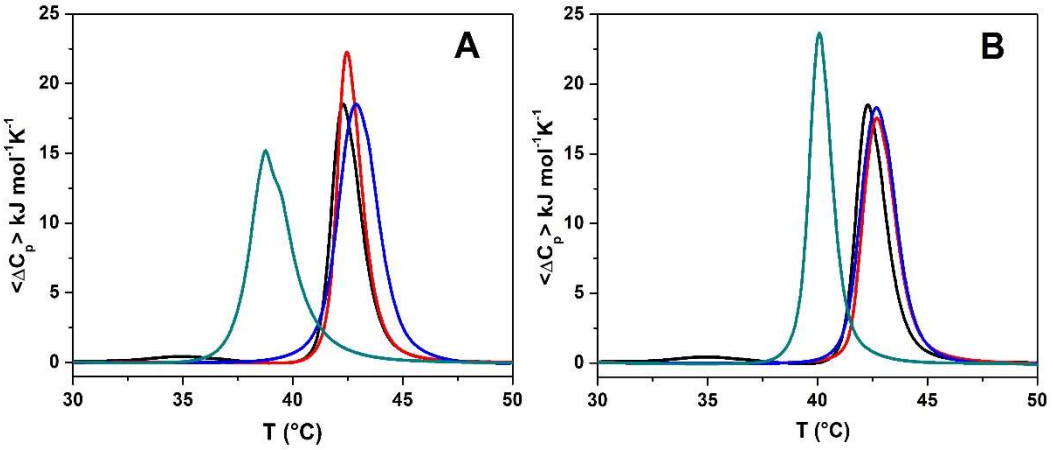

Fig. 4.2 DSC thermograms of DPPC/DPPG multilamellar vesicles (black line) in the presence of (A) P9Nal(SR) and (B) P9Trp(SS) at lipid-to-peptide ratio of 10 (red line), 5 (blue line) and 1 (green line). All the experiments were carried out in 20 mM phosphate buffer, pH 7.4

As described in the section 3.5.2, the DSC thermogram of liposomes composed by DPPC/DPPG (8/2 mol/mol) is characterized by the presence of two transitions [184,207]: the pre-transition, at about 35 °C, is due to the rearrangement of lipid

polar head groups; the main transition, at 42.4 °C, is due to the melting of acyl chains of lipids. Thus, the peptides' effects on two distinct regions of the membrane, surface and hydrophobic core, can be followed.
The addition of P9Nal(SR) or P9Trp(SS) completely abolish the DPPC/DPPG pre-transition already at lowest peptide concentrations used (L/P = 10). These results clearly indicate that both peptides interact with lipid polar head groups perturbing their transitions from the lamellar gel phase to rippled gel phase.
The most surprising result, which differs from that observed for the parent peptide P9Nal(SS), is that the main transition, i.e. lipid acyl chains packing, seems not significantly perturbed by the presence of peptides, up to L/P = 5 (high peptide concentrations). In fact, only a small increase of transition temperature coupled with a slightly broadening of transition peaks were observed, suggesting a binding at hydrophilic/hydrophobic interface [185]. In contrast, already at L/P = 10 P9Nal(SS) was able to penetrate inside the bilayer strongly perturbing the lipid packing (section 3.5.2, Fig. 3.6).
An evident perturbation of the main transition was observed only at very high peptide concentration (L/P = 1). At this ratio, in the presence of P9Nal(SR), the main transition temperature decreases from 42.3 °C to 38.8 °C. Moreover, the peak looks broader and composed by at least two peaks (with a shoulder centered at about 39.5 °C) suggesting the formation of domains which differ in their lipid compositions and melt at different temperatures, as observed for P9Nal(SS). These results indicate that P9Nal(SR) is able to perturb the lipids packing inducing the formation of lipid domains and penetrating at some extent in the bilayer [185].
Similarly, also for P9Trp(SS) a very high peptide concentration is required to clearly perturb the main transition peak (Fig. 4.2, panel B). At this high peptide concentration, the DSC peak looks sharper respect to that in the absence of peptide and it does not appear as composed by the superposition of two or more peaks. This result suggest that P9Trp(SS) does not penetrate in the membrane hydrophobic core and is not able to perturb the lipid packing. Most likely, the preferential interaction of P9Trp(SS) with DPPG caused a demixing of DPPC and DPPG molecules leading to the formation of lipid domains. The formed domains (with acyl chains unperturbed by the presence of peptide) of DPPC and DPPG have similar transition temperatures. Their sharp transitions sum to each other leading to the formation of the observed DSC peak. The localization of the peptide at the hydrophilic/hydrophobic interface is also supported by the particular preference of Trp residues in localizing in this membrane region [32,208]. Thus, it seems that P9Nal(SR) and P9Trp(SS) have different penetration abilities inside the membrane. P9Trp(SS) doesn't perturb strongly the lipid acyl chains packing, because it cannot distribute in the hydrophobic core of the membrane leading to thermogram similar to that observed for 2Nal-containing peptide.

To better highlight the ability of P9Trp(SS) to induce the formation of lipid domains, the DSC experiment was repeated by replacing DPPG with POPG, producing multilamellar vesicles composed by DPPC/POPG (8/2 mol/mol). As stated in section 3.5.3, POPG vesicles have a transition temperature below 0°C. Thus, POPG incorporation affects the observed transition of DPPC only indirectly, by changing its local distribution. This replacement has several advantages: i) at the mole fraction used, the two lipids are completely miscible [189]; ii) the melting temperature of pure POPG vesicles is below 0 °C and, thus, it can affect the observed phase transition of DPPC/POPG indirectly, by changing its local distribution. If the added peptide preferentially interacts with the low-melting component of the membrane (POPG), it will promote its segregation leaving the rest of the membrane enriched in the high-melting component (DPPC), which melts at higher temperature [209]. In Fig. 4.3 are reported the DSC thermograms of DPPC/POPG vesicles in the absence and in the presence of P9Trp(SS) at L/P = 50.

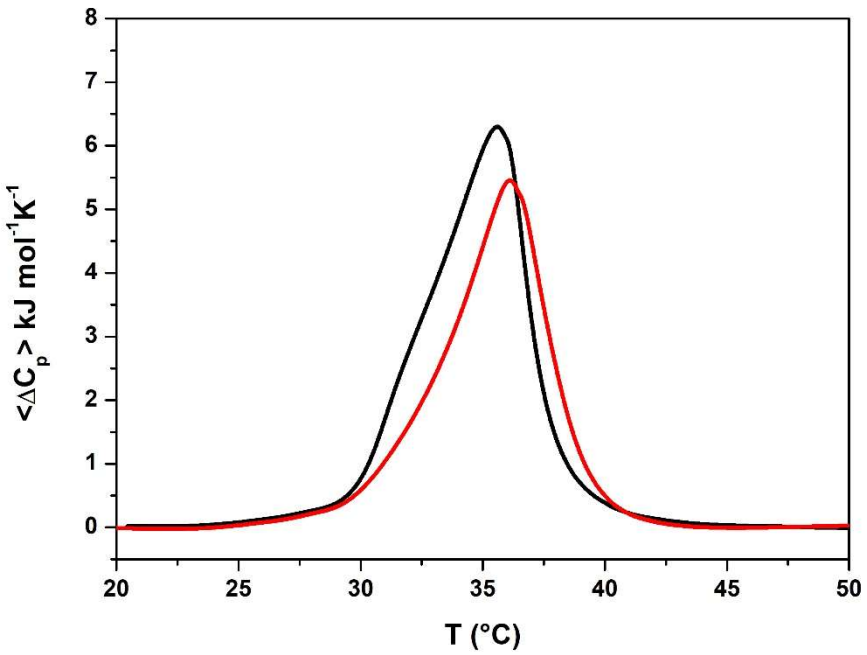

Fig. 4.3 DSC thermograms of DPPC/POPG multilamellar vesicles in the absence (black line) and in the presence (red line) of P9Trp(SS) at L/P = 50. The experiments were carried out in 20 mM phosphate buffer, pH 7.4.

The DSC thermogram of DPPC/POPG vesicles has a transition temperature at about 35.6 °C. After the addition of P9Trp(SS) an increase of the transition temperature to 36.1 °C was observed coupled with an increase of the transition cooperativity

(sharper peak). This result is consistent with a preferential interaction with negatively charged lipids leaving a DPPC enriched domain which melts more cooperatively and at higher temperature.

4.3.3 Abilities of Peptides to Penetrate in the Membrane

To better understand the effects of peptides insertion on the bilayer stability, fluorescence anisotropy measurements with the probe DPH were carried out. DPH is a very poor-soluble water fluorescent molecule that partitions inside the hydrophobic core of the lipid bilayer [175,210]. Since the DPH anisotropy values depend on the lipid acyl chains packing, this technique is an invaluable tool to study the peptides insertion in the membrane [211].
In Fig. 4.4 are reported the anisotropy values of DPH embedded in DPPC/DPPG unilamellar vesicles in the presence of increasing concentration of P9Nal(SR) and P9Trp(SS) peptides in panel A and B, respectively.

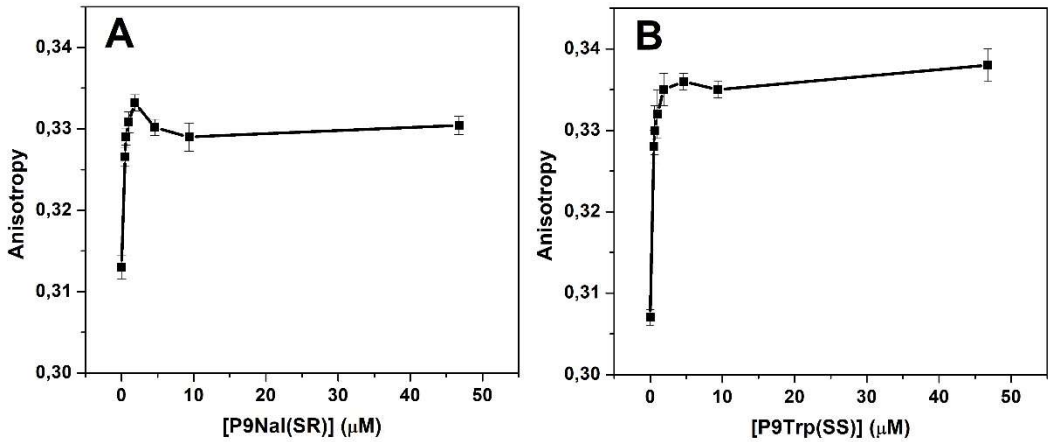

Fig. 4.4 Fluorescence anisotropy for DPH embedded in DPPC/DPPG unilamellar vesicles in the presence of increasing concentration of (A) P9Nal(SR) and (B) P9Trp(SS). The total lipid concentration was ~50 μM. All the experiments were carried out in 20 mM phosphate buffer, pH 7.4 at the temperature of 25 °C.

The addition of P9Nal(SR) peptide causes an increase of the anisotropy values of DPH up to peptide concentration of about 2 μM. Then, increasing peptide concentration, a decrease of anisotropy was observed. This result indicate that the effect of peptide is concentration dependent. At low concentration (below 2 μM) the peptide doesn't penetrate in membrane but rather it interacts with lipid polar heads groups. These interactions could stabilize the bilayer, reducing the repulsion between polar head groups [185,212]. At higher concentration, P9Nal(SR) is able to penetrate

in the membrane destabilizing the regular lipid packing. Consequentially, a decrease of anisotropy was detected. For the P9Trp(SS), a different phenomenon was observed. Its addition to DPPC/DPPG vesicles increases the anisotropy value of DPH up to 0.335 at 2 μM which is compatible with a surface binding which stabilize the bilayer. Then, the further increase of peptide concentration doesn't affect the anisotropy values. These findings point out that P9Trp(SS) is not able to perturb the lipid packing. Probably, as noted for DSC measurements, this could be due to the weak capacity of this peptide to penetrate inside the hydrophobic core of the membrane. Overall, the obtained results are in very good agreement with the results obtained by means of DSC measurements.

Finally, fluorescence quenching measurements with acrylamide were performed. Fluorescence emission spectra of peptide in buffer or in the presence of DPPC/DPPG at L/P = 100 were recorded at different acrylamide concentrations. According to the equation reported in "Fluorescence quenching" section, a plot of F_0/F versus acrylamide concentration gives a straight line whose slope is the Stern-Volmer constant, indicated as K_{SV}. The value of K_{SV} is an index of the degree of exposure to the aqueous solvent of the two fluorophores in the primary sequence of the peptide [175,190]. A more exposed residue will be more quenched respect a less exposed one. In the first case, the value of K_{SV} will be greater than the value obtained in the second case. In Fig. 4.5 are reported the Stern-Volmer plots obtained from the acrylamide quenching of P9Nal(SR) and P9Trp(SS) peptides in buffer or in the presence of unilamellar vesicles composed by DPPC/DPPG.

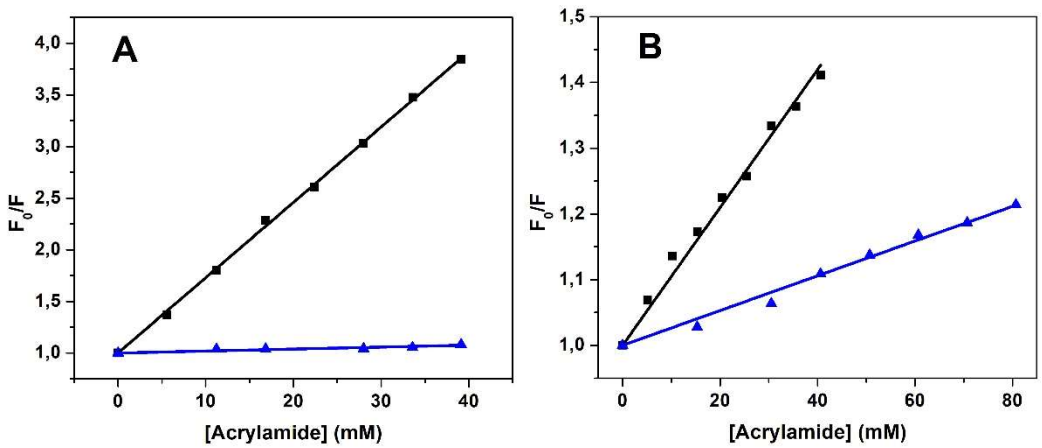

Fig. 4.5 Stern-Volmer plots obtained from the fluorescence quenching experiments with acrylamide of (A) P9Nal(SR) and (B) P9Trp(SS) in the absence (black squares) and in the presence (blue triangles) of DPPC/DPPG unilamellar vesicles at L/P = 100. Note that the scales of the two graphs are different.

For P9Nal(SR) in the absence of DPPC/DPPG lipid vesicles, the value of the K_{SV} is 72.9±0.5 M^{-1}. It is important to note that, despite that the fluorophores in P9Nal(SS) and P9Nal(SR) are the same, the value of K_{SV} are completely different. In fact, the value obtained for P9Nal(SS) was of 16.9±0.4 M^{-1} (section 3.5.4). This discrepancy could be ascribed by the presence of Cys(S^{t}Bu) and Cys(^{t}Bu) in P9Nal(SS) and P9Nal(SR), respectively. In fact, the longer and more flexible side chains of Cys(S^{t}Bu) residues could shield more the 2Nal residues from the aqueous medium respect to the shorter and less flexible Cys(^{t}Bu) residues.
In the presence of DPPC/DPPG vesicles at L/P = 100, a strong decrease of K_{SV} was observed (2.0±0.6 M^{-1}), suggesting that the peptide and the 2Nal residues are inserted in the membrane and are hidden to acrylamide presents in solution.
For P9Trp(SS) in solution without lipid vesicles, a value of K_{SV} of 10.5±0.2 M^{-1} was obtained. Upon the addition of DPPC/DPPG vesicles, the value of K_{SV} decreases to 2.6±0.6 M^{-1}. Again, this result suggest that the P9Trp(SS) is able to insert inside the membrane.
The K_{SV} values for both peptides are similar, even though DSC and anisotropy measurements suggested different degrees of penetration. The incongruence with fluorescence quenching results could be explained considering that, probably, the quenching test is not able to discriminate among different levels of insertion in the bilayer. This sounds reasonable, since the hydrophilic acrylamide doesn't partition in the membrane [190,213,214].

4.4 Discussion

In this chapter, the results obtained from biophysical studies of two P9Nal(SS) derived peptides with DPPC/DPPG liposomes as model of cytoplasmic bacterial membrane were presented. The two peptides, named P9Nal(SR) and P9Trp(SS), were obtained from the replacement of some residues in the primary sequence of P9Nal(SS). In particular P9Nal(SR) was obtained after the substitution of the two Cys(S^{t}Bu) with Cys(^{t}Bu) residues. On the contrary, in P9Trp(SS) peptide the two 2Nal residues were replaced by Trp residues. These substitutions led to peptides with comparable hydrophobicities and more hydrophilic respect to the parent peptide P9Nal(SS). The final goal of this study was to clarify if these substitutions could have an impact on the perturbation of bacterial model membranes.
All the reported data reveal similarities and differences in the interaction process and perturbation activities of the two studied peptides. As demonstrated by CD spectra, both peptides change their conformation upon binding to liposomes and it seems that they assume a helix-like conformation. The conformational changes of both peptides well correlate with their antimicrobial activities *in vivo* (section 3.4.1).

From the reported DSC measurements (Fig. 4.2) is evident that both peptides act through a concentration dependent mechanism. Up to L/P = 5, only a binding with lipid polar head groups was observed. At the threshold value of L/P = 1, a clear effect on the main transition peak of DPPC/DPPG liposomes can be revealed.
The DSC experiments at this very high peptide concentration point out some differences in the mode of interaction of these two peptides. In fact, for P9Nal(SR) the formation of a broad multicomponent peak suggest the formation of lipid domains and penetration of the peptide in the membrane which perturbs the regular lipid packing. In contrast, for P9Trp(SS) these features are not immediately revealed. In fact, due to the preference of Trp residues to locate at the membrane-water interface, P9Trp(SS) penetrates to a less extent in the bilayer [32,208]. Nevertheless, it is able to induce lipid segregation as demonstrated by the result obtained with DPPC/POPG mixture (Fig. 4.3). The different degrees of peptides penetration in the bilayer are well supported by fluorescence anisotropy measurements (Fig. 4.4). In fact, for P9Nal(SR) the increase of DPH anisotropy at low concentration and the decrease at high peptide concentration indicate that the surface binding is followed by an insertion in the hydrophobic core of the membrane. For P9Trp(SS), at low concentration an increase of anisotropy was detected. The further addition of peptide doesn't change the DPH anisotropy embedded in DPPC/DPPG vesicles. This is a clear proof that the peptide does not penetrate in the hydrophobic core of the membrane and, consequentially, it cannot perturb the lipid packing remaining at hydrophobic/hydrophilic interface.
At this point it is useful to compare P9Nal(SR) and P9Trp(SS) with the parent peptide P9Nal(SS). Overall, the reported data in this chapter and in the chapter 3 suggest that the key step in membrane destabilization is the same for all the three peptides: the formation of lipid domains. It is known that the interface between domains can act as defects in destabilizing the membrane promoting membrane permeabilization [12,87,199,200].
The main difference among the three peptides is related to their penetration capacities inside the bilayer which are correlated with the overall peptides' hydrophobicities. As demonstrated by retention of peptides in reverse phase HPLC experiment (Fig. 3.3) the parent peptide P9Nal(SS) is the most hydrophobic, followed by P9Nal(SR) and P9Trp(SS). However, the difference between the two analog peptides is little. It seems that P9Nal(SS) has the highest penetration ability according with its higher hydrophobicity, followed by P9Nal(SR) and P9Trp(SS). This is demonstrated by DSC measurements (Fig. 3.6 and Fig. 4.2). In fact, the strong perturbation of the DSC peak of DPPC/DPPG vesicles, compatible with P9Nal(SS) insertion in the membrane, took place already at L/P = 10. In contrast, only at very high peptide concentrations (L/P = 1), P9Nal(SR) gave a similar (but less pronounced) phenomenon. Instead, the results obtained for the P9Trp(SS) revealed

no deep insertion in the hydrophobic core of the membrane even at L/P = 1, but the localization at the hydrophobic/hydrophilic interface. These ideas are also well supported by DPH fluorescence anisotropy experiments (Fig. 3.7 and Fig. 4.4). Thus, the penetration abilities seem to be in the order: P9Nal(SS) >> P9Nal(SR) ≥ P9Trp(SS).

To conclude, the three peptides act through the same general action mechanism which involve peptides absorption on membrane surface, conformational changes and formation of lipid domains. Upon reaching a threshold L/P value, the peptides insert in the bilayer at different levels perturbing, or not, the regular lipid packing. Since all the peptides have similar antimicrobial activities especially against gram-negative bacteria (Table 1, section 3.4.1), it seems that the partition inside the membrane is not fundamental in destabilizing the membrane. Rather, it is sufficient that the peptides are able to induce lipid segregation and domains formation. This is also supported by the observation that an increase of hydrophobicity in L-V13K peptide does not alter its activity against *Pseudomonas aeruginosa* [46]. The reported data cannot explain the reduced activities against gram-positive bacteria, since it is widely accepted that the target of AMPs is the cytoplasmic membrane in both kinds of bacteria (section 1.4 and 2.4) [215]. As reported in literature [179] the activity against gram-positive bacteria is correlated to hydrophobicity, since a decrease of this parameter lead to a decrease of antimicrobial potency. Most likely, the hydrophobicity could modulate the interaction of peptides with cell wall components (e.g. teichoic acids) which can retain peptides preventing their interaction with the cytoplasmic membrane [138]. Thus, higher peptides concentrations in biological tests should be used to have the inhibition of gram-positive bacterial growth.

Chapter 5

The Cytotoxic and Antimicrobial Activities of the Human Thrombin-derived Peptide (P)GKY20: A Biophysical Study

5.1 Introduction

The antimicrobial peptide (P)GKY20 is a natural peptide modelled on the Gly^{271} to Ile^{290} sequence of the C-terminus region of the human thrombin [178]. The region corresponding to the peptide sequence in the protein is highlighted in red in Fig. 5.1. The sequence of (P)GKY20 peptide is: (P)GKYGFYTHVFRLKKWIQKVI. The proline residue is not present in the original sequence of the peptide [178], but it is the result of the expression and the purification procedure of the peptide (see Materials section). The (P)GKY20 possesses a net positive charge of 5 at physiological pH of 7.4 and no protecting groups (e.g. amidation and acetylation) at the termini.

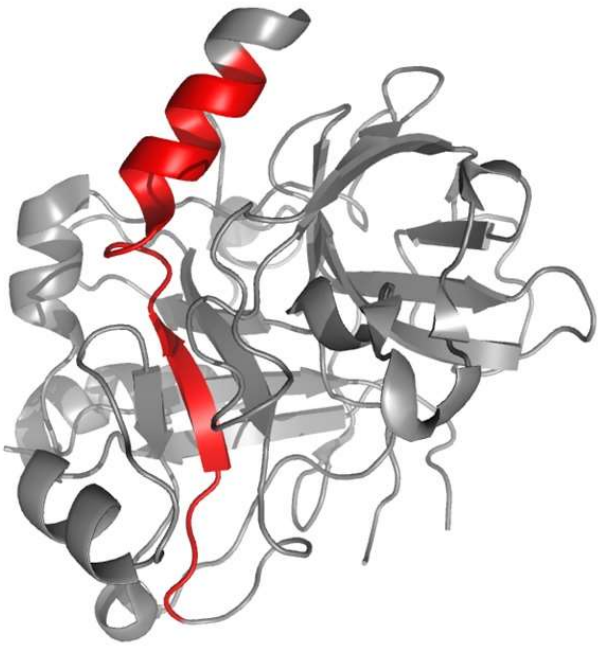

Fig. 5.1 The three-dimensional structure of the human thrombin (pbd: 3U69) [216]. In red is highlighted the portion of protein which corresponds to the sequence of (P)GKY20 peptide.

It was shown that this peptide is effective against both gram-negative and gram-positive bacteria as well as against the fungus *Candida albicans* [178]. For example,

the MIC value for the gram-negative bacterium *Escherichia coli* is in the range 2.5-10 μM. Instead the MIC value for the gram-positive bacterium *Staphylococcus aureus* is in the range 20-40 μM. Moreover, it was shown that permeabilization of human skin fibroblasts after the exposure at 60 μM of (P)GKY20 peptide was largely absent, revealing the low cytotoxic effects of the peptide. Consequentially, (P)GKY20 peptide could be very suitable as drug for biomedical applications.
Unfortunately, the molecular basis of the action mechanism, which underlying the observed (P)GKY20 antimicrobial activity, is still unknown. Thus, in order to study the interaction process with the membrane, a detailed biophysical study was carried out by using liposomes composed by POPC and POPG as a simplified model of the cytoplasmic bacterial membrane. For comparison, the same study was carried out with POPC liposomes as model of the eukaryotic membrane to find the key determinants able to explain the low observed cytotoxicity.
The reported data clearly indicate that, although (P)GKY20 binds both the membranes, its effect is strongly dependent on the membrane lipid composition. In particular, the peptide is able to drastically perturb the microstructure and stability of the bacterial-like membrane whereas no significant perturbation of the eukaryotic-like membrane was observed. These findings are fully consistent with the reported (P)GKY20 selectivity toward bacterial membranes. In addition, a complex action mechanism which involves peptide conformational changes, lipid segregation, domain formation and micellization as key steps in promoting membrane disruption was revealed. The reported results shed a first light on the action mechanism of (P)GKY20 providing molecular details at the level of peptide-lipid interaction and could represent an important contribution for the development of new peptides serving as antimicrobial agents.

5.2 Materials and Methods

Materials. The recombinant peptide (P)GKY20 (molecular weight: 2609.16 g/mol) was prepared by heterologous expression in *E. coli* through fusion to the C-terminus of a carrier derived from a modified ribonuclease as previously described [170]. After purification the peptide was released by selective hydrolysis of an aspartyl-prolyl sequence present at the carrier/peptide boundary. Hydrolysis leaves an additional proline residue at the N-terminus of the peptide which does not influence the biological activity of the peptide [170]. The peptide was expressed in collaboration with the research group of Prof. E. Notomista of the Department of Biology, University of Naples Federico II.
The lipids 1-palmitoyl-2-oleoyl-*sn*-glycero-3-phosphocholine (POPC), 1-palmitoyl-2-oleoyl-*sn*-glycero-3- phospho-1'-rac-glycerol (POPG), 1,2-dipalmitoyl-*sn*-glycero-3-phosphocholine (DPPC), 1,2-dipalmitoyl-*sn*-glycero-3-phospho-1'-rac

glycerol (DPPG) and N-(Lissamine rhodamine B sulfonyl) phosphatidylethanolamine (N-Rh-DHPE) were purchased from Avanti Polar Lipids Inc. (Alabaster, AL, USA) and used without further purifications. The fluorescent probe Laurdan (6-dodecanoyl-2-dimethylaminonaphtalene), acrylamide solution (40% w/v), chloroform, methanol and dimethylformamide were purchased from Sigma Aldrich Chemical. Deionized water was used for the phosphate buffer and all sample preparations.

Liposome Preparation. Appropriate amounts of lipids were weighed and dissolved in a chloroform/methanol (2/1 v/v) mixture. A thin film was produced by gentle evaporation of the organic solvent with nitrogen gas. To remove final traces of organic solvent, the sample was placed under vacuum overnight. Then, the sample was hydrated with an appropriate volume of 10 mM phosphate buffer, pH 7.4, and vigorously mixed obtaining a suspension of multilamellar vesicles (MLVs). Small unilamellar vesicles (SUVs) were produced by sonication of multilamellar vesicles at room temperature with a Sonics VCX130 (Sonics and Materials Newtown, USA) until the suspension appeared clear (~15-20 min). Large unilamellar vesicles (LUVs) containing the fluorescent probe Laurdan (6-dodecanoyl-2-dimethylaminonaphtalene) were obtained by adding to the lipids dissolved in the organic mixture a definite amount of a solution of Laurdan in DMF (dimethylformamide) at the lipid/Laurdan molar ratio of 500. Large unilamellar vesicles (LUVs) were produced by the extrusion method using a Mini-Extruder (Avanti Polar Lipid Inc.) passing the MLVs suspension through a 100 nm pore size polycarbonate membrane twenty-one times. Dynamic light scattering measurements were performed to check the size of the vesicles after both sonication and extrusion. The average hydrodynamic radii (R_H) of pure and mixed lipids vesicles were ~90 nm for SUVs and ~120 nm for LUVs, compatible with the formation of unilamellar vesicles. Liposomes with different composition were prepared: POPC, DPPC, POPC/POPG (8/2 mol/mol), DPPC/DPPG (8/2 mol/mol), DPPC/POPG (8/2 mol/mol), and DPPG. Vesicle samples in the presence of peptide were prepared by mixing appropriate volumes of peptide solution and liposomes suspension to yield the desired lipid-to-peptide (L/P) ratio.

Circular Dichroism (CD). Far-UV circular dichroism spectra of the (P)GKY20 peptide were recorded using a JASCO J-715 spectropolarimeter (Jasco Corporation, Tokyo, Japan) in a 0.1 cm path length quartz cuvette as an average of 3 scans, using the following parameters: scan speed of 20 nm/min, 4 s response time, 2 nm bandwidth. Samples were prepared in 10 mM phosphate buffer, pH 7.4, at the peptide concentration of 17 μM in the absence and presence of SUVs at a total lipid concentration of 0.17 mM, 0.85 mM and 1.7 mM. For each sample, a background

blank (buffer or lipid suspension alone) was subtracted. An estimation of the secondary structure content was obtained from the spectra using "PEPFIT Analyses" software [217].

Steady-state Fluorescence. The steady-state fluorescence binding and quenching measurements were performed with a Fluoromax-4 spectrofluorimeter (Horiba, Edison, NJ, USA) using a quartz cuvette of 1 cm path length (volume ~1 mL). Instead, Laurdan fluorescence emission spectra were acquired with a K2 fluorescence spectrometer from ISS (Champaign, Illinois, USA) using a full volume (~2 mL) quartz cuvette of 1 cm path length. During the measurements, the samples were under gentle stirring.

Binding Experiments. The ability of (P)GKY20 peptide to interact with POPC and POPC/POPG (8/2 mol/mol) large unilamellar vesicles (LUVs) was studied by monitoring the changes in the Trp fluorescence emission spectra of the peptide. The titrations were performed, at 25 °C, by recording the spectra of solutions of the peptide at a fixed peptide concentration of about 6 μM and lipid vesicles concentrations ranging from 0 to ~10^{-3} M. The excitation wavelength was set to 280 nm, and the emission spectra were collected from 300 to 500 nm. The slit widths for excitation and emission wavelengths were set to 8-10 nm and 10-12 nm, respectively. The acquisition of good fluorescence spectra is not straightforward because of light scattering associated with liposomes, especially at high lipid concentrations [218]. Light scattering can affect the emission spectra leading to erroneous conclusions about the interaction of peptides with liposomes (e.g. apparent blue shift). Since the light scattered by liposomes has the same polarization of incident light, the experiments were carried out by exciting the sample with plane-polarized light and recording the light emission in a plane perpendicular to that of exciting light, as described in detail in [218]. The binding isotherms were obtained by plotting the relative fluorescence intensity at 355 nm as a function of lipid concentration. The mole fraction partition constant (K_x) was obtained by fitting the binding curves with the following equation [218]:

$$F = 1 + (F_\infty - 1) \cdot \frac{(K_x \cdot [L])}{([W] + K_x \cdot [L])}$$

where F is the relative fluorescence intensity at each point of the titration, F_∞ is the relative fluorescence at saturation, [L] is the lipid concentration, [W] = 55.3 M is the molar concentration of water, and K_x is the mole fraction partition constant. The mole fraction partition constant is defined as [219]:

$$K_x = \frac{[P_b]/[L]}{[P_f]/[W]}$$

where $[P_b]$, $[P_f]$, [L] and [W] are the molar concentration of the membrane-associated peptide, free peptide in the aqueous phase, lipids and water, respectively.

Laurdan Generalized Polarization. Laurdan fluorescence emission spectra were recorded by exciting LUVs labelled with Laurdan at 340 nm. The emission spectra were collected from 390 to 620 nm. The slit widths for both excitation and emission wavelengths were 8 nm. The final lipid concentration was 50 μM. For DPPC/DPPG vesicles, spectra of Laurdan as a function of the temperature in the absence and in the presence of (P)GKY20 peptide (L/P = 10) were recorded. For POPC and POPC/POPG LUVs, emission spectra of Laurdan were recorded by varying the peptide concentration. The Laurdan generalized polarization (GP) is defined as [220]:

$$GP = \frac{(I_{440} - I_{490})}{(I_{440} + I_{490})}$$

where I_{440} and I_{490} are the fluorescence intensities at 440 nm and 490 nm, respectively.

Quenching Experiments. Fluorescence quenching experiments were performed at 25 °C. A 6 μM solution of (P)GKY20 peptide, in the absence or in the presence of LUVs at L/P of 200, was titrated with acrylamide solution (40% w/v). The titrations were performed at fixed peptide concentration in the absence and presence of acrylamide concentrations up to ~ 50 mM. The excitation wavelength was set to 280 nm. The emission spectra were collected from 300 nm to 500 nm. The slit widths for the excitation and emission were 2 nm and 4 nm, respectively. The obtained data were analyzed using the Stern-Volmer equation [175]:

$$\frac{F_0}{F} = 1 + K_{SV}[Q]$$

where F_0 is the fluorescence intensity of the peptide at its maximum in the absence of the quencher, F is the fluorescence intensity at each step of titration in the presence of the quencher, [Q] is the concentration of acrylamide, and K_{SV} is the Stern-Volmer

quenching constant. The obtained spectra were corrected for the acrylamide absorbance at the excitation wavelength as reported in [177].

Differential Scanning Calorimetry (DSC). DSC measurements were carried out by means of a nano-DSC from TA Instruments (New Castle, DE, USA) for DPPC and DPPC/DPPG vesicles. Instead, the DSC measurements for the mixture DPPC/POPG were performed with a MicroCal VP-DSC from Microcal (now Malvern Instruments. MLVs were used for all DSC experiments since they provide the better resolution of the phase transition peaks [174]. Briefly, 300 µL of 0.4 mM vesicles suspension (DPPC, DPPC/DPPG or DPPC/POPG) in the absence or in the presence of peptide was placed in the calorimetry vessel, and successive heating and cooling scans were performed at the scan speed of 1 °C/min. The excess heat capacity function ($<\Delta C_p>$) was obtained after baseline subtraction. A buffer-buffer scan was subtracted from the sample scan. The samples composed by lipid suspension and peptide were freshly prepared just before the experiments, by adding the appropriate amount of peptide to the lipid suspension and waiting at least 30 min to ensure that the equilibrium was reached. The reversibility of the process was ensured by the superposition of successive heating scans. The data obtained were analyzed by means of the NanoAnalyze software supplied with the instrument and plotted using the Origin software package (OriginLab, Northampton, MA, USA).

Dynamic Light Scattering (DLS). DLS measurements were carried out to evaluate the liposomes mean size before and after the addition of the (P)GKY20 peptide. Briefly, 1 mL of 100 µM LUVs suspension in the absence or in the presence of (P)GKY20 peptide, at different lipid-to-peptide ratios, was placed in a polystyrene cuvette at the temperature of 25 °C and analyzed at the scattering angle of 90° using a Zetasizer nano ZSP (Malvern Instruments Ltd., Malvern, Worcestershire, UK) equipped with a 10-mW He-Ne laser operating at the wavelength of 633 nm. All measurements were carried out as triplicate.

Atomic Force Microscopy (AFM). Samples for atomic force microscopy (AFM) experiments were prepared by direct fusion of LUVs composed by POPC/POPG in 20 mM Tris, 5 mM $MgCl_2$, pH 7.4. The vesicle fusion on mica was performed by depositing 300 µL of LUVs suspension, at a total lipid concentration of 2 mg/mL, on freshly cleaved mica and incubation for 2 h in a wet chamber at 70 °C. After the fusion, to remove the unspread vesicles, the sample was rinsed with Tris buffer. The peptide-containing sample was obtained by injecting peptide solution into the AFM fluid cell. AFM measurements were performed in tapping mode, at room temperature, on a MultiMode scanning probe microscope equipped with a NanoScope IIIa controller (Digital Instruments) and usage of a J-scanner (scan size

125 μm). Images were obtained in liquid with sharp nitride lever (SNL) probes mounted on a fluid cell (MTFML, both Veeco, Karlsruhe, Germany). Tips with nominal force constants of 0.24 N m^{-1} were used at driving frequencies of 9 kHz and drive amplitudes between 200 and 800 mV. Scan frequencies were between 1.0 and 1.94 Hz. Height and phase images of sample regions were acquired with resolutions of 512x512 pixels. All measurements were analyzed by using the analysis and processing software NanoScope version 5.

Confocal Fluorescence Microscopy. Giant unilamellar vesicles (GUVs) composed by POPC/POPG were produced by the electroformation method [221]. Briefly, 25 μL of 2 mg/mL of lipid mixtures, labelled with N-Rh-DHPE at 0.2 mol%, in organic solvent were spread on ITO-coated slides (SPI Supplies, West Chester, USA). The slides were placed under vacuum overnight to remove the organic solvent. Afterwards, the slides were mounted on a temperature-controlled preparation chamber consisting of a closed bath imaging chamber RC-21B (360 μL) mounted on a P-2 platform (both Warner Instruments). Then, after addition of a solution of 10 mM phosphate, 100 mM sucrose, pH 7.4 (via an injection-channel) the electroformation was performed at the frequency of 500 Hz at 400 mV for 5 min, 1.25 V for 20 min and 3.5 V for 90 min. Fluorescence microscopy of GUVs, in buffer in the absence or in the presence of (P)GKY20 peptide, was performed by using a confocal laser scanning microscope (Biorad MRC 1024) coupled via a side port to an inverted microscope (Nikon; Eclipse TE-300DV), enabling fluorescence excitation in the focal plane of an objective lens (Nikon Plan Apo 60 WI, NA 1.2). A 568-nm line of a Kr/Ar laser (Dynamic Laser, Salt Lake City, UT, USA) was used to excite N-Rh-DHPE. Image acquisition was controlled using the software LaserSharp2000 (Biorad). The analysis of the data was performed using the software ImageJ [222].

5.3 Results

5.3.1 The Interaction and the Conformational Behavior of (P)GKY20 with Model Membranes

To verify the ability of the peptide (P)GKY20 to interact with liposomes composed by POPC and POPC/POPG (8/2 mol/mol) as simplified models of eukaryotic and bacterial membranes, respectively, steady state fluorescence spectroscopy experiments were performed. Due to the presence of aromatic residues [175], the measurements were carried out by exciting the peptide at λ_{ex} = 280 nm and following the changes in emission intensity at the maximum of emission. To avoid spectral

distortions due to light scattering induced by liposomes, all the spectra were acquired using polarized [218] (see section 5.2).
In Fig. 5.2 are reported the binding isotherms and emission spectra obtained from the titration of a peptide solution with POPC (Panel A) and POPC/POPG (Panel B) large unilamellar vesicles.

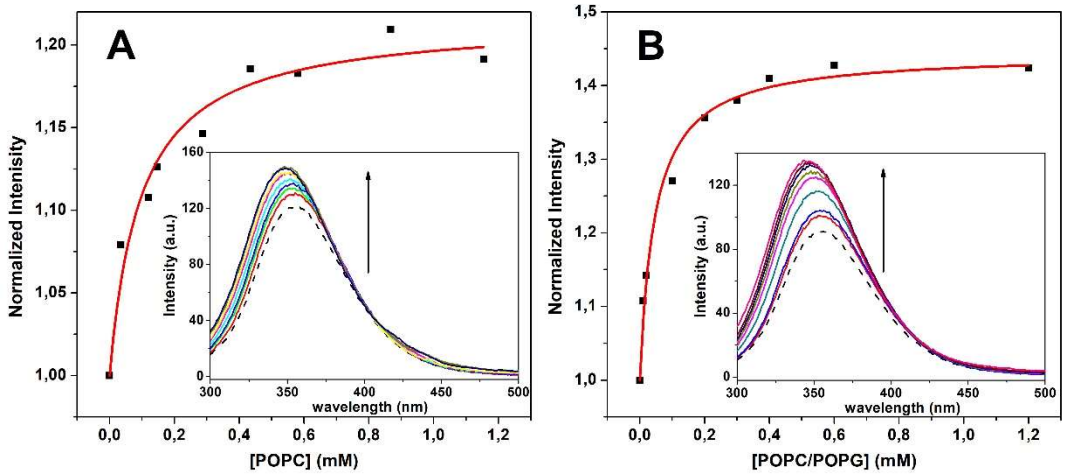

Fig. 5.2 Binding isotherms obtained from the titration of a solution of (P)GKY20 peptide with unilamellar vesicles of (A) POPC and (B) POPC/POPG (8/2 mol/mol). Solid lines are the best fit to the experimental data using the equation reported in Materials and Methods, Binding Experiments section. In the insets are collected the fluorescence spectra.

The experimental points, obtained by following the changes in fluorescence intensity at wavelength maximum (λ_{max} = 355 nm) and normalized relative to the emission intensity of peptide in the absence of lipid, were fitted in order to obtain the mole fraction partition constant (K_x) [218]. The value of K_x is an index of the peptide affinity for the membrane. The obtained values of K_x are $(1.4\pm0.4)\cdot10^6$ and $(4.7\pm1.0)\cdot10^5$ for POPC/POPG and POPC, respectively, indicating that (P)GKY20 interacts with both model membranes with a difference in the binding constant less than one order of magnitude. The small difference on K_x does not account for the observed low cytotoxicity towards eukaryotic cells and good antimicrobial activities against bacteria [178].
Far-UV circular dichroism (CD) spectroscopy experiments were carried out to explore the ability of (P)GKY20 peptide to change its secondary structure upon interaction with model membranes. Thus, CD spectra of (P)GKY20 in buffer or in the presence of POPC and POPC/POPG at lipid-to-peptide ratio of 10, 50 and 100 were recorded. In Fig. 5.3 are reported the CD spectra of (P)GKY20 peptide in buffer and in the presence of SUVs at L/P = 100. In these experiments, SUVs were used in order to minimize the liposomes scattering [223].

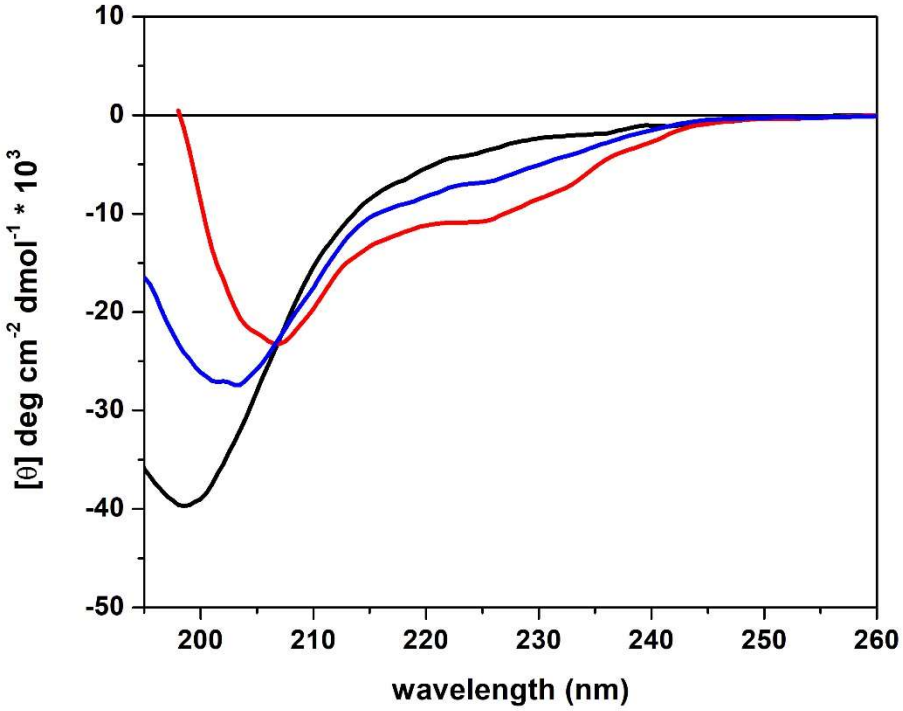

Fig. 5.3 CD spectra of (P)GKY20 peptide in 10 mM phosphate buffer, pH 7.4 (black line) and in the presence of POPC (blue line) and of POPC/POPG (red line) at L/P = 100. All CD spectra were recorded at T = 25°C.

In the absence of liposomes, the CD spectrum of (P)GKY20 peptide is typical of a disordered structure as evidenced by the presence of a minimum at about 200 nm [173] This is a common feature of many linear AMPs [12]. Upon the addition of unilamellar vesicles at L/P = 100, the peptide changes its conformation. In the presence of POPC, the spectrum is characterized by a minimum at about 203 nm. A very weak band appears at about 225 nm. Moreover, the spectrum in the region below 200 nm becomes more positive. In the presence of POPC/POPG vesicles similar features were observed. The band around 200 nm of the random-coil peptide shifts at about 207 nm. The band at 225 nm is now more intense. In addition, the rise of the positive band below 200 nm is evident. These data suggest that the peptide assumes a helix-like conformation in the presence of lipid vesicles. However, the conformational change is more pronounced in the presence of POPC/POPG. Thus, (P)GKY20 assumes a more ordered structure upon interaction with bacterial-like membrane.

To quantify the percentage of secondary structures adopted by the peptide, deconvolution of the recorded CD spectra with the software PEPFIT at different L/P ratios were performed (Table 1) [217,224].

Table 1 Percentage of secondary structure elements of (P)GKY20 peptide obtained from CD spectra deconvolution by means of PEPFIT at different lipid-to-peptide molar ratios.

System	L/P ratio	% random coil	% α-helix	% β-turn
(P)GKY20		100	0	0
+POPC	10	90	0	10
	50	79	14	7
	100	77	13	10
+POPC/POPG	10	84	0	16
	50	34	39	27
	100	37	46	17

An inspection of Table 1 reveals that increasing lipid concentration, the percentage of α-helix content increases in the presence of both lipid vesicles. In the presence of POPC, a maximum value of ~14% is reached. On the contrary, in the presence of POPC/POPG the percentage of α-helix is greater, reaching ~46%. This result is very important as the ability to perturb membrane integrity is related to the ability of the peptide to adopt helical structure [29,34].

5.3.2 The Effects of (P)GKY20 on Stability of Eukaryotic and Bacterial Model Membranes

The effect of the peptide on the stability of lipid bilayer can provide valuable information on the action mechanism as AMPs perform their activity through a destabilization of the membrane. Thus, differential scanning calorimetry (DSC) measurements were performed on model membranes in the presence of (P)GKY20. Since POPC and POPG show a phase transition temperature below 0°C [152,225], not suitable for DSC, they were replaced by DPPC and DPPG, respectively. The DSC thermogram of DPPC and DPPC/DPPG (8/2 mol/mol) multilamellar vesicles in the absence and in the presence of (P)GKY20 at L/P = 10 are reported in Fig. 5.4. The thermodynamic parameters for the gel-to-liquid phase transition obtained from the analysis of the DSC thermogram are reported in Table 2.

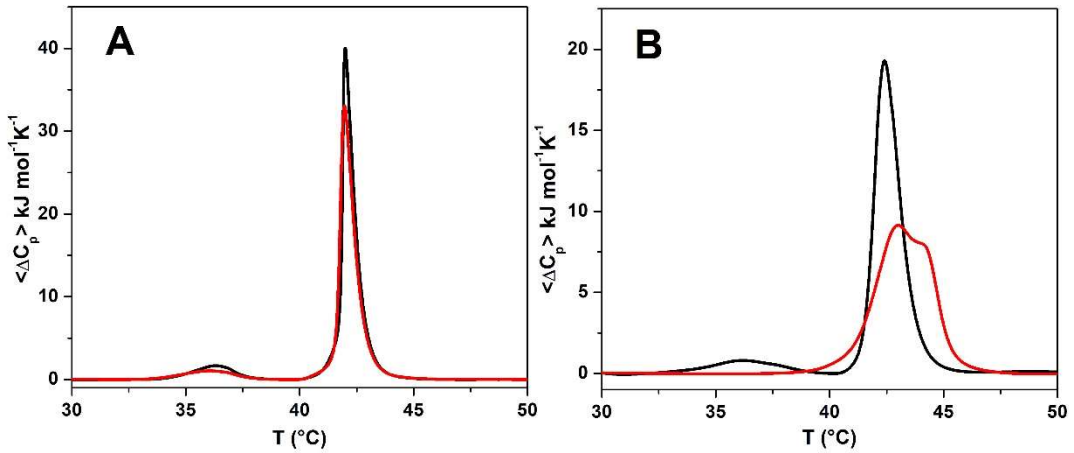

Fig. 5.4 DSC thermograms of multilamellar vesicles of (A) DPPC and (B) DPPC/DPPG in the absence (black line) and in the presence (red line) of (P)GKY20 at L/P = 10. All the experiments were carried out in 10 mM phosphate buffer, pH 7.4.

Table 2 Thermodynamic parameters obtained by means of DSC for the phase transitions of DPPC and DPPC/DPPG (8/2 mol/mol) liposomes in the absence and presence of (P)GKY20 at a lipid to peptide ratio of 10.

System	T_p (°C)[a]	ΔH_p (kJ/mol)[a]	T_m (°C)[b]	ΔH_m (kJ/mol)[b]
DPPC	36.3±0.2	3.6±0.2	42.0±0.1	31.2±1.6
+(P)GKY20	36.0±0.2	2.8±0.3	41.9±0.1	28.4±1.5
DPPC/DPPG	36.1±0.2	1.7±0.3[c]	42.4±0.1	29.5±1.5[c]
+(P)GKY20	-	-	43-44±0.1[d]	28.4±1.4[c]

[a] Enthalpy change and temperature of the pre-transition peak.
[b] Enthalpy change and temperature of the main transition peak.
[c] Normalization against total lipid moles.
[d] The reported temperatures refer to the first and second maxima in the DSC thermogram, respectively.

As stated in section 3.5.2, the DSC thermograms of DPPC and DPPC/DPPG liposomes are quite similar and characterized by the presence of two transitions. The first one is the pre-transition at about 36 °C and the second one, named main transition, at about 42 °C [93]. The pre-transition is due to the rearrangement of lipid polar head groups, whereas the main transition is due to the melting of acyl chains of lipids. Analysis of the DSC profile of DPPC in the presence of peptide reveals very weak perturbation of both transitions. This result is compatible with the low cytotoxicity exhibited by (P)GKY20. On the contrary, the presence of peptide drastically perturbs the thermotropic properties of DPPC/DPPG liposomes. The pre-transition is completely abolished revealing a strong interaction with lipid polar heads. The main transition peak is turned into a multicomponent DSC profile which

consists of two overlapping peaks which indicates phase segregation and the presence of domains of different lipid composition [206]. Moreover, the peak is shifted at higher temperature suggesting that the peptide, interacting with lipid polar heads, stabilizes the membrane without penetrating deeply in the hydrophobic core. Otherwise, a suppression of the main transition peak should be observed [185]. In fact, the enthalpy change of the gel-to-liquid phase transition, due to the melting of lipid acyl chains (Table 2), of DPPC/DPPG liposomes is not affected by the presence of the peptide, confirming that (P)GKY20 peptide is not inserted deeply in the membrane and consequently is not able to perturb the lipid packing.

To better highlight the effects of peptide in the lateral membrane organization and lipid order, fluorescence experiments with the probe Laurdan were performed [220]. Laurdan, an amphiphilic probe, partitions between polar head groups and the hydrophobic core of the membrane with no lipid phase preference [226]. Its fluorescence spectrum is sensitive to the accessibility and mobility of water molecules near itself (water dipolar relaxation process). Accessibility and mobility strictly depend on the packing of lipids in the membrane, making Laurdan a reporter of lipid phases. The fluorescence spectrum of Laurdan is composed by two bands centered at about 440 nm and 490 nm. The emission from 440 nm is attributed to Laurdan molecules in the lipid gel phase, whereas emission from 490 nm is attributed to probe molecules in the liquid phase [220,227]. Generalized Polarization (GP) function (as defined in Materials and Methods, Laurdan Generalized Polarization section) is a way to quantify the degree of order in the membrane. GP values change from about 0.5 to -0.3 passing from gel (more compact, high degree of order) to the fluid-like phase (less compact, low degree of order). In Fig. 5.5 are reported the GP values for Laurdan embedded in DPPC/DPPG large unilamellar vesicles as a function of the temperature in the absence and in the presence of (P)GKY20 peptide at L/P = 10.

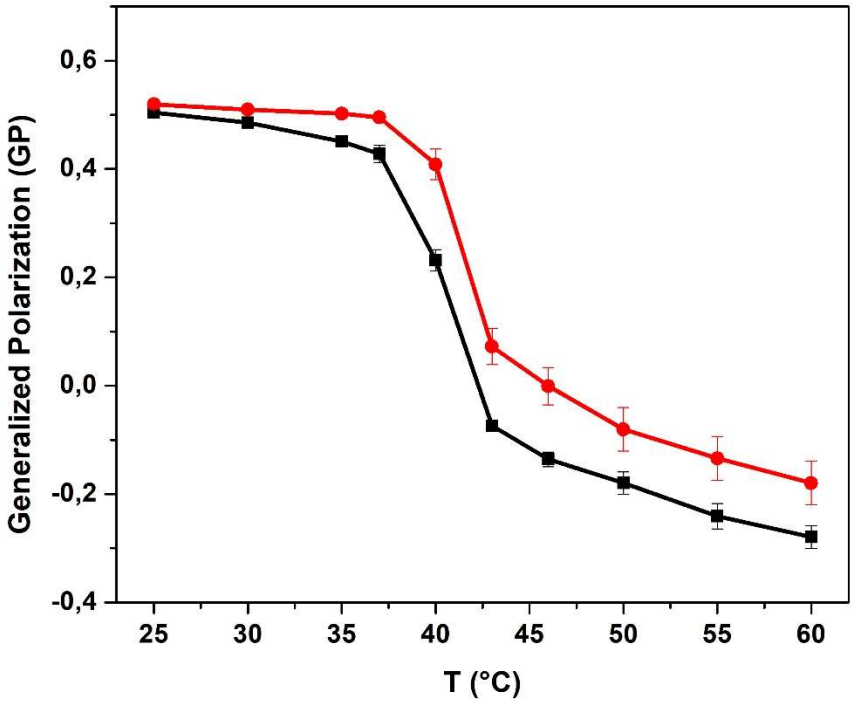

Fig. 5.5 Generalized Polarization (GP) function for Laurdan embedded in DPPC/DPPG (50 μM) large unilamellar vesicles in buffer (black line) and in the presence of (P)GKY20 peptide (red line) at L/P = 10. The temperature was varied in the range 25-60 °C.

Interestingly, the GP values are found to be higher in the presence of (P)GKY20 peptide. This result suggests that the peptide is able to induce order, especially in the fluid-like phase, leading to a more compact membrane. Thus, in good agreement with DSC data, the peptide does not penetrate inside the hydrophobic core of the membrane but interacts superficially at the level of lipid head groups. A similar result was reported for penetratin [227].

Finally, the ability of the peptide to induce order was also checked on POPC/POPG liposomes. In Fig. 5.6 are reported the GP values of Laurdan embedded in POPC/POPG LUVs as a function of peptide concentration at the temperature of 25 °C. For comparison, the same experiment with POPC was also performed. It is important to note that being these vesicles in the fluid phase at 25 °C, GP value in the absence of peptide is lower compared to that obtained for DPPC/DPPG in the same conditions. The reported results confirm that the peptide has only a minor effect on eukaryotic-like liposomes, whereas it orders the POPC/POPG bilayer (as shown for DPPC/DPPG).

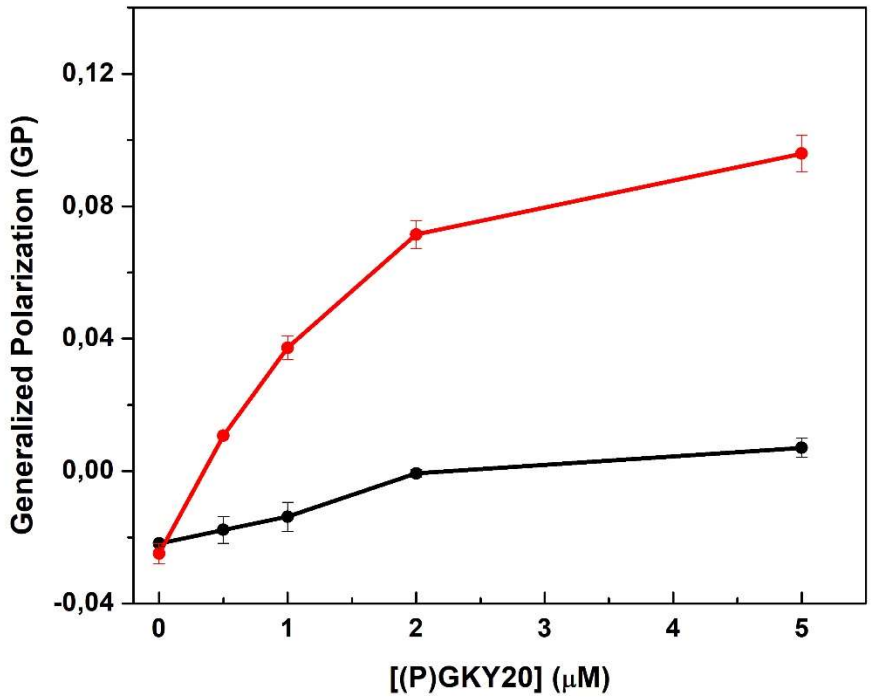

Fig. 5.6 Generalized Polarization (GP) function for Laurdan embedded in POPC (black line) and POPC/POPG (red line) as a function of peptide concentration. All the experiments were carried out in 10 mM phosphate buffer, pH 7.4 at the temperature of 25 °C.

5.3.3 (P)GKY20 Clusters Anionic Lipids: Formation of Lipid Domains

As noted in Fig. 5.4, the DSC profile of DPPC/DPPG vesicles in the presence of (P)GKY20 at L/P = 10 appears composed by at least two overlapping peaks. This suggest the formation of lipid domains. Most likely, the formation of domains is triggered by the preferential interaction of cationic peptide (net charge of +5) with the anionic DPPG lipids [209]. To experimentally verify the ability of (P)GKY20 peptide to induce segregation, a new DSC experiment was performed by replacing DPPG with POPG (see section 3.5.3) forming the mixture DPPC/POPG (8/2 mol/mol). POPG has a transition temperature below 0 °C and is miscible with DPPC. Thus, the presence of POPG can affect the transition of DPPC/POPG only by changing its local distribution. In Fig. 5.7 are reported the DSC thermogram of DPPC/POPG multilamellar vesicles in the absence and in the presence of (P)GKY20 peptide at different lipid-to-peptide ratios.

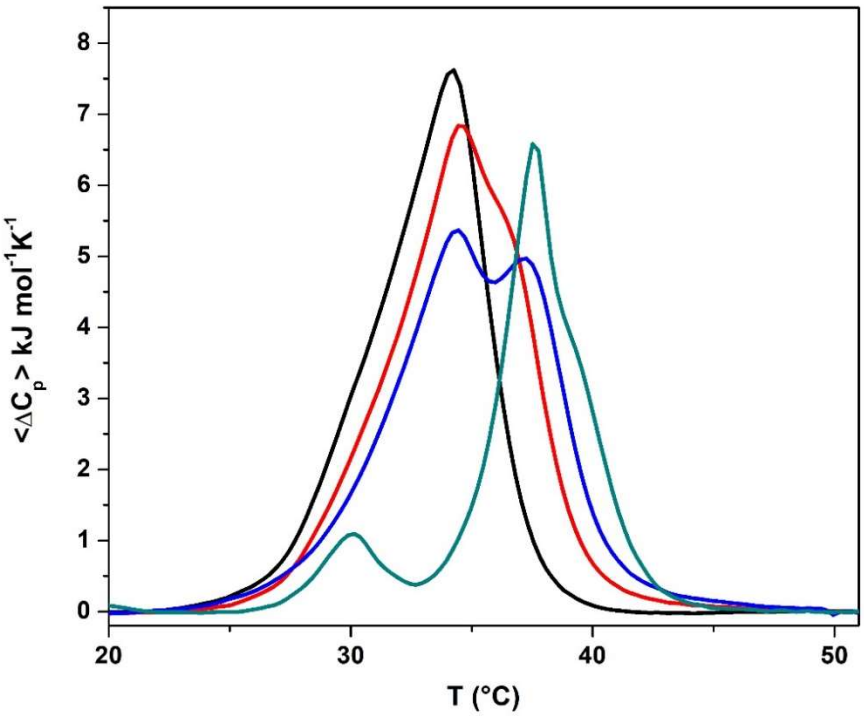

Fig. 5.7 DSC thermograms of DPPC/POPG multilamellar vesicles in the absence (black line) and in the presence of (P)GKY20 peptide at L/P of 100 (red line), 50 (blue line) and 10 (dark cyan line). All the experiments were performed in 10 mM phosphate buffer, pH 7.4.

The DSC profile of this DPPC/POPG mixture has a transition temperature around 34.4 °C. After the addition of the peptide, at L/P = 100, the peak shape changes. The transition temperature is now centered at about 34.6 °C. In addition, it is possible to note the appearance of a little shoulder at about 36.5 °C. At L/P = 50, the DSC profile is now composed by two distinct peaks. The first one has a transition temperature very close to that obtained at L/P = 100 (34.6 °C). The second peak instead, is centered at about 37.2 °C. This phenomenon is more evident after a further addition of peptide, at L/P = 10. In fact, the thermogram appears as formed by at least two well separated peaks centered at lower and at higher temperatures revealing DPPC domains enriched and depleted of POPG, respectively. The peak at lower temperature (~30 °C) can be attributed to a domain of DPPC particularly enriched of POPG. On the other hand, the peak at higher temperature (~37.2 °C) appears to be due to DPPC enriched domains with a DPPC/POPG ratio higher than 8/2 mol/mol. This scenario is also supported by the comparison of DPPC/POPG thermograms obtained by varying the relative lipid proportions and reported in the literature [189]. In fact, the progressive addition of POPG to DPPC liposomes leads to a decrease of

the gel-to-liquid phase transition temperature coupled with a reduction of the peak area (enthalpy change).
Since the (P)GKY20 possess a net positive charge of 5 at pH 7.4, it sounds reasonable that the domains formation is due to its preferential interaction with the negatively charged PGs. To strongly support this hypothesis, DSC experiments with multilamellar vesicles composed by only DPPG were performed. In Fig. 5.8 are reported the DSC thermograms of DPPG liposomes in the absence and in the presence of peptide at L/P = 10.

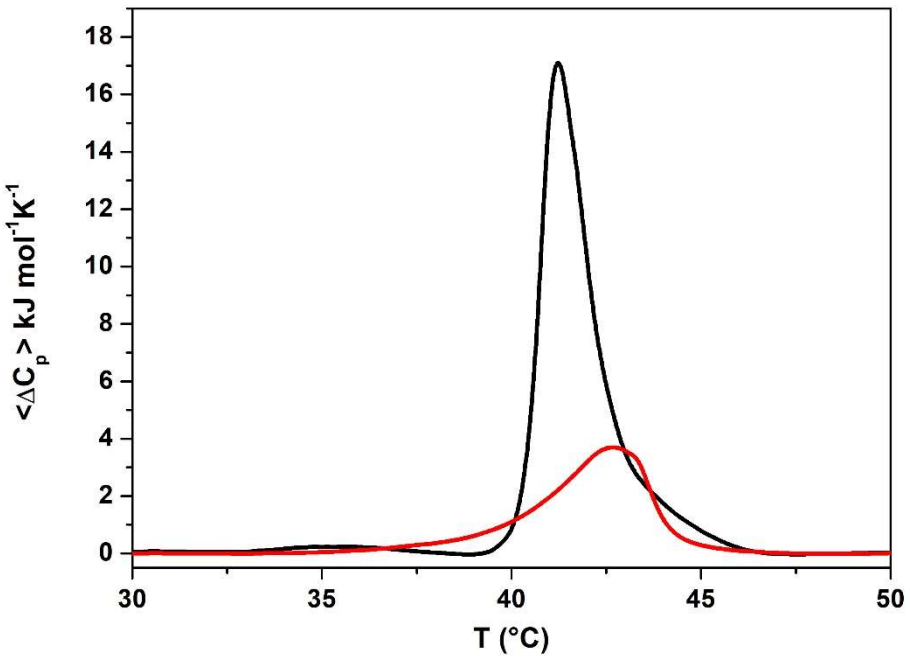

Fig. 5.8 DSC thermograms of DPPG multilamellar vesicles in the absence (black line) and in the presence of (P)GKY20 (red line) at L/P = 10. The experiments were carried out in 10 mM phosphate buffer, pH 7.4.

The DSC profile of DPPG vesicles is characterized by the presence of a pre-transition at about 34.5 °C and a main transition at 41.2 °C, in good agreement with data previously reported [228]. The little shoulder in the temperature range 43-46 °C is typical of DPPG vesicles at low ionic strength [229]. The presence of (P)GKY20 peptide at L/P = 10 causes a strong perturbation of the DSC profile of DPPG. The pre-transition is abolished, revealing a strong interaction on the surface. The gel-to-liquid phase transition temperature increases of about 1.5 °C. Moreover, in this case a perturbation of lipid acyl chains occurred. Upon the interaction with DPPG the

peptide is able to induce a different lipid packing which reflects in a different shape of the DSC thermogram. However, this result clearly indicates that there is a very strong interaction of (P)GKY20 peptide with the anionic DPPG. Combing this result with the observation that the DSC thermogram of pure DPPC is only slightly affected by the presence of peptide (Fig. 5.4, panel A), the preferential interaction of (P)GKY20 peptide with anionic lipids can be revealed.

5.3.4 The Localization of (P)GKY20 Upon Interaction with the Membrane

To explore the ability of peptide to insert in the membrane, fluorescence quenching experiments with acrylamide were performed. Fluorescence emission spectra of the peptide in the absence and presence of LUVs of POPC and POPC/POPG at L/P = 200 were recorded at different acrylamide concentrations. Acrylamide is a water-soluble molecule which cannot partition inside the hydrophobic core of the membrane and it is a quencher of fluorescence emission of Trp [175,190]. According to the equation reported in "Quenching Experiments" section, a plot of F_0/F versus acrylamide concentration gives a straight line whose slope is the Stern-Volmer constant, indicated as K_{SV}. The value of K_{SV} is an index of the degree of exposure to the aqueous solvent of the aromatic residue in the primary sequence of the peptide. Fig. 5.9 shows the Stern-Volmer plots for the acrylamide fluorescence quenching experiments of (P)GKY20 peptide in the absence and in the presence of POPC and POPC/POPG LUVs.

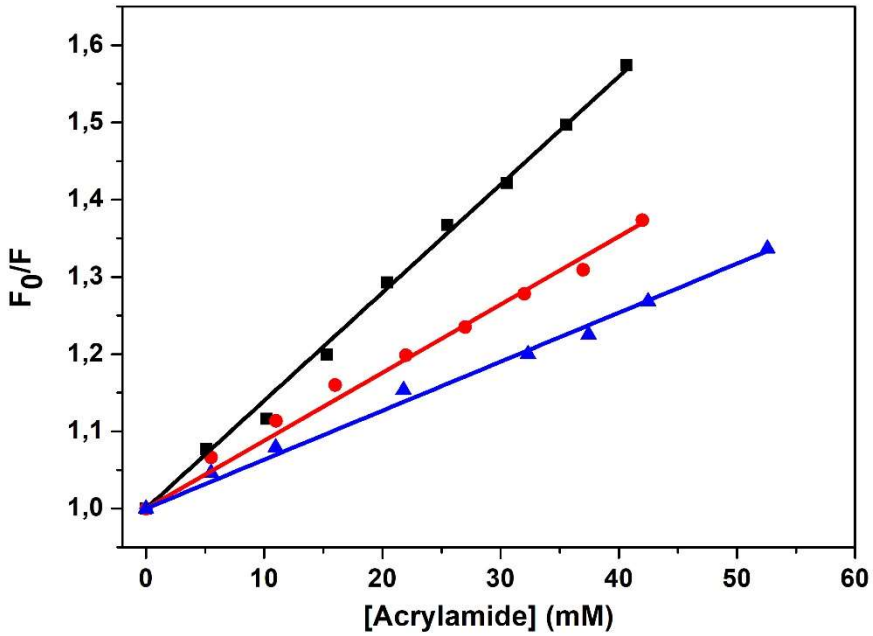

Fig. 5.9 Stern-Volmer plots for the fluorescence quenching of (P)GKY20 peptide in the absence (black line) and in the presence of POPC (red line) and POPC/POPG (blue line) at L/P = 200. All the experiments were carried out in 10 mM phosphate buffer, pH 7.4 at the temperature of 25 °C.

As expected, in the absence of vesicles, the highest value of K_{SV} was obtained (14.0±0.6 M^{-1}), because of the complete exposure to the aqueous solvent of the Trp residue. In the presence of lipid vesicles lower values of the constants were obtained. The values of K_{SV} were 8.8±0.6 M^{-1} and 6.3±0.4 M^{-1} in the presence of POPC and POPC/POPG, respectively. These results indicate that the peptide penetrates, to some extent, both lipid vesicles and that it is slightly deeper inserted into POPC/POPG bilayer. Additional information on penetration ability can be obtained by comparing the shifts on λ_{max} (wavelength position at the maximum of intensity) in the emission spectrum of the peptide, obtained in the titration experiments (Fig. 5.2). In fact, the position of λ_{max} strongly depends on the polarity of the microenvironment in which the residue of Trp is embedded [175]. In particular, the position of λ_{max} shifts from $\lambda_{max} > 350$ nm when a Trp residue is completely exposed to a polar environment (e.g. aqueous solution) to up 310 nm when the residue is in apolar environment (e.g. cyclohexane) [175]. In Fig. 5.10 are reported the normalized emission spectra of (P)GKY20 in buffer and in the presence of POPC and POPC/POPG at L/P = 200.

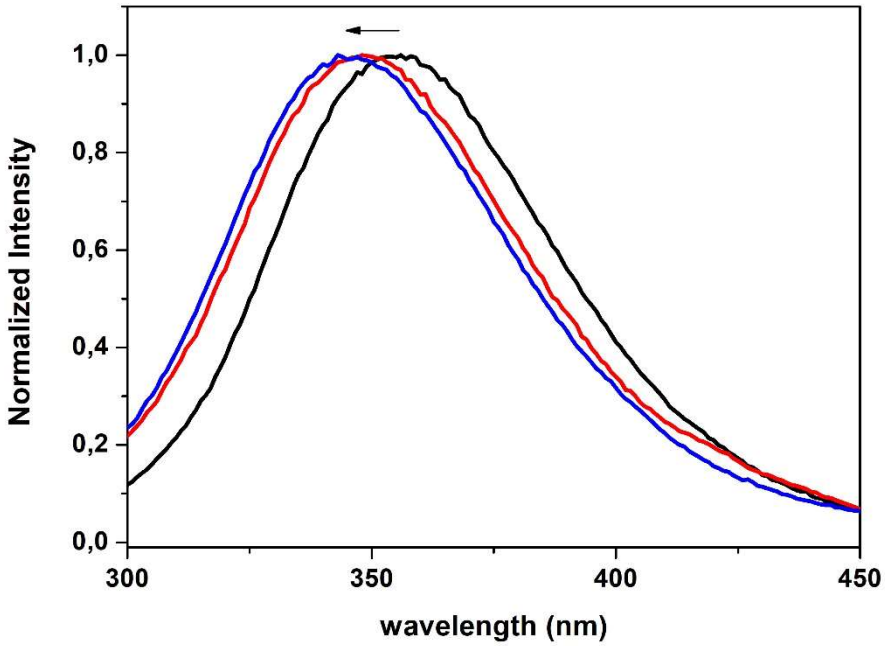

Fig. 5.10 Normalized fluorescence emission spectra of (P)GKY20 peptide in phosphate buffer (black line) and in the presence of POPC (red line) and POPC/POPG (blue line) unilamellar vesicles at a lipid-to-peptide ratio of 200.

An inspection of the spectra reported in Fig. 5.10 revealed that λ_{max} is 355 nm, 349 nm and 346 nm for (P)GKY20 peptide in buffer, in the presence of POPC (L/P~200) and in the presence of POPC/POPG (L/P~200), respectively. This trend indicates that going from buffer to POPC to POPC/POPG, the Trp residue of the peptide is localized in a less polar environment. However, the observed shifts suggest that, despite the strong interaction, the aromatic residue is not significantly inserted in the hydrophobic core of both membranes, as observed for other peptides [230,231]. Thus, it is possible to conclude that (P)GKY20 doesn't penetrate deeply inside the hydrophobic core of the membrane and it remains localized, probably, at the membrane-water interface. These data support the previous hypothesis reported in section 5.3.2.

5.3.5 Visualizing the Effect of (P)GKY20 on Bacterial Model Membrane: Atomic Force Microscopy

Atomic Force Microscopy (AFM) is a powerful technique with which the effects of the peptide on model membranes can be directly visualized [232]. In Fig. 5.11 are

reported the AFM images of supported bilayer composed by POPC/POPG in the absence and in the presence of 50 µM and 100 µM of (P)GKY20 peptide. The experiments were carried out in collaboration with Prof. Roland Winter, Technical University of Dortmund (Germany). These peptide concentrations roughly correspond to L/P = 50 and L/P = 25. Since after the formation of the supported bilayer, the fluid cell was rinsed with buffer to remove unspread liposomes, these ratios should be considered as a very rough over-estimation of the lipid-to-peptide ratios.

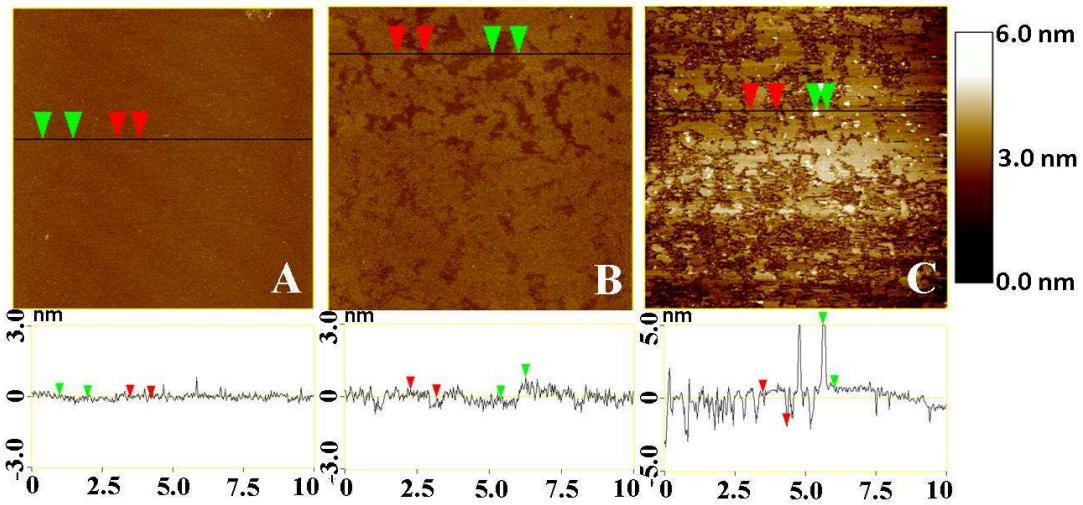

Fig. 5.11 AFM height images of a POPC/POPG bilayer (A) before and after the addition of (B) 50 µM and (C) 100 µM of (P)GKY20 peptide solution into the AFM fluid cell. In the lower part the section profiles of the corresponding AFM images are reported.

The interaction process was followed by imaging the same membrane region 60 min after the addition of the peptide. Before peptide addition, it was checked if a uniform bilayer has formed on the mica support. The flat image reported in Fig. 5.11, panel A, indicate that a uniform bilayer was obtained. Upon the addition of 50 µM of peptide, the formation of dark regions was observed (Fig. 5.11, panel B). The inspection of the section profile of the acquired image revealed that, on average, the height of the dark regions is slightly smaller compared to that of surrounding lipid regions (the difference is less than 1 nm). Such scenario is consistent with the formation of lipid domains, as suggested by DSC measurements reported above. Even more dramatically, upon the addition of a 100 µM peptide solution, complete disruption of the membrane took place (Fig. 5.11, panel C). In particular, the line profile reveals that the average height of the bilayer has become thinner and that part of the lipids has been extracted (as indicated by the occurrence of deep dips) forming

mixed peptide-lipids clusters - most likely of micellar type – remaining, at least in part, localized on the surface of the membrane.

5.3.6 The Effects of (P)GKY20 on Size and Morphology of Lipid Vesicles

Dynamic light scattering (DLS) measurements were carried out to verify the influence of peptide on the size of lipid vesicles. In Fig. 5.12 are reported the hydrodynamic radius distribution functions for POPC and POPC/POPG in the absence and in the presence of (P)GKY20 peptide at different L/P ratios.

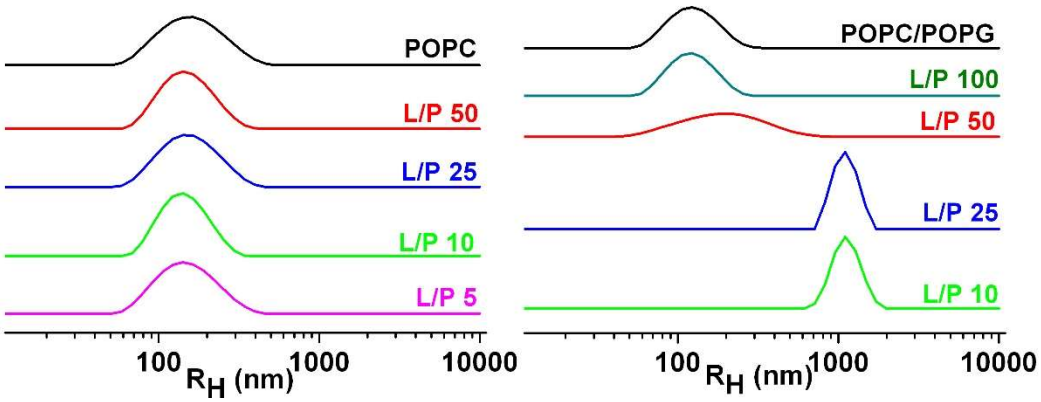

Fig. 5.12 Hydrodynamic radius distribution functions for POPC (left panel) and POPC/POPG (right panel) large unilamellar vesicles as a function of lipid-to-peptide mole ratio. All the experiments were carried out in 10 mM phosphate buffer at the temperature of 25 °C.

In the absence of peptide, both lipid systems form a single population of LUVs with similar average hydrodynamic radius (R_H) of about 120 nm, as a result of the extrusion procedure. The addition of peptide to POPC vesicles does not affect their size distribution, even at very high peptide concentration. This result confirms the low perturbation activity with eukaryotic-like membrane. For POPC/POPG the addition of (P)GKY20 peptide does not affect the size distribution at L/P = 100. At L/P = 50 a slight modification occurred and starting from L/P = 25 the presence of a population of liposomes with a very large R_H was observed. These results suggest that the peptide induces the formation of large aggregates or it favours the fusion (or even hemifusion) among liposomes composed by POPC/POPG.
Unfortunately, from this experiment it is not possible to know if the formation of the large population is due to an aggregation or a (hemi)fusion process among lipid vesicles. A way to try to answer this question is to verify the reversibility of the observed process. If an aggregation process occurs, a high dilution of the lipid suspension should favour the dissociation of vesicles. In fact, due to a high energetic cost is very unlikely that two or more fused vesicles separate in distinct ones. In Fig.

5.13 are reported the hydrodynamic radius distribution functions for POPC/POPG LUVs in the presence of peptide at L/P = 10 before and after 10-time dilution with phosphate buffer. For comparison, the sample composed by POPC/POPG without the peptide is also reported.

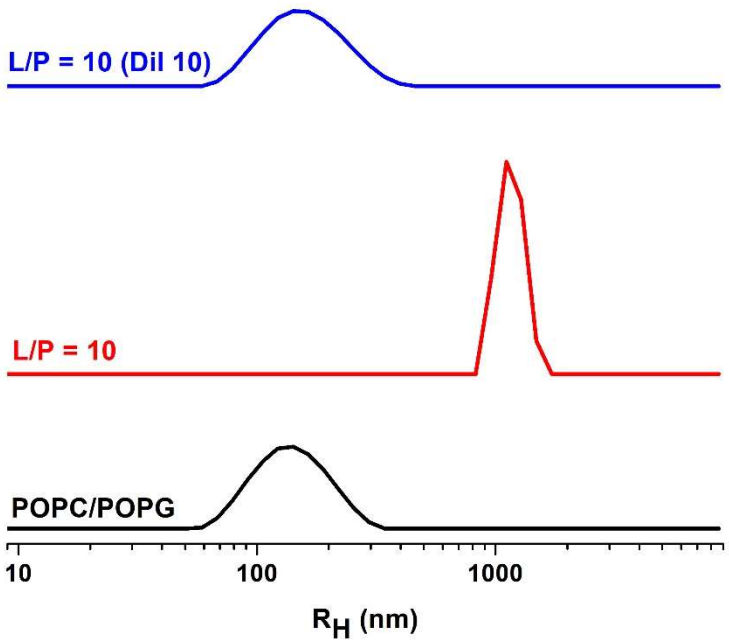

Fig. 5.13 Hydrodynamic radius distribution functions for POPC/POPG unilamellar vesicles: i) in buffer (black line), ii) in the presence of peptide at L/P = 10 (red line) and iii) as the same in ii) but diluted 10 times (blue line).

Surprisingly, the formation of the large population is a reversible process. This observation strongly supports the idea that an aggregation process among liposomes took place and not (hemi)fusion. This unusual phenomenon was already observed for the antimicrobial peptide LAH4 [233] and it was ascribed to the ability of the positively charged peptide to neutralize the negative charge of liposomes and the formation of weak peptide-peptide interactions between peptides on different liposomes.

To directly visualize vesicles topological changes and further support the hypothesis of aggregation, confocal fluorescence microscopy experiments were carried out, in collaboration with Prof. Roland Winter at the Technical University of Dortmund (Germany). The experiments were performed using giant unilamellar vesicles (GUVs) labelled with the fluorescent probe N-Rh-DHPE. In Fig. 5.14 are reported

the images of POPC/POPG GUVs before and after the addition of 10 μM of (P)GKY20 peptide.

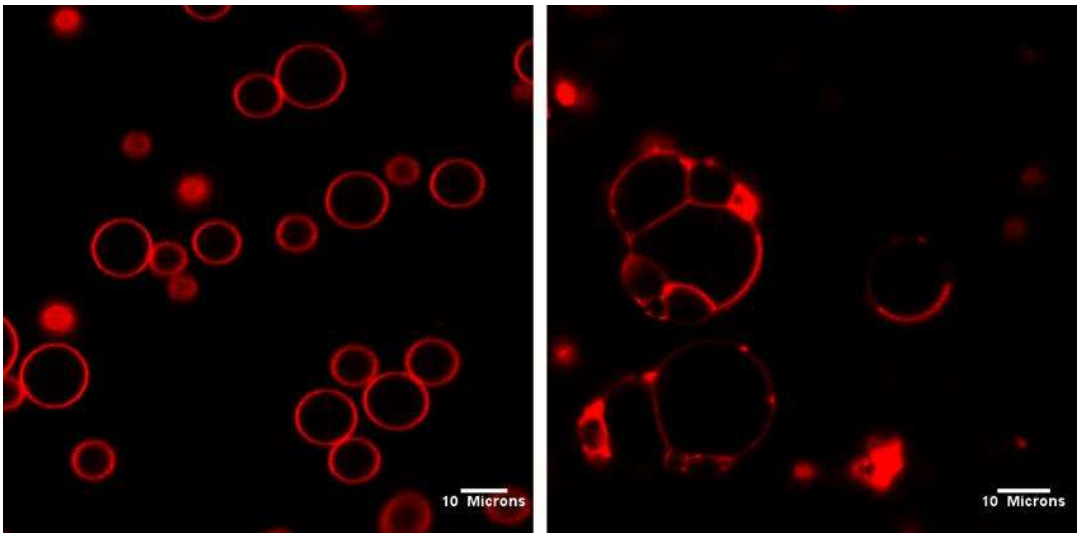

Fig. 5.14 Confocal fluorescence microscopy images of POPC/POPG GUVs before (left) and after (right) the addition of 10 μM of peptide solution.

The image of GUVs before the addition of the peptide confirms that the electroformation protocol was successfully applied and giant unilamellar vesicles were formed. Upon the addition of peptide (right panel), dramatic changes both in size and shape of GUVs were observed. As suggested by DLS measurements, the peptide induces the formation of aggregates. Moreover, upon aggregation, the shape of vesicles changes, revealing the ability of the peptide to modulate the morphology of the lipid vesicles. These results reflect the ability of the peptide to mediate lipid-lipid interactions [233]. Most likely, similar peptide-mediated interactions are involved in the lipid extraction process and formation of mixed peptide-lipid micelles, noted in the AFM measurements.

5.4 Discussion

Antimicrobial peptides (AMPs) comprise a particular class of amino acids-based antibiotics [52]. Since they interact in a non-specific way with the lipid matrix of the bacterial membrane [12], they can overcome the problem of resistance to antibiotics in bacteria [6,8], thereby representing an alternative to conventional drugs. Understanding the molecular basis of the interaction process with the membrane is mandatory for biomedical applications. Moreover, such knowledge is critical for the development on AMPs with improved antimicrobial activity and low cytotoxicity.

The antimicrobial peptide (P)GKY20 is a peptide composed by 21 amino acids. It is modelled on the Gly^{271} to Ile^{290} sequence in the C-terminus region of the human thrombin [178]. It possesses a net positive charge of 5 at physiological pH of 7.4, a low hemolytic activity and a good antimicrobial activity especially against gram-negative bacteria. However, the underlying mechanism of its action is still unknown. Thus, a detailed biophysical study was carried out to elucidate the interaction process of (P)GKY20 with model membrane systems. Liposomes with two different lipid composition were used. Liposomes composed by POPC can be considered as a model of the eukaryotic plasma membrane. Liposomes composed by a mixture of POPC and POPG were used as simplified model of the cytoplasmic bacterial membrane, since it is mainly composed by zwitterionic and negatively charged lipids [12,234].

The binding isotherms obtained by means of fluorescence experiments (Fig. 5.2) revealed that (P)GKY20 is able to interact with both model membranes with binding constants which differ less than one order of magnitude. This small difference does not account for the low hemolytic activity and good antimicrobial activity of (P)GKY20. Instead, circular dichroism experiments (Fig. 5.3) clearly reveal a difference in the secondary structure adopted by the peptide. The deconvolution of CD spectra indicate that the percentage of α-helix is sensitive higher in the presence of POPC/POPG (46%) than in the presence of POPC (14%). Thus, the capacity of (P)GKY20 to adopt a helix structure could be related to membrane perturbation activity [29,34,235,236]. The DSC measurements (Fig. 5.4) carried out on DPPC and DPPC/DPPG vesicles confirmed the different perturbation ability of (P)GKY20 peptide on eukaryotic and bacterial model membranes. The presence of peptide does not perturb the thermotropic properties of DPPC liposomes. This result was confirmed by fluorescence experiments with the probe Laurdan, where only a slight increase of the GP value on POPC was detected. In addition, DLS measurements showed that the peptide does not perturb the size distribution of POPC LUVs. Thus, in good agreement with the low cytotoxicity of (P)GKY20, the peptide is able to interact with eukaryotic model membranes, but the lack of a definite secondary structure upon interaction prevent the membrane destabilization.

In the case of bacterial model membrane composed by PCs and PGs, the peptide changes significantly its secondary structure adopting a α-helix structure, as suggested by CD experiments. Most likely, the conformational change leads to an amphipathic structure which facilitates the interaction with and the perturbation of the membrane (section 1.2). The value of the mole fraction partition constant (K_x) for the interaction with POPC/POPG is $(1.4\pm0.4)\cdot10^6$. From this value is possible to determine the fraction of bound peptide in the CD experiments at L/P = 100 (Fig. 5.3). A simple calculation reveals that about 98% of peptide should be bound to the membrane. Since the deconvolution of the CD spectra at L/P = 100 indicate that the

percentage of α-helix is 46%, this means that about half of the peptide amino acids should be in helical conformation. Most likely, the portion of peptide that adopts the helical structure comprises the amino acids RLKKWIQKVI on the C-terminus side of the peptide. This idea is supported by several observations. First, this region leads to a perfect amphipathic structure when represented by means of helical wheel projection (Fig. 5.15), as evidenced by the calculated hydrophobic moment $<\mu_H>$ of 0.778. It is widely accepted that linear AMPs adopt an amphipathic helical structure upon binding to membrane and it is fundamental for the antimicrobial activity.

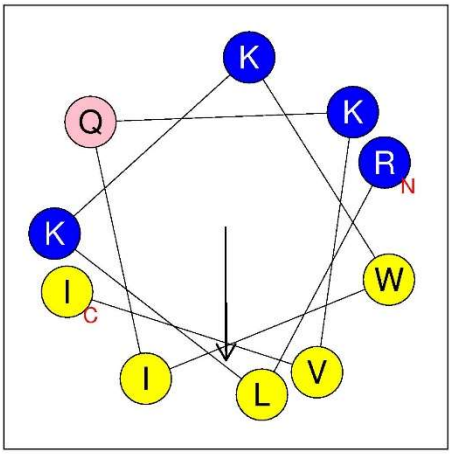

Fig. 5.15 The helical wheel projection of the RLKKWIQKVI segment of (P)GKY20. The arrow represents the hydrophobic moment vector (0.778). Yellow circles represent hydrophobic residues, blue circles positively charged residues and pink circles polar residues with no charge. The projection was made by means of Heliquest software [40].

Second, it is interesting to note that the same region in the human thrombin is in the α-helix conformation. The other part assumes a small β-strand with turns and unstructured portions (Fig. 5.1) [216]. Finally, a systematic study carried out on the antimicrobial potency of (P)GKY20 analog peptides of different lengths showed that the peptide composed by GKYGFYTHVF sequence has no antimicrobial activity [178]. This region corresponds to the N-terminus region of (P)GKY20. Thus, on these bases it is possible to speculate that the region which adopts the amphipathic helical structure in the peptide (P)GKY20 is the C-terminus portion with the sequence RLKKWIQKVI.

The interaction with POPC/POPG liposomes and the conformational change of (P)GKY20 peptide has several consequences on the stability of the bilayer. Differential scanning calorimetry measurements on DPPC/DPPG multilamellar vesicles suggest that, upon interaction, (P)GKY20 peptide is able to induce the

formation of lipid domains which differ in lipid composition and melt at different temperatures (Fig. 5.4). The formation of domains was confirmed by DSC experiments where DPPG was replaced by POPG (Fig. 5.6). In these experiments, the progressive addition of (P)GKY20 induces the formation of DPPC enriched and POPG enriched domains. At L/P = 10 the DSC thermogram is composed by two well defined peaks which gave two transitions at higher and lower temperature. The peak at higher temperature could be attributed to the DPPC enriched domain. On the contrary, the peak at lower temperature could be due to a DPPC domain particularly enriched of POPG. The formation of domains has a deep impact on the stability of the membrane. The interface among domains act as defects in destabilizing the membrane promoting membrane permeabilization [12,87,199,200]. The formation of domains is triggered by the preferential interaction of the cationic (P)GKY20 peptide with the negatively charged lipids PGs, as observed in many other cases [86,88,198,237]. The selective interaction with anionic lipids was revealed by DSC measurements with liposomes composed by only DPPG (Fig. 5.8). In fact, a strong perturbation of the DSC thermogram was observed. In contrast, the DSC thermogram of pure DPPC is only slightly affected.

The DSC results obtained for DPPC/DPPG vesicles in the presence of peptide suggested additional features on the action mechanism. An increase of the transition temperature compared to that in the absence of peptide strongly suggest that the peptide is not able to penetrate inside the hydrophobic core of the membrane but remains at the membrane-water interface. This is also supported by the observation that the enthalpy change of DPPC/DPPG liposomes is not affected by the presence of peptide. The interaction on the surface leads to a more compact membrane, because the presence of peptide screens the repulsion among lipid head groups [185,212]. This scenario is supported by several experiments. The variation of the GP parameter for Laurdan embedded in DPPC/DPPG LUVs confirms this idea (Fig. 5.5). In fact, in the presence of peptide at L/P = 10, the GP parameter is higher, clearly indicating that the peptide leads to a more compact membrane which can be rationalized by only assuming that the peptide cannot penetrate deeply in the membrane [227]. The same experiment on the GP values obtained for Laurdan in POPC/POPG as a function of peptide concentration led to the same conclusion. The localization of the peptide at membrane-water interface was finally supported by fluorescence quenching experiments and the spectral shifts in the λ_{max} of the fluorescence emission spectra of (P)GKY20 (section 5.3.4). In fact, usually peptides which insert in the hydrophobic core of the membrane give lower values of K_{SV} [238,239]. In addition, the position of λ_{max} is only 346 nm. The shift is quite modest compared to the peptide in the absence of lipid vesicles (355 nm). This result indicate that the peptides is inserted at some extent in the membrane, but not inside the

hydrophobic core, otherwise a more consistent shift toward shorter wavelengths should be observed [175].
Atomic force microscopy (AFM) experiments gave the possibility to direct visualize the effects of (P)GKY20 on the bacterial model membrane composed by POPC/POPG (Fig. 5.11). The acquired images revealed the formation of lipid domains upon the addition of 50 μM (P)GKY20, as evidenced in DSC experiments. In fact, the presence of some dark regions slightly smaller compared to the surrounding lipids was detected. At 100 μM of peptide solution (Fig. 5.11, panel C), a complete destabilization of the membrane occurred. The inspection of the corresponding line profile reveals that the in some membrane regions lipids have been extracted (as indicated by the occurrence of deep dips) forming peptide-lipid clusters which can remain (in part) localized on the surface of the membrane justifying the very high peaks in the section profile. The AFM results pointed out the peptide-concentration dependent nature of the action mechanism of (P)GKY20, a common feature of many AMPs [12].
In agreement with the DSC and AFM results, it is possible to conclude that domain formation induced by recruiting anionic lipids is a crucial step in the mechanism of the (P)GKY20 peptide-membrane interaction process. It is known that the packing defects at the boundaries of such domains represent instability regions of the lipid bilayer [12,200]. The concomitant increase of line tension at domain boundaries could lead to further accumulation of peptide and formation of larger domains. It is reasonable to assume that the increase in the cross-sectional area per lipid in the PG-enriched domains due to peptide binding induces a local positive curvature of the membrane, facilitating lipid extraction and formation of mixed peptide-lipid micelles as observed by AFM experiments (Fig. 5.11).
Finally, dynamic light scattering experiments evidenced that (P)GKY20 is able to induce aggregation of POPC/POPG liposomes. As reported in section 5.3.6, it was found that the aggregation of liposomes is a reversible process suggesting that only weak interaction among peptides on different liposomes are involved. A similar phenomenon was reported for the peptide LAH4 [233] and it was ascribed to the ability of the positively charged peptide to neutralize the negative charge of liposomes. For LAH4 peptide it was conclude that the association of liposomes is only driven by electrostatic interactions. This is because the aggregation was only observed at a well-defined L/P ratio where the overall liposome charge was neutralized by the positive charge of the peptide. In fact, below this L/P, the peptide causes an excess of positive charge which leads to the disaggregation of liposomes [233]. In the case of (P)GKY20, a complete neutralization of liposomes charge should be accomplished at L/P = 25 where the formation of aggregates was observed. With the further addition of peptide (L/P = 10) the disaggregation of liposomes was not observed, as in the case of LAH4 peptide. This observation strongly indicates

that the aggregation of liposomes is mediated not only by electrostatic interactions but also by others weak peptide-peptide interactions on different liposomes, as hydrophobic ones. The application of confocal fluorescence confirmed the formation of aggregates. In addition, it was revealed the ability of peptide to modulate the morphology of lipid vesicles. Overall these results strongly support the idea that the peptide can modulate interactions among liposomes and, probably, similar forces are involved in the lipid extraction and formation of mixed peptide-lipid clusters as detected by AFM. The uncommon capacity of (P)GKY20 peptide to induce reversible aggregation merits further attentions and it will be explored in detail in the future.

To summarize, the combined array of data suggests that probably the (P)GKY20 peptide act through a carpet mechanism [80]. The (P)GKY20 peptide, remaining at the membrane-water interface, induces irreversible lesions to the bilayer through a lipid extraction process promoted by the accumulation of peptides at domains enriched in anionic lipids. On these bases, it is possible to summarize the key steps in the action mechanism of (P)GKY20 on bacterial model membrane as follows (Scheme 1): i) recruitment and preferential electrostatic binding of the random-coil peptide to negatively charged lipids, coupled with peptide folding in a helix-like conformation; ii) subsequent formation of large domains enriched in negatively charged lipids and peptides, which results in a local positive curvature of the membrane; iii) finally, upon reaching a certain threshold concentration of the peptide, through peptide-mediated lipid-lipid interactions, (P)GKY20 extracts lipids from the bilayer leading to a complete disruption of the membrane and formation of lipid-peptide clusters which can remain, in part, on the surface of the membrane.

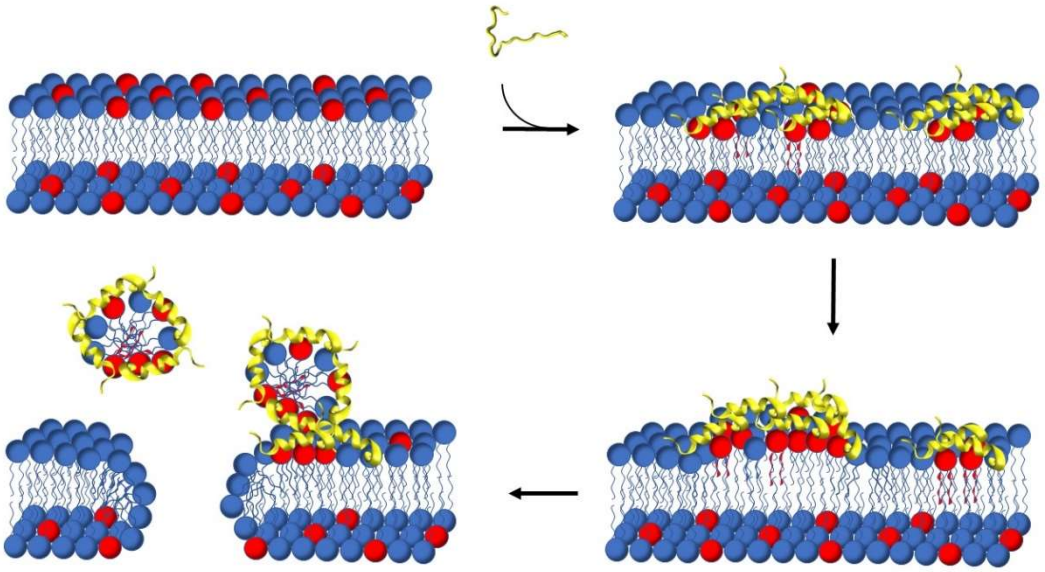

Scheme 1. Proposed mechanism of action of the (P)GKY20 peptide with bacterial model membranes: i) preferential binding of the disordered peptide to the negatively charged lipids coupled with peptide folding adopting a helical conformation; ii) consequential formation of large domains enriched of negatively charged lipids and peptides which leads to local positive membrane curvature; iii) finally, upon reaching a threshold peptide concentration, through peptide-mediated interactions, (P)GKY20 extracts lipids from the lipid bilayer leading to formation of mixed lipid-peptide micelles and complete disruption of the membrane.

The reported data have shed a first light on the molecular basis of the action mechanism of the natural antimicrobial peptide (P)GKY20, pointing out important features at the level of peptide-lipid interactions. Such knowledge can be useful in the development of new peptides serving as antimicrobial agents for biomedical applications.

Chapter 6

The Complexation of (P)GKY20 Peptide with Cyclodextrins

6.1 Introduction

In this chapter are reported some results concerning the interaction of the antimicrobial peptide (P)GKY20 with cyclodextrins.
As stated in section 1.5, the final goal in studying AMPs is their use in medicine. However, the application of natural amino acids containing peptides is seriously limited. In fact, peptides are not chemically e physically stable. They are prone to hydrolysis and oxidation which can modify the biological activity. In addition, once inside the human body, proteases [92] can cleave the peptide at specific site or at the C- or N- terminus, reducing the peptides' half-life in the plasma. Finally, the possibility that AMPs can interact with serum proteins (e.g. human serum albumin) should be considered [240]. Clearly, all these aspects inevitably lead to the unfavorable pharmacological profile of antimicrobial peptides. Encapsulation of AMPs could represent a way to protect the peptides improving their pharmacological properties. Cyclodextrins (CDs) are cyclic oligosaccharides [241] widely used in pharmaceutical, food and cosmetic industries as drug encapsulating agents to increase solubility and stability of compounds [242,243]. They are composed by glucopyranose units linked through α-(1-4)-glycosidic bonds. There are three naturally occurring CDs: α-, β- and γ-CD composed by 6, 7 and 8 glucopyranose units, respectively [241] (Fig. 6.1).

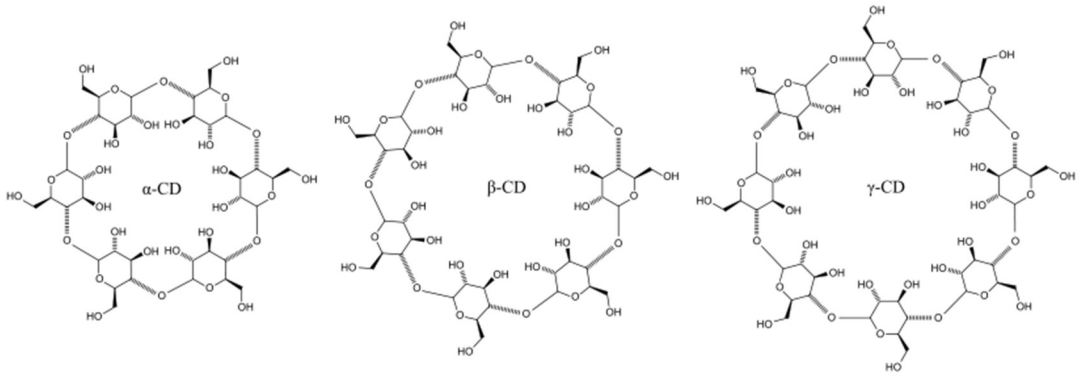

Fig. 6.1 The chemical structures of natural cyclodextrins: α-, β- and γ-CDs. Taken from https://en.wikipedia.org/wiki/Cyclodextrin.

Given the low solubility of natural CDs, a series of modified ones were developed [241]. Several chemical groups, such as hydroxypropyl o methyl, can replace the OH

groups in the sugar rings improving the affinity for the peptide and/or enhancing its solubility and safety. CDs can form inclusion complex in solution where a lipophilic guest molecule inserts inside the hydrophobic cavity of the sugar ring [244]. In proteins and peptides, CDs interact with hydrophobic side chains of amino acids. The type of side chains incorporated inside the cavity depends on the size of CDs. The most used CDs are the β-CDs which have the right size to accommodate aromatic residues, such as tryptophan and tyrosine [245]. The extent of complexation is strongly dependent on the binding constant (K_b) between peptide and CDs [241]. It is known that the binding constants for such interaction is very low (in the range 50-2000 M^{-1}) [244]. Thus, to reach an efficient extent of complexation, a high amount of CD is required. Even if CDs are regarded as safety compounds, a high amount of the sugar could have adverse effects on human health. In fact, the ability of CDs to extract lipids [241,245], such as cholesterol, from the membrane is widely known. Thus, it is important to find, for a particular drug (such as AMPs), the right CDs which can interact with a suitable binding constant (neither too much low, nor to much high) without affecting the drug properties. In this way a good encapsulation efficiency can be reached by using a small amount of CDs.

In this chapter, some preliminary data on the characterization of the interaction between the AMP (P)GKY20 and the anionic sulfobutylether-β-cyclodextrin (SBE-β-CD) serving as encapsulating agent are reported. For comparison, the interaction with the widely used [246,247] neutral hydroxypropyl-β-cyclodextrin (HP-β-CD) was also explored. The chemical structures of SBE-β-CD and HP-β-CD are reported in Fig. 6.2

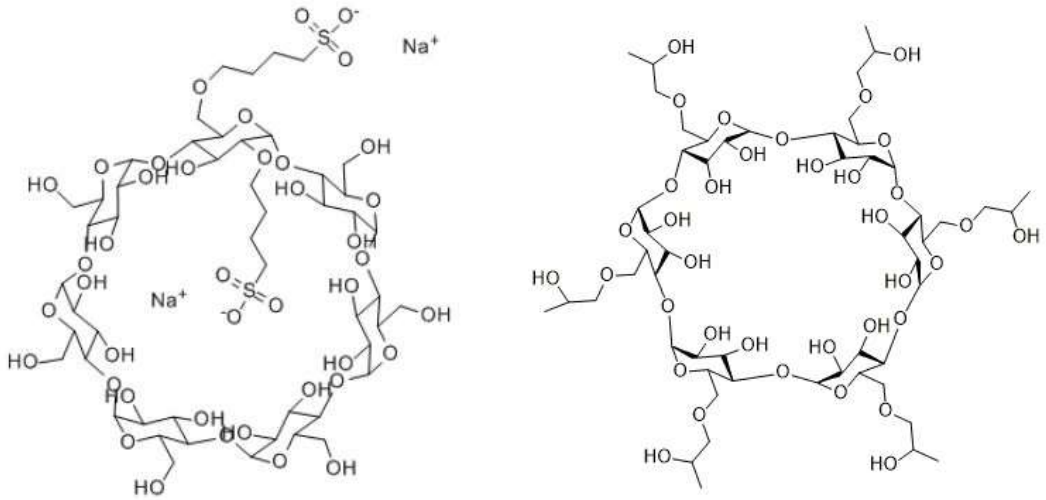

Fig. 6.2 The chemical structures of SBE-β-CD (left) and HP-β-CD. Adapted from www.medkoo.com

In chapter 5 it was shown that the antimicrobial peptide (P)GKY20 is able to drastically perturb the bacterial model membrane, whereas no effect on eukaryotic

model membrane was detected. The reported results well correlate with the observed good antimicrobial activity and the low cytotoxicity [178] making (P)GKY20 a good candidate for biomedical application. However, being susceptible to the proteases action, (P)GKY20 is not stable [93]. Thus, it could be useful to find a suitable encapsulating agent that can protect the peptide without compromising its biological activity.
The obtained results indicate that the (P)GKY20 interacts with the anionic SBE-β-CD forming a 1:1 complex. Most likely the interaction takes place through the formation of an inclusion complex where the Trp residue of the peptide inserts inside the hydrophobic cavity of the sugar ring. It was found that the binding constant (K_b) is in the order of 10^4 M^{-1}, which is sensitive higher respect to the binding constant found for the widely used neutral HP-β-CD (~ 10^2 M^{-1}). This difference could be ascribed to the presence of sulfobutylether groups which confer a net negative charge to SBE-β-CD enhancing the affinity for the positively charged peptide. Finally, differential scanning calorimetry data revealed that the peptide, even in the presence of SBE-β-CD, is still active towards the bacterial model membrane.
These preliminary data demonstrated that, in principle, SBE-β-CD could be used as efficient encapsulating agent for the (P)GKY20 peptide with the intent to improve its pharmacological properties.

6.2 Materials and Methods

Materials. The antimicrobial peptide (P)GKY20 was obtained as described in the Materials section 5.2. The sulfobutylether-β-cyclodextrin (SBE- β-CD, MW: 1451 Da, average degree of substitution: 0.28) was purchased from Sigma Aldrich Chemical. The hydroxypropyl-β-cyclodextrin (HP-β-CD, MW: 1501 Da, average degree of substitution: 0.85-1) was purchased from CycloLab (Budapest, Hungary). The lipids 1,2-dipalmitoyl-*sn*-glycero-3-phosphocholine (DPPC), 1,2-dipalmitoyl-*sn*-glycero-3-phospho-1'-*rac*-glycerol (DPPG) were obtained from Avanti Polar Lipids Inc and used without further purifications. Chloroform and methanol were purchased from Sigma Aldrich Chemical. The phosphate buffer, 10 mM pH 7.4, was prepared by using deionized water.

Liposomes Preparation. Appropriate amounts of lipids were weighed and dissolved in a chloroform/methanol (2/1 v/v) mixture. Then, a thin film was produced by evaporation of the organic solvent with nitrogen gas. To remove final traces of organic solvent, the sample was placed under vacuum overnight. Then, the sample was hydrated with an appropriate volume of 10 mM phosphate buffer, pH 7.4, and vigorously mixed obtaining a suspension of multilamellar vesicles (MLVs). Liposomes composed by a mixture of DPPC/DPPG (8/2 mol/mol) were prepared as

simplified model of the cytoplasmic bacterial membrane, since the bacterial membrane is mainly composed by zwitterionic and negatively charged lipids [12].

Fluorescence. Fluorescence spectroscopy experiments were carried to check the ability of the (P)GKY20 peptide to bind to SBE-β-CD and HP-β-CD. Fluorescence emission spectra were acquired by means of K2 spectrofluorometer from ISS (Champaign, Illinois, USA), using a quartz cuvette with a path length of 1 cm at the temperature of 25 °C and under constant stirring. The excitation wavelength was set to 280 nm and emission spectra were recorded in the range 315-525 nm. The slit widths for excitation and emission wavelengths were set both to 8 nm. The titrations were performed by recording the spectra of a solution of peptide at fixed concentration of 4.5 μM and SBE-β-CD concentrations ranging from 0 to 800 μM. In the case of HP-β-CD, the cyclodextrin concentration was in the range 0-24 mM. The binding curve was obtained by plotting F_0/F versus cyclodextrin concentration, where F_0 is fluorescence intensity of the peptide in the absence of CD at 355 nm and F is the intensity in the presence of CD at the same wavelength. The binding constant was determined by fitting the experimental points with a 1:1 binding model equation as reported in detail in [248].

Job's Plot. To verify and confirm the binding stoichiometry between (P)GKY20 and SBE- β-CD, the continuous variations method (also known as Job's plot) was applied [176] by means of UV/Vis spectrophotometry. The UV/Vis spectra were recorded on a Cary 5000 from Agilent Technologies by using a 1-cm quartz cuvette at the temperature of 25 °C. In this experiment, the mole fraction of the peptide was varied from 0.1 to 1 and the total molar concentration (peptide + CD) was fixed at 200 μM. As blank measurements, the same experiment was repeated in the absence of SBE-β-CD. A plot of $\Delta A=A_{complex}-A_{peptide}$ versus the peptide mole fraction (where $A_{complex}$ is the absorbance of the complex at 280 nm and $A_{peptide}$ was the absorbance at the same wavelength of the peptide alone) was done to determine the final binding stoichiometry. The experiments were carried out in triplicate.

Isothermal Titration Calorimetry (ITC). ITC measurements were performed using a Nano-ITC III from TA instruments (New Castle, DE, USA) at the temperature of 25 °C. Briefly, 30 μM of peptide solution was placed in the calorimetry vessel (about 1 mL) and titrated by injecting a 4 mM SBE-β-CD solution (250 μL) in 16 aliquots of 15.15 μL with 600 s intervals between the individual injections. To account for the heats of dilution of the injected SBE-β-CD, a control experiment where the same solution of SBE-β-CD was titrated in the phosphate buffer without peptide was performed. The heat peaks obtained from the titration

experiment were integrated by using NanoAnalyze software supplied with the instruments.
The binding enthalpy change ($\Delta_b H$) was determined by dividing the cumulative heat $\sum_1^n \Delta h_k$, calculated by summing over all the n = 16 injections the recorded heats at each step of titration (Δh_k), by the moles of peptide in the calorimetry vessel. To determine the binding constant (K_b), a plot of the cumulative heat $\sum_1^n \Delta h_k$, normalized by peptide moles, as function of SBE-β-CD concentration was fitted with a 1:1 binding model equation [205]. The cumulative heat $\sum_1^n \Delta h_k$ at the k-th injection of CD was obtained by summing the recorded heat from the first to the k-th injection. The binding Gibbs energy and its entropic contribution were calculated using the relationships $\Delta_b G° = -RT \ln K_b$ (R = 8.314 J mol^{-1} K^{-1}, T = 298 K) and $T\Delta_b S = \Delta_b H - \Delta_b G°$. The experiments were carried out in duplicate.

Circular Dichroism (CD). Far-UV CD spectra of the peptide were recorded in order to verify the peptide secondary structure upon interaction with SBE-β-CD. CD spectra were recorded by using a JASCO J-715 spectropolarimeter (Jasco Corporation, Tokyo, Japan) in a 0.1 cm path length quartz cuvette as an average of 3 scans, using the following parameters: scan speed of 20 nm/min, 4 s response time, 2 nm bandwidth. Samples were prepared in 10 mM phosphate buffer, pH 7.4, at the peptide concentration of 20 μM in the absence and presence of SBE-β-CD at the concentration of 100 μM. For each sample, a background blank (buffer or buffer with CDs) was subtracted.

Differential Scanning Calorimetry (DSC). DSC experiments were carried out by means of a nano-DSC from TA Instruments (New Castle, DE, USA) MLVs were used since they provide the better resolution of the phase transition peaks [174]. Briefly, 300 μL of 0.5 mM vesicles suspension of DPPC/DPPG in 10 mM phosphate buffer, pH 7.4 was placed in the calorimetry vessel, and successive heating and cooling scans were performed at the scan speed of 1 °C/min. Then, DSC experiments of the same lipid mixture in the presence of 50 μM of SBE-β-CD, or 50 μM of (P)GKY20 or in the presence of 50 μM SBE-β-CD + 50 μM pf (P)GKY20 were performed.
The excess heat capacity function ($<\Delta C_p>$) was obtained after baseline subtraction. A buffer-buffer scan was subtracted from the sample scan. The samples were freshly prepared just before the experiments, by adding the appropriate amount of peptide and/or cyclodextrin to the lipid suspension and waiting at least 30 min to ensure that the equilibrium was reached. The reversibility of the process was ensured by the superposition of successive heating scans. The data obtained were analyzed by

means of the NanoAnalyze software supplied with the instrument and plotted using the Origin software package (OriginLab, Northampton, MA, USA).

6.3 Results

6.3.1 The Interaction of (P)GKY20 with CDs: SBE-β-CD versus HP-β-CD

In order to verify the ability of SBE-β-CD to interact with (P)GKY20 peptide, the changes in fluorescence emission spectra of peptide as function of cyclodextrin concentration was followed. For comparison, the same experiment was performed with the widely used HP-β-CD. In Fig. 6.3 are reported the fluorescence emission spectra of (P)GKY20 in the presence of increasing amount of SBE-β-CD (panel A) and HP-β-CD (panel B) upon excitation at 280 nm.

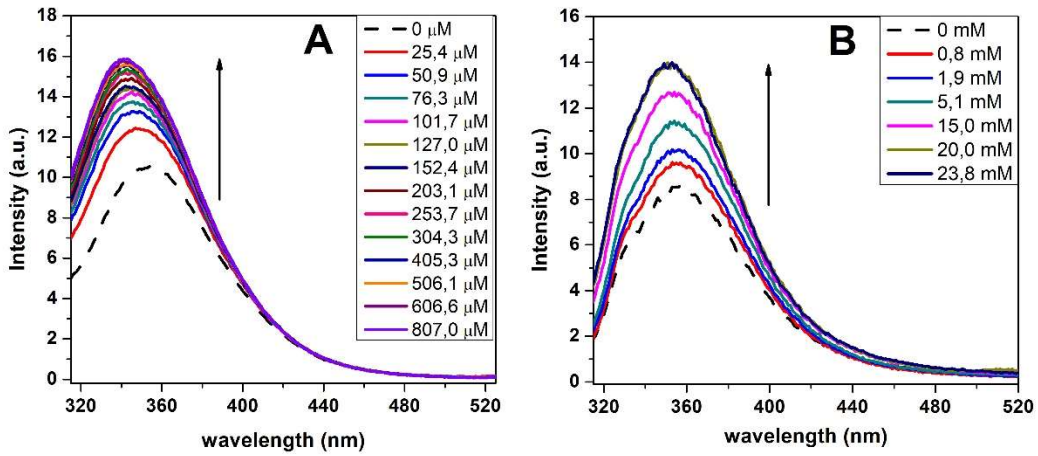

Fig. 6.3 Fluorescence emission spectra of (P)GKY20 peptide in the presence of increasing amounts of SBE-β-CD (panel A) and HP-β-CD (panel B). The dashed lines represent the spectra of peptide in the absence of CDs. All the experiments were carried out in 10 mM phosphate buffer, pH 7.5 at 25 °C.

The fluorescence emission spectra of (P)GKY20 is centered at about 355 nm. Upon the addition of SBE-β-CD, an increase of fluorescence emission was observed. Moreover, the position at the maximum of intensity (λ_{max}) shifts to the lowest value of 341 nm in the presence of ~800 μM of SBE-β-CD. This result indicates that, most likely, the cyclodextrin forms an inclusion complex with the Trp residue of the peptide. The Trp residue is the main responsible of the fluorescence emission in peptides and proteins [175]. In addition, Trp is the only environment-sensitive fluorescent residue in the peptide. Thus, the observed spectral shift indicates that the Trp residue is experiencing a more hydrophobic environment, i.e. the cavity of the

cyclodextrin. In contrast, in the presence of HP-β-CD the shift in the λ_{max} is modest. In fact, a shift to 352 nm at about 24 mM of HP-β-CD coupled with an increase of fluorescence emission was observed. It is important to note the great difference in the concentration used for the two experiments: in the range 0-800 μM for SBE-β-CD, whereas in the range 0-24 mM for HP-β-CD. This observation pointed out that the two cyclodextrins have very different affinities for (P)GKY20 peptide.
In order to obtain the values of binding constants (K_b), isotherm binding curves were obtained from the fluorescence spectra in Fig. 6.3 by plotting F_0/F versus cyclodextrin concentration, where F_0 is fluorescence intensity of the peptide in the absence of CD at 355 nm and F is the intensity in the presence of CD at the same wavelength (Fig. 6.4). Then, to determine the final values of K_b the experimental points were fitted with 1:1 binding model equation [248] where the interaction of one peptide molecule with one CD is supposed.

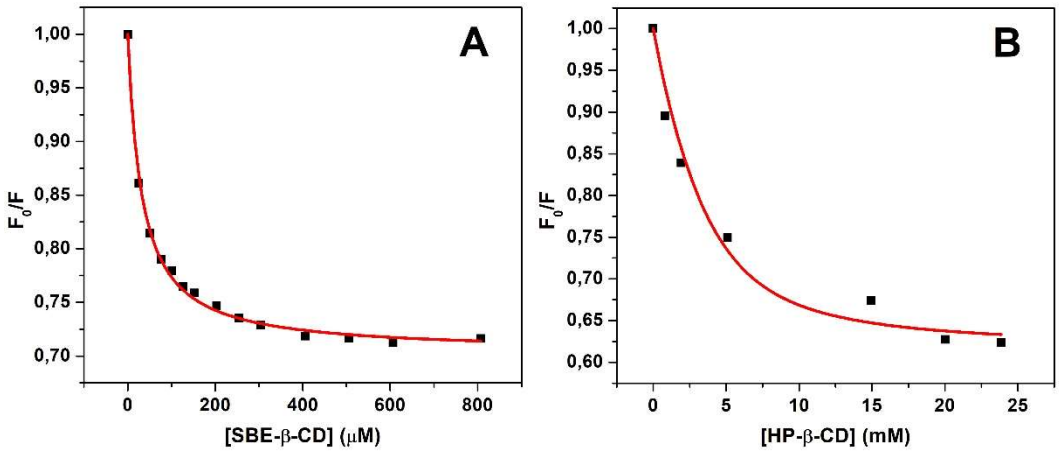

Fig. 6.4 The binding curves obtained from the fluorometric titration of a solution of (P)GKY20 peptide with SBE-β-CD (panel A) and HP-β-CD (panel B). All the experiments were carried out in 10 mM phosphate buffer, pH 7.4 at the temperature of 25 °C.

Data analysis revealed that the binding constant for SBE-β-CD is $(3.9\pm1.5)\cdot10^4$ M^{-1}. On the contrary, the binding constant for HP-β-CD is only $(6.4\pm4.0)\cdot10^2$ M^{-1}. Thus, the sulfobutylether CD has an affinity two order of magnitude higher respect to hydroxypropylated CD. These data clearly show that the anionic CDs could be a better encapsulating agent for (P)GKY20 peptide. For this reason, only the characterization with SBE-β-CD was further explored.

6.3.2 The (P)GKY20 Peptide Forms a 1:1 Complex with SBE-β-CD

In the previous section, the K_b of (P)GKY20 for the SBE-β-CD was determined. In data analysis a 1:1 stoichiometry was supposed, as commonly done in the literature

in treating the formation of inclusion complexes involving CDs. To further support the formation of 1:1 complex, the continuous variation method, also known as Job's plot, was applied [176,249]. In this method, UV spectra of (P)GKY20 in the presence of SBE-β-CD were recorded. The peptide mole fraction was varied in the range 0.1-1 by holding the total concentration of both compounds, [(P)GKY20] + [SBE-β-CD], at 200 μM. Then, spectra of peptide in the absence of CD at the same concentrations used before were recorded. A plot of $\Delta A = A_{complex} - A_{peptide}$ versus the peptide mole fraction (where $A_{complex}$ is the absorbance of the complex at 280 nm and $A_{peptide}$ was the absorbance at the same wavelength of the peptide alone) was done in order to determine the final binding stoichiometry. In Fig. 6.5 is reported the Job's plot for this system.

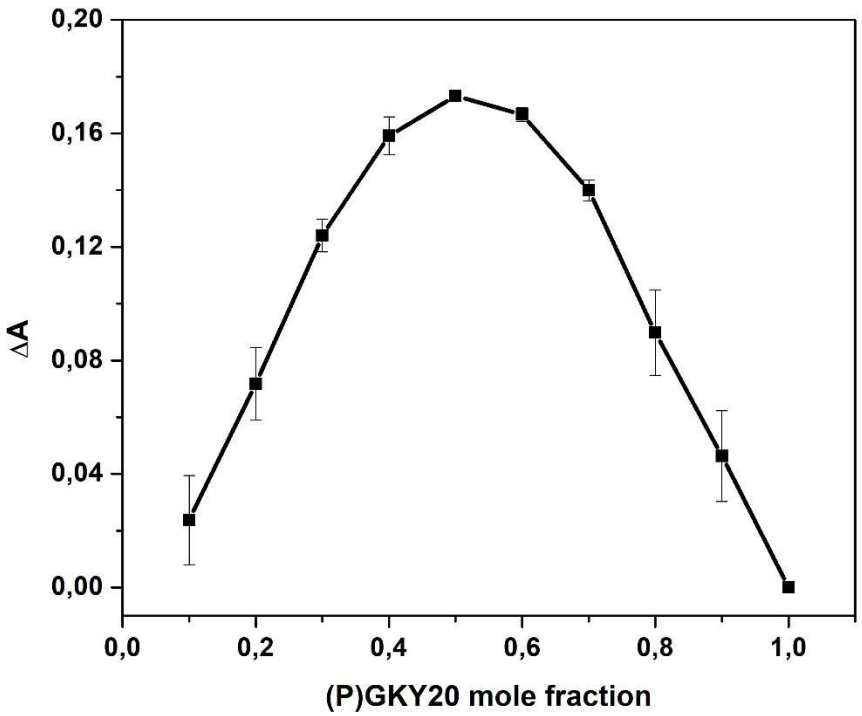

Fig. 6.5 The Job's plot for the system composed by (P)GKY20 and SBE-β-CD. The experiment was carried out in 10 mM phosphate buffer, pH 7.4 at 25 °C.

The reported Job's plot shows only one intersection point at peptide mole fraction of 0.5, clearly indicating the formation of 1:1 complex, i.e. one peptide molecule interacts with one molecule of SBE-β-CD. This result completely validates the previous analysis of fluorescence data.

6.3.3 (P)GKY20 Secondary Structure upon Interaction with SBE-β-CD

Circular dichroism (CD) spectroscopy was carried out to check the secondary structure adopted by the peptide in the presence of sulfobutylether-β-CD. In Fig. 6.6 are reported the CD spectra of 20 μM (P)GKY20 peptide solution in the absence and in the presence of 100 μM SBE-β-CD in 10 mM phosphate buffer, pH 7.4 at the temperature of 25 °C.

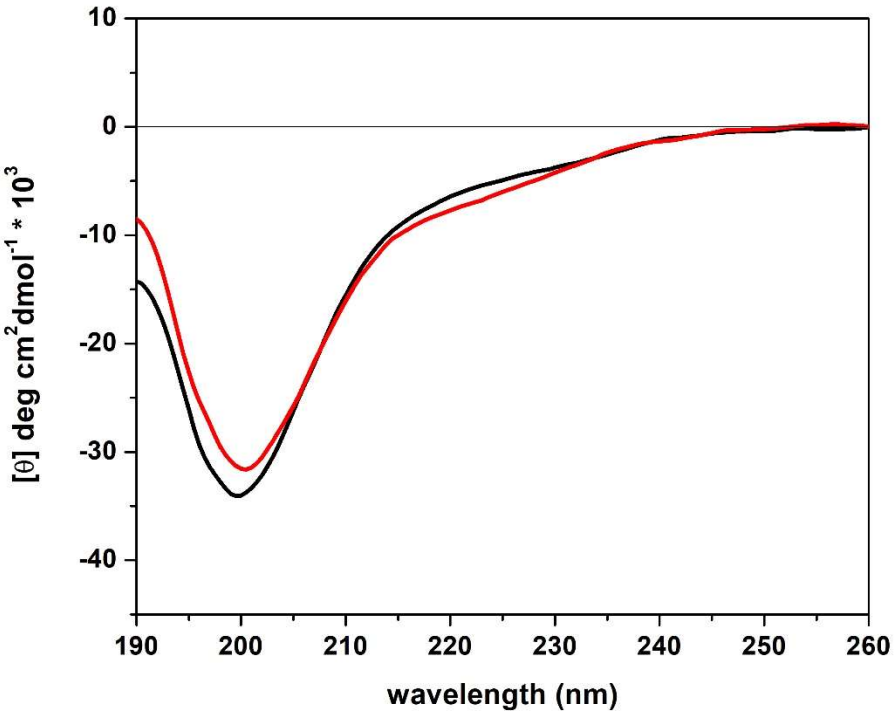

Fig. 6.6 CD spectra of (P)GKY20 in the absence (black line) and in the presence of SBE-β-CD (red line) at cyclodextrin-to-peptide ratio of 5.

As described in the section 5.3.1 of the chapter 5, the peptide adopts a random structure in solution, as evidenced by the presence of a minimum at about 200 nm. Upon the addition of SBE-β-CD at the CD-to-peptide ratio of 5, only minor changes in the spectrum are revealed, indicating that the peptide essentially does not change its secondary structure. This result supports the formation of complex through an inclusion process where the Trp residue is inserted in the hydrophobic cavity of the sugar ring. In fact, the strong shift in the fluorescence spectra (Fig. 6.3) can be only due to this process since the technique has evidenced no conformational variations that could be change the Trp local environment.

6.3.4 Thermodynamics of Interaction between (P)GKY20 and SBE-β-CD

To further characterize the interaction process between the AMP (P)GKY20 and the sulfobutylether CD, isothermal titration calorimetry (ITC) experiment was carried out. ITC is a high-accuracy method for measuring binding affinities [250]. Moreover, it is the only technique that directly measures the binding enthalpy. ITC also allows to determine enthalpic and entropic components of the free energy of binding revealing the overall nature of the forces that drive the binding reaction [251]. In Fig. 6.7 are reported the ITC trace and the corresponding binding isotherm obtained from the titration of 30 μM solution of (P)GKY20 with 4 mM of SBE-β-CD.

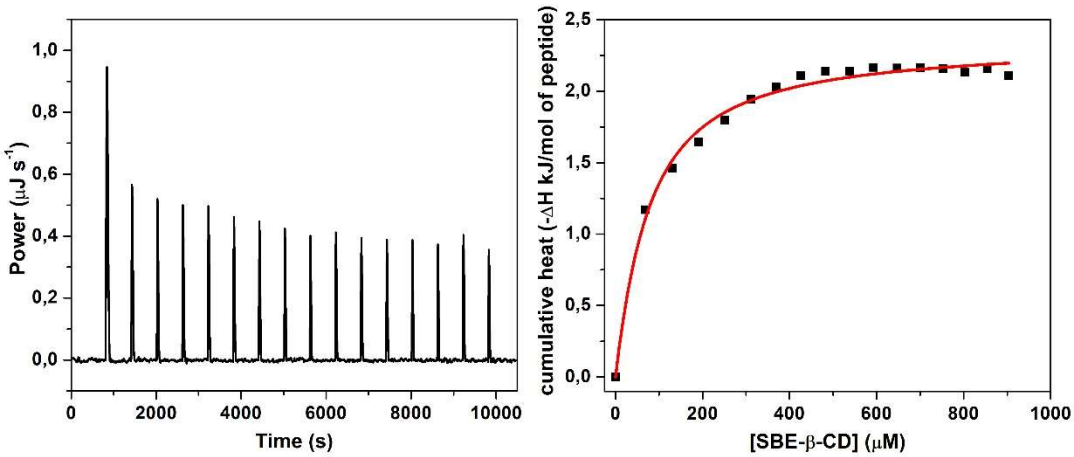

Fig. 6.7 The ITC trace (left panel) and the corresponding binding isotherm (right panel) obtained from the titration of a solution of (P)GKY20 peptide with SBE-β-CD. The red line represents the best curve fit obtained using a 1:1 binding model equation. The experiment was carried out in 10 mM phosphate buffer, pH 7.4 at 25 °C.

In the ITC experiment, the peptide solution is placed in the calorimeter vessel and a solution of SBE-β-CD is injected via the titration syringe. After each addition of SBE-β-CD, peptide is bound to the sugar and it is removed from bulk solution. Hence with increasing SBE-β-CD concentration in the reaction vessel less and less peptide is available for binding. The heat of reaction is therefore no constant but decreases with each injection. This leads to the ITC trace reported in Fig. 6.7, left panel. The binding enthalpy change ($\Delta_b H$) was calculated by summing all the recorded heats at each step of titration (corrected for the heat of dilution of the injected SBE-β-CD) divided by the peptide moles in the calorimetry vessel. Instead, from the plot of the cumulative heat versus the SBE-β-CD concentration (Fig. 6.7, right panel) it was possible to determine the K_b by fitting the experimental points with 1:1 binding model equation. The use of this binding model was validated by the Job's plot

reported in Fig. 6.5. With Δ_bH and K_b determined, using the well-known relations $\Delta_bG° = -RT \ln K_b$ ($R = 8.314$ J mol^{-1} K^{-1}, $T = 298$ K) and $T\Delta_bS = \Delta_bH - \Delta_bG°$, a full thermodynamic characterization was obtained. In Table 1 are summarized the thermodynamic parameters.

Table 1 Thermodynamic parameters obtained from the titration of a solution of (P)GKY20 peptide with a solution of SBE-β-CD at the temperature of 25 °C.

K_b (M^{-1})	Δ_bH (kJ/mol)	$\Delta_bG°$ (kJ/mol)	$T\Delta_bS$ (kJ/mol)
$(1.6\pm0.6)\cdot10^4$	-2.3±0.5	-24.0±1.0	21.7±1.2

The obtained binding constant (K_b) is in excellent agreement with the one determined by means of fluorescence experiment. An inspection of the Table 1 reveals that the enthalpy change for the binding is low and exothermic, suggesting that weak non-bonding interactions are involved in the formation of the complex [252]. In addition, its contribution to the binding free energy is quite modest. The entropy change for the interaction process is positive. This could be due to the release of water molecules, that form the hydration shells of the Trp and CD, to the bulk solvent. This process leads to an increase of entropy change, as detected. A comparison of the obtained enthalpy and entropy changes reveal that the formation of the complex is entropically driven.

6.3.5 The Effect of (P)GKY20/SBE-β-CD Complex on the Thermotropic Properties of DPPC/DPPG Liposomes

Finally, the effect of the complex formed by a mixture of (P)GKY20 and SBE-β-CD on the thermotropic properties of DPPC/DPPG (8/2 mol/mol) liposomes was studied. This experiment was carried out to verify if the peptide complexed with cyclodextrin is able to perturb the membrane. In Fig. 6.8 are reported the DSC thermogram of DPPC/DPPG multilamellar vesicles (0.5 mM) alone and in the presence of a mixture composed by 50 μM of (P)GKY20 and 50 μM of SBE-β-CD. For comparison, DSC thermograms of DPPC/DPPG in the presence of peptide or cyclodextrin at the same concentrations are reported. In Table 2 are reported the thermodynamic parameters for the gel-to-liquid phase transition of DPPC/DPPG liposomes in the absence and in the presence of peptide, cyclodextrin or both (complex).

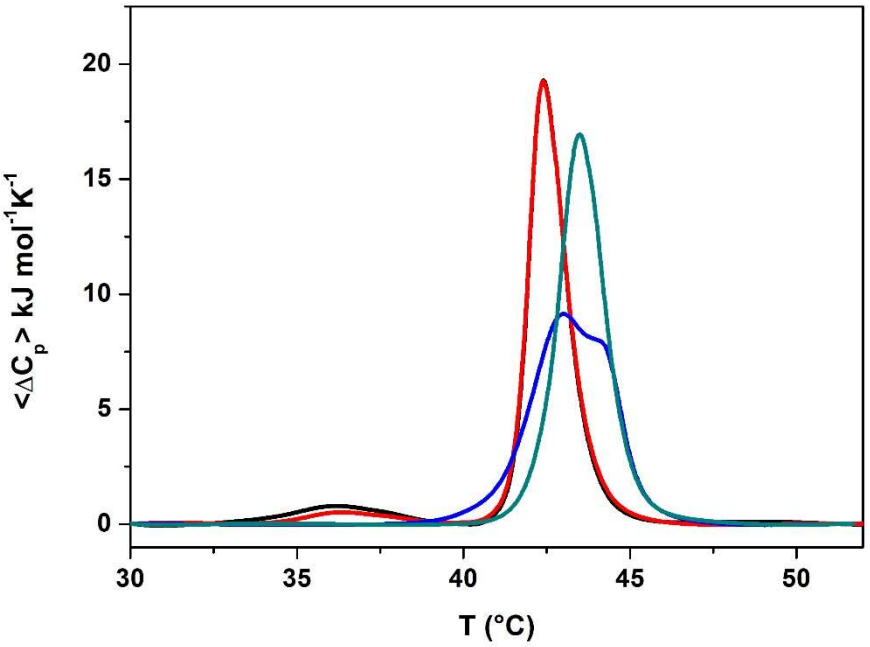

Fig. 6.8 DSC thermograms of 0.5 mM DPPC/DPPG multilamellar vesicles in the absence (black line) and in the presence of 50 μM of SBE-β-CD (red line), 50 μM of (P)GKY20 (blue line) and in the presence of a mixture of 50 μM (P)GKY20 + 50 μM SBE-β-CD (dark cyan line). All the experiments were carried out in 10 mM phosphate buffer, pH 7.4.

Table 2 Thermodynamic parameters obtained by means of DSC for the phase transitions of DPPC/DPPG (8/2 mol/mol) liposomes in the absence and presence of 50 μM SBE-β-CD, 50 μM (P)GKY20 and a mixture of 50 μM SBE-β-CD + 50 μM (P)GKY20 (complex).

System	T_p (°C)[a]	ΔH_p (kJ/mol)[a,c]	T_m (°C)[b]	ΔH_m (kJ/mol)[b,c]
DPPC/DPPG	36.1±0.2	1.7±0.3	42.4±0.1	29.5±1.5
+SBE-β-CD	36.2±0.2	1.5±0.3	42.4±0.1	29.6±1.6
+(P)GKY20	-	-	43-44±0.1[d]	28.4±1.4
+Complex	-	-	43.5±0.1	31.2±1.8

[a] Enthalpy change and temperature of the pre-transition peak.
[b] Enthalpy change and temperature of the main transition peak.
[c] Normalization against total lipid moles.
[d] The reported temperatures refer to the first and second maxima in the DSC thermogram, respectively.

The DSC thermogram of DPPC/DPPG multilamellar vesicles is characterized by the presence of two transitions. A pre-transition at about 36 °C and a main transition at about 42.4 °C, as reported in section 4.3.2. Upon the addition of SBE-β-CD at the

concentration of 50 μM, the DSC thermogram of DPPC/DPPG vesicles does no change, pointing out that the cyclodextrin has no effect on the stability of the bilayer. In the presence of 50 μM of (P)GKY20, as noted in chapter 5, a strong perturbation of the DSC profile was detected. The obtained result was interpreted as the surface binding of peptide coupled with the preferential interaction with the anionic lipid which leads to the formation of lipid domains (section 5.3.2). Finally, in the presence of both peptide and cyclodextrin a complete suppression of the pre-transition was observed, indicating again a strong interaction on the surface. In addition, also the main-transition is affected by the presence of the complex. The melting temperature (T_m) increases from 42.4 °C to 43.5 °C, instead the enthalpy change is not affected by the presence of the complex (Table 2), indicating a binding on the surface without penetration inside the hydrophobic core of the membrane [185]. However, the effect of the complex seems less pronounced respect to the peptide alone. Nevertheless, this experiment demonstrated that even in the presence of cyclodextrin, the peptide is able to interact and perturb the lipid bilayer.

6.4 Discussion

In this chapter, some preliminary data on the interaction of (P)GKY20 peptide with sulfobutylether-β-CD (SBE-β-CD) and of the obtained complex with bacterial model membrane were reported. The final goal was to verify if the peptide can interact with the cyclodextrin to develop, in the near future, a formulation which can increase the pharmacological properties of the peptide. In fact, it is known that peptides are not physically and chemically stable [91,253]. In addition, AMPs are subject to the proteases action which can seriously limit their application as drugs [92]. Finally, the interaction with serum proteins can limit their availability [240]. Thus, it is important to find some compounds which can improve the pharmacological properties of peptides. Clearly, these compounds must not interfere with the biological activity of peptides and should be no dangerous for human health. Cyclodextrins (CDs) are a class of cyclic oligosaccharides which are very suitable for this purpose [241]. CDs are generally recognized as safe for humans and they are used in a wide variety of pharmacological applications to increase the stability, the solubility and the safety of drugs [241]. In particular, it was demonstrated that SBE-β-CD is safe, and only at very high concentration could have some light adverse effects [241]. In addition, this CD is already commercialized as Captisol® [254]. Thus, it is available in high amount and it is not expensive. For this reason, the complexation of (P)GKY20 peptide with sulfobutylether-β-CD was studied. For comparison, the interaction with the widely used hydroxypropyl-β-CD (HP-β-CD) was also studied. The extent of complexation is strongly dependent on the binding constant (K_b) between peptide and CD [241,244]. In fact, the value of binding constant should be neither too much

low, nor to much high. This is because a good level of complexation must be achieved (high K_b) by using a small amount of CD to avoid side effects at high sugar concentration. On the other hand, a too much high K_b could prevent the interaction of the peptide with the membrane. Thus, the determination of K_b is of fundamental importance.

The reported data demonstrated that the SBE-β-CD has a binding constant of about 10^4 M^{-1} for (P)GKY20. In contrast, HP-β-CD showed a very weak binding to the peptide ($K_b \sim 6 \cdot 10^2$ M^{-1}). Thus, the sulfobutylether CD is more efficient as encapsulating agent. For this reason, only the interaction with SBE-β-CD was further explored. Most likely, the interaction of SBE-β-CD with peptide occurs through the formation of inclusion complex [255] where the Trp residue is inserted in the hydrophobic cavity of the sugar ring. This is supported by the strong blue shift in the fluorescence emission spectra of the peptide. In fact, tryptophan is the only environment-sensitive natural residue in peptides and proteins [175]. In addition, the ability of β-CDs to interact with aromatic residues was already reported [245,252]. The strong interaction of SBE-β-CD compared to neutral HP-β-CD could be attributed to the presence of negatively charge sulfonate groups (two in the used SBE-β-CD) which enhance the affinity for the peptide. It is important to note that in the primary sequence of (P)GKY20 peptide (GKYGFYTHVFRLKK**W**IQKVI) the Trp residue is very close to positively charged residues (Lys and Arg) leading to a cluster of positive charges on the C-terminus region of the peptide. This can drive the initial interaction of SBE-β-CD with this region of the peptide, just before the formation of the inclusion complex.

The reported circular dichroism spectrum of peptide in the presence of cyclodextrin (Fig. 6.6) revealed no conformational changes in its secondary structure, supporting the formation of inclusion complex. Indeed, the strong spectral shift in fluorescence spectra is not due to conformational changes which can alter the environment surrounding the Trp residue. In addition, the result obtained from the Job's plot experiment revealed the formation of 1:1 complex, where one peptide molecule interacts with one CD. Even if the Job's plot is not a direct proof, it supports the formation of the inclusion complex, since only one Trp residue is present in the primary sequence of (P)GKY20. Finally, the formation of the complex was further studied by means of isothermal titration calorimetry (Fig. 6.7). The obtained value for K_b is in excellent agreement with the value obtained from the spectrofluorimetric titration, thus confirming that the K_b is in the order of 10^4 M^{-1}. The direct measurements of the heats involved in the interaction process allowed the determination of the binding enthalpy and, consequentially, of the entropy and free energy changes. First of all, the free energy change is negative pointing out the spontaneity of the interaction process (Table 1). The low and exothermic value of $\Delta_b H$ (-2.3 kJ/mol of peptide) suggests that only non-bonding weak interactions are

involved in the interaction, as expected in the formation of an inclusion complex. On the contrary, a strong entropy change was detected, highlighting that the formation of the inclusion complex is entropically driven [252]. It is known that cyclodextrins contains several water molecules inside their cavity [256,257]. Upon the formation of the inclusion complex, structured water molecules inside the CD cavity are released into the bulk water [255] leading to the positive entropy variation.
Finally, the interaction of the peptide/CD complex with liposomes mimicking the cytoplasmic bacterial membrane was explored by means of differential scanning calorimetry (Fig. 6.8). This is an important step, since the complexation of the peptide with the cyclodextrin should not influence the peptide antimicrobial activity. The obtained data showed that, at the concentration used in the experiment, SBE-β-CD has no effect on the bilayer stability. The presence of peptide alone, as reported in chapter 5, led to a multicomponent peak which suggest the formation of lipid domains. The contemporary presence of cyclodextrin and peptide also influences the bilayer stability. The suppression of the pre-transition peak indicates that the peptide is able to interact superficially even in the presence of CD. In addition, the main transition peak seems halfway between the DSC peak of liposomes in the absence and in the presence of peptide (Fig. 6.8). In particular, it seems that the formation of domains didn't take place. Most likely, the presence of CD could lower the concentration of the membrane-bound peptide leading to a less pronounced effect on the recorded DSC peak. Another explanation is represented by the possibility that the peptide in the complexed form could directly interact with the membrane, lowering the membrane perturbation activity of the peptide. However, this result clearly demonstrated that even in the presence of the anionic SBE-β-CD, the (P)GKY20 peptide is able to interact with the bacterial model membrane.
Collectively, the reported preliminary data showed that for (P)GKY20 the SBE-β-CD should be a good encapsulating agent. The binding constant (K_b) is of the right value which allows a good extent of encapsulation without using high amount of sugar. In addition, the peptide is able to perturb the bilayer stability in the presence of CD, even if the effect is less pronounced respect to the case when the peptide is alone.
Clearly, a lot of work must be done to deeply characterized the interaction of the complex with bacterial model membrane. DSC experiments with different peptide-CD ratios should be performed in order to find the best ratio value which represents the right compromise between encapsulation and membranotropic activity. In addition, there is the possibility that the peptide could interact with the membrane in the complexed form with CD. Thus, the possible involvement of the CD in the interaction with the membrane must be verified.
Biological assays on bacterial strains must be performed in the presence of SBE-β-CD to verify *in vivo* the antibacterial activity of the complex. Another important

biological assays to perform is the stability to proteases of the complex in serum. Finally, the interaction of (P)GKY20 peptide in the absence and in the presence of the cyclodextrin with serum proteins (e.g. human serum albumin) should be verified. This full characterization could lead to the preparation of a peptide/CD formulation which can render possible the pharmacological (and not only) applications of the antimicrobial peptide (P)GKY20.

References

[1] C.L. Ventola, The antibiotic resistance crisis: part 1: causes and threats, P T Peer-Rev. J. Formul. Manag. 40 (2015) 277–283.

[2] Antibiotic resistance, World Health Organ. (n.d.). http://www.who.int/news-room/fact-sheets/detail/antibiotic-resistance (accessed August 25, 2018).

[3] J.M. Munita, C.A. Arias, Mechanisms of Antibiotic Resistance, Microbiol. Spectr. 4 (2016). doi:10.1128/microbiolspec.VMBF-0016-2015.

[4] F.D. Lowy, Antimicrobial resistance: the example of Staphylococcus aureus, J. Clin. Invest. 111 (2003) 1265–1273. doi:10.1172/JCI200318535.

[5] B. Spellberg, J.H. Powers, E.P. Brass, L.G. Miller, J.E. Edwards, Trends in antimicrobial drug development: implications for the future, Clin. Infect. Dis. Off. Publ. Infect. Dis. Soc. Am. 38 (2004) 1279–1286. doi:10.1086/420937.

[6] M. Zasloff, Antimicrobial peptides of multicellular organisms, Nature. 415 (2002) 389–395. doi:10.1038/415389a.

[7] L.W. Hamoen, M. Wenzel, Editorial: Antimicrobial Peptides - Interaction with Membrane Lipids and Proteins, Front. Cell Dev. Biol. 5 (2017). doi:10.3389/fcell.2017.00004.

[8] J. Lakshmaiah Narayana, J.-Y. Chen, Antimicrobial peptides: Possible anti-infective agents, Peptides. 72 (2015) 88–94. doi:10.1016/j.peptides.2015.05.012.

[9] F. Schweizer, Cationic amphiphilic peptides with cancer-selective toxicity, Eur. J. Pharmacol. 625 (2009) 190–194. doi:10.1016/j.ejphar.2009.08.043.

[10] L. Nyström, M. Malmsten, Membrane interactions and cell selectivity of amphiphilic anticancer peptides, Curr. Opin. Colloid Interface Sci. 38 (2018) 1–17. doi:10.1016/j.cocis.2018.06.009.

[11] G. Diamond, N. Beckloff, A. Weinberg, K.O. Kisich, The roles of antimicrobial peptides in innate host defense, Curr. Pharm. Des. 15 (2009) 2377–2392.

[12] V. Teixeira, M.J. Feio, M. Bastos, Role of lipids in the interaction of antimicrobial peptides with membranes, Prog. Lipid Res. 51 (2012) 149–177. doi:10.1016/j.plipres.2011.12.005.

[13] G. Wang, Post-translational Modifications of Natural Antimicrobial Peptides and Strategies for Peptide Engineering, Curr. Biotechnol. 1 (2012) 72–79.

[14] L.-J. Zhang, R.L. Gallo, Antimicrobial peptides, Curr. Biol. CB. 26 (2016) R14-19. doi:10.1016/j.cub.2015.11.017.

[15] G. Wang, Human Antimicrobial Peptides and Proteins, Pharmaceuticals. 7 (2014) 545–594. doi:10.3390/ph7050545.

[16] A. Fleming, On a Remarkable Bacteriolytic Element Found in Tissues and Secretions, Proc. R. Soc. B Biol. Sci. 93 (1922) 306–317. doi:10.1098/rspb.1922.0023.

[17] D. Voet, J.G. Voet, Biochemistry, 4th ed, John Wiley & Sons, Hoboken, NJ, 2011.

[18] M. Lobanovska, G. Pilla, Penicillin's Discovery and Antibiotic Resistance: Lessons for the Future?, Yale J. Biol. Med. 90 (2017) 135–145.
[19] R.J. Dubos, STUDIES ON A BACTERICIDAL AGENT EXTRACTED FROM A SOIL BACILLUS : I. PREPARATION OF THE AGENT. ITS ACTIVITY IN VITRO, J. Exp. Med. 70 (1939) 1–10.
[20] N. Kessler, H. Schuhmann, S. Morneweg, U. Linne, M.A. Marahiel, The Linear Pentadecapeptide Gramicidin Is Assembled by Four Multimodular Nonribosomal Peptide Synthetases That Comprise 16 Modules with 56 Catalytic Domains, J. Biol. Chem. 279 (2004) 7413–7419. doi:10.1074/jbc.M309658200.
[21] A.K. Balls, W.S. Hale, T.H. Harris, A Crystalline Protein Obtained from a Lipoprotein of Wheat Flour, Cereal Chem. 19 (1942) 279–288.
[22] G. Kiss, H. Michl, Uber das Giftsekret der Gelbbauchunke, Bombina variegata L., Toxicon. 1 (1962) 33–34. doi:10.1016/0041-0101(62)90006-5.
[23] D. Phoenix, S.R. Dennison, F. Harris, Antimicrobial peptides, Wiley-VCH, Weinheim, 2013.
[24] D. Hultmark, H. Steiner, T. Rasmuson, H.G. Boman, Insect immunity. Purification and properties of three inducible bactericidal proteins from hemolymph of immunized pupae of Hyalophora cecropia, Eur. J. Biochem. 106 (1980) 7–16.
[25] H. Steiner, D. Hultmark, A. Engström, H. Bennich, H.G. Boman, Sequence and specificity of two antibacterial proteins involved in insect immunity, Nature. 292 (1981) 246–248.
[26] M. Zasloff, Magainins, a class of antimicrobial peptides from Xenopus skin: isolation, characterization of two active forms, and partial cDNA sequence of a precursor, Proc. Natl. Acad. Sci. U. S. A. 84 (1987) 5449–5453.
[27] G. Wang, X. Li, Z. Wang, APD3: the antimicrobial peptide database as a tool for research and education, Nucleic Acids Res. 44 (2016) D1087-1093. doi:10.1093/nar/gkv1278.
[28] M.N. Melo, R. Ferre, M.A.R.B. Castanho, Antimicrobial peptides: linking partition, activity and high membrane-bound concentrations, Nat. Rev. Microbiol. 7 (2009) 245–250. doi:10.1038/nrmicro2095.
[29] O.G. Travkova, H. Moehwald, G. Brezesinski, The interaction of antimicrobial peptides with membranes, Adv. Colloid Interface Sci. 247 (2017) 521–532. doi:10.1016/j.cis.2017.06.001.
[30] H.G. Boman, Peptide antibiotics and their role in innate immunity, Annu. Rev. Immunol. 13 (1995) 61–92. doi:10.1146/annurev.iy.13.040195.000425.
[31] A. Tossi, L. Sandri, A. Giangaspero, Amphipathic, alpha-helical antimicrobial peptides, Biopolymers. 55 (2000) 4–30. doi:10.1002/1097-0282(2000)55:1<4::AID-BIP30>3.0.CO;2-M.
[32] W.-M. Yau, W.C. Wimley, K. Gawrisch, S.H. White, The Preference of Tryptophan for Membrane Interfaces †, Biochemistry. 37 (1998) 14713–14718. doi:10.1021/bi980809c.

[33] B. Bechinger, M. Zasloff, S.J. Opella, Structure and orientation of the antibiotic peptide magainin in membranes by solid-state nuclear magnetic resonance spectroscopy, Protein Sci. 2 (1993) 2077–2084. doi:10.1002/pro.5560021208.
[34] Z. Oren, Y. Shai, Selective lysis of bacteria but not mammalian cells by diastereomers of melittin: structure-function study, Biochemistry. 36 (1997) 1826–1835. doi:10.1021/bi962507l.
[35] J. Shi, L.-Y. So, F. Chen, J. Liang, H.-Y. Chow, K.-Y. Wong, S. Wan, T. Jiang, R. Yu, Influences of disulfide connectivity on structure and antimicrobial activity of tachyplesin I, J. Pept. Sci. 24 (2018) e3087. doi:10.1002/psc.3087.
[36] J. Gesell, M. Zasloff, S.J. Opella, Two-dimensional 1H NMR experiments show that the 23-residue magainin antibiotic peptide is an alpha-helix in dodecylphosphocholine micelles, sodium dodecylsulfate micelles, and trifluoroethanol/water solution, J. Biomol. NMR. 9 (1997) 127–135.
[37] A. Laederach, A.H. Andreotti, D.B. Fulton, Solution and micelle-bound structures of tachyplesin I and its active aromatic linear derivatives, Biochemistry. 41 (2002) 12359–12368.
[38] M. Fernández-Vidal, S. Jayasinghe, A.S. Ladokhin, S.H. White, Folding amphipathic helices into membranes: amphiphilicity trumps hydrophobicity, J. Mol. Biol. 370 (2007) 459–470. doi:10.1016/j.jmb.2007.05.016.
[39] D. Eisenberg, R.M. Weiss, T.C. Terwilliger, The helical hydrophobic moment: a measure of the amphiphilicity of a helix, Nature. 299 (1982) 371–374.
[40] R. Gautier, D. Douguet, B. Antonny, G. Drin, HELIQUEST: a web server to screen sequences with specific alpha-helical properties, Bioinforma. Oxf. Engl. 24 (2008) 2101–2102. doi:10.1093/bioinformatics/btn392.
[41] A. Hollmann, M. Martínez, M.E. Noguera, M.T. Augusto, A. Disalvo, N.C. Santos, L. Semorile, P.C. Maffía, Role of amphipathicity and hydrophobicity in the balance between hemolysis and peptide–membrane interactions of three related antimicrobial peptides, Colloids Surf. B Biointerfaces. 141 (2016) 528–536. doi:10.1016/j.colsurfb.2016.02.003.
[42] Z. Jiang, A.I. Vasil, J.D. Hale, R.E.W. Hancock, M.L. Vasil, R.S. Hodges, Effects of net charge and the number of positively charged residues on the biological activity of amphipathic alpha-helical cationic antimicrobial peptides, Biopolymers. 90 (2008) 369–383. doi:10.1002/bip.20911.
[43] H.-T. Chou, T.-Y. Kuo, J.-C. Chiang, M.-J. Pei, W.-T. Yang, H.-C. Yu, S.-B. Lin, W.-J. Chen, Design and synthesis of cationic antimicrobial peptides with improved activity and selectivity against Vibrio spp., Int. J. Antimicrob. Agents. 32 (2008) 130–138. doi:10.1016/j.ijantimicag.2008.04.003.
[44] M.J. Oudhoff, J.G.M. Bolscher, K. Nazmi, H. Kalay, W. van ’t Hof, A.V.N. Amerongen, E.C.I. Veerman, Histatins are the major wound-closure stimulating factors in human saliva as identified in a cell culture assay, FASEB J. Off. Publ. Fed. Am. Soc. Exp. Biol. 22 (2008) 3805–3812. doi:10.1096/fj.08-112003.

[45] K.D. Saint Jean, K.D. Henderson, C.L. Chrom, L.E. Abiuso, L.M. Renn, G.A. Caputo, Effects of Hydrophobic Amino Acid Substitutions on Antimicrobial Peptide Behavior, Probiotics Antimicrob. Proteins. 10 (2018) 408–419. doi:10.1007/s12602-017-9345-z.
[46] Y. Chen, M.T. Guarnieri, A.I. Vasil, M.L. Vasil, C.T. Mant, R.S. Hodges, Role of peptide hydrophobicity in the mechanism of action of alpha-helical antimicrobial peptides, Antimicrob. Agents Chemother. 51 (2007) 1398–1406. doi:10.1128/AAC.00925-06.
[47] A. Giangaspero, L. Sandri, A. Tossi, Amphipathic alpha helical antimicrobial peptides, Eur. J. Biochem. 268 (2001) 5589–5600.
[48] M. Dathe, H. Nikolenko, J. Meyer, M. Beyermann, M. Bienert, Optimization of the antimicrobial activity of magainin peptides by modification of charge, FEBS Lett. 501 (2001) 146–150.
[49] M.R. Yeaman, N.Y. Yount, Mechanisms of antimicrobial peptide action and resistance, Pharmacol. Rev. 55 (2003) 27–55. doi:10.1124/pr.55.1.2.
[50] N. Uematsu, K. Matsuzaki, Polar angle as a determinant of amphipathic alpha-helix-lipid interactions: a model peptide study, Biophys. J. 79 (2000) 2075–2083. doi:10.1016/S0006-3495(00)76455-1.
[51] B. Mojsoska, H. Jenssen, Peptides and Peptidomimetics for Antimicrobial Drug Design, Pharmaceuticals. 8 (2015) 366–415. doi:10.3390/ph8030366.
[52] K.A. Brogden, Antimicrobial peptides: pore formers or metabolic inhibitors in bacteria?, Nat. Rev. Microbiol. 3 (2005) 238–250. doi:10.1038/nrmicro1098.
[53] B. Bechinger, The structure, dynamics and orientation of antimicrobial peptides in membranes by multidimensional solid-state NMR spectroscopy, Biochim. Biophys. Acta. 1462 (1999) 157–183.
[54] L.M. Gottler, A. Ramamoorthy, Structure, membrane orientation, mechanism, and function of pexiganan--a highly potent antimicrobial peptide designed from magainin, Biochim. Biophys. Acta. 1788 (2009) 1680–1686. doi:10.1016/j.bbamem.2008.10.009.
[55] S. Fruitwala, D.W. El-Naccache, T.L. Chang, Multifaceted immune functions of human defensins and underlying mechanisms, Semin. Cell Dev. Biol. (2018). doi:10.1016/j.semcdb.2018.02.023.
[56] P. Bulet, C. Hetru, J.L. Dimarcq, D. Hoffmann, Antimicrobial peptides in insects; structure and function, Dev. Comp. Immunol. 23 (1999) 329–344.
[57] J.A. Mackintosh, D.A. Veal, A.J. Beattie, A.A. Gooley, Isolation from an ant Myrmecia gulosa of two inducible O-glycosylated proline-rich antibacterial peptides, J. Biol. Chem. 273 (1998) 6139–6143.
[58] D. Vanhoye, F. Bruston, S. El Amri, A. Ladram, M. Amiche, P. Nicolas, Membrane association, electrostatic sequestration, and cytotoxicity of Gly-Leu-rich peptide orthologs with differing functions, Biochemistry. 43 (2004) 8391–8409. doi:10.1021/bi0493158.
[59] B. Agerberth, J.Y. Lee, T. Bergman, M. Carlquist, H.G. Boman, V. Mutt, H. Jörnvall, Amino acid sequence of PR-39. Isolation from pig intestine of a new

member of the family of proline-arginine-rich antibacterial peptides, Eur. J. Biochem. 202 (1991) 849–854.
[60] H.G. Boman, B. Agerberth, A. Boman, Mechanisms of action on Escherichia coli of cecropin P1 and PR-39, two antibacterial peptides from pig intestine, Infect. Immun. 61 (1993) 2978–2984.
[61] S.T. Henriques, M.N. Melo, M.A.R.B. Castanho, Cell-penetrating peptides and antimicrobial peptides: how different are they?, Biochem. J. 399 (2006) 1–7. doi:10.1042/BJ20061100.
[62] S. Futaki, I. Nakase, A. Tadokoro, T. Takeuchi, A.T. Jones, Arginine-rich peptides and their internalization mechanisms, Biochem. Soc. Trans. 35 (2007) 784–787. doi:10.1042/BST0350784.
[63] M.E. Selsted, M.J. Novotny, W.L. Morris, Y.Q. Tang, W. Smith, J.S. Cullor, Indolicidin, a novel bactericidal tridecapeptide amide from neutrophils, J. Biol. Chem. 267 (1992) 4292–4295.
[64] A. Rozek, C.L. Friedrich, R.E. Hancock, Structure of the bovine antimicrobial peptide indolicidin bound to dodecylphosphocholine and sodium dodecyl sulfate micelles, Biochemistry. 39 (2000) 15765–15774.
[65] I.H. Lee, C. Zhao, Y. Cho, S.S. Harwig, E.L. Cooper, R.I. Lehrer, Clavanins, alpha-helical antimicrobial peptides from tunicate hemocytes, FEBS Lett. 400 (1997) 158–162.
[66] O.N. Silva, E.S.F. Alves, C. de la Fuente-Núñez, S.M. Ribeiro, S.M. Mandal, D. Gaspar, A.S. Veiga, M.A.R.B. Castanho, C.A.S. Andrade, J.M. Nascimento, I.C.M. Fensterseifer, W.F. Porto, J.R. Correa, R.E.W. Hancock, S. Korpole, A.L. Oliveira, L.M. Liao, O.L. Franco, Structural Studies of a Lipid-Binding Peptide from Tunicate Hemocytes with Anti-Biofilm Activity, Sci. Rep. 6 (2016). doi:10.1038/srep27128.
[67] T. Manabe, K. Kawasaki, D-form KLKLLLLLKLK-NH2 peptide exerts higher antimicrobial properties than its L-form counterpart via an association with bacterial cell wall components, Sci. Rep. 7 (2017) 43384. doi:10.1038/srep43384.
[68] W.C. Wimley, Describing the mechanism of antimicrobial peptide action with the interfacial activity model, ACS Chem. Biol. 5 (2010) 905–917. doi:10.1021/cb1001558.
[69] N. Papo, Y. Shai, Can we predict biological activity of antimicrobial peptides from their interactions with model phospholipid membranes?, Peptides. 24 (2003) 1693–1703. doi:10.1016/j.peptides.2003.09.013.
[70] R.E. Hancock, Peptide antibiotics, Lancet Lond. Engl. 349 (1997) 418–422. doi:10.1016/S0140-6736(97)80051-7.
[71] N. Malanovic, K. Lohner, Antimicrobial Peptides Targeting Gram-Positive Bacteria, Pharmaceuticals. 9 (2016) 59. doi:10.3390/ph9030059.
[72] S. Omardien, S. Brul, S.A.J. Zaat, Antimicrobial Activity of Cationic Antimicrobial Peptides against Gram-Positives: Current Progress Made in

Understanding the Mode of Action and the Response of Bacteria, Front. Cell Dev. Biol. 4 (2016). doi:10.3389/fcell.2016.00111.
[73] J. Seelig, Thermodynamics of lipid-peptide interactions, Biochim. Biophys. Acta. 1666 (2004) 40–50. doi:10.1016/j.bbamem.2004.08.004.
[74] G. Beschiaschvili, J. Seelig, Melittin binding to mixed phosphatidylglycerol/phosphatidylcholine membranes, Biochemistry. 29 (1990) 52–58.
[75] E.S. Salnikov, A.J. Mason, B. Bechinger, Membrane order perturbation in the presence of antimicrobial peptides by (2)H solid-state NMR spectroscopy, Biochimie. 91 (2009) 734–743.
[76] M.S. Sansom, Alamethicin and related peptaibols--model ion channels, Eur. Biophys. J. EBJ. 22 (1993) 105–124.
[77] A. Rahaman, T. Lazaridis, A thermodynamic approach to alamethicin pore formation, Biochim. Biophys. Acta. 1838 (2014) 1439–1447.
[78] R.A. Cruciani, J.L. Barker, S.R. Durell, G. Raghunathan, H.R. Guy, M. Zasloff, E.F. Stanley, Magainin 2, a natural antibiotic from frog skin, forms ion channels in lipid bilayer membranes, Eur. J. Pharmacol. 226 (1992) 287–296.
[79] E. Gallucci, D. Meleleo, S. Micelli, V. Picciarelli, Magainin 2 channel formation in planar lipid membranes: the role of lipid polar groups and ergosterol, Eur. Biophys. J. EBJ. 32 (2003) 22–32. doi:10.1007/s00249-002-0262-y.
[80] E. Gazit, I.R. Miller, P.C. Biggin, M.S. Sansom, Y. Shai, Structure and orientation of the mammalian antibacterial peptide cecropin P1 within phospholipid membranes, J. Mol. Biol. 258 (1996) 860–870. doi:10.1006/jmbi.1996.0293.
[81] S. Yamaguchi, D. Huster, A. Waring, R.I. Lehrer, W. Kearney, B.F. Tack, M. Hong, Orientation and dynamics of an antimicrobial peptide in the lipid bilayer by solid-state NMR spectroscopy, Biophys. J. 81 (2001) 2203–2214. doi:10.1016/S0006-3495(01)75868-7.
[82] R.J. van Abel, Y.Q. Tang, V.S. Rao, C.H. Dobbs, D. Tran, G. Barany, M.E. Selsted, Synthesis and characterization of indolicidin, a tryptophan-rich antimicrobial peptide from bovine neutrophils, Int. J. Pept. Protein Res. 45 (1995) 401–409.
[83] R. Rathinakumar, W.F. Walkenhorst, W.C. Wimley, Broad-Spectrum Antimicrobial Peptides by Rational Combinatorial Design and High-Throughput Screening: The Importance of Interfacial Activity, J. Am. Chem. Soc. 131 (2009) 7609–7617. doi:10.1021/ja8093247.
[84] R.E. Hancock, D.S. Chapple, Peptide antibiotics, Antimicrob. Agents Chemother. 43 (1999) 1317–1323.
[85] M. Wu, E. Maier, R. Benz, R.E. Hancock, Mechanism of interaction of different classes of cationic antimicrobial peptides with planar bilayers and with the cytoplasmic membrane of Escherichia coli, Biochemistry. 38 (1999) 7235–7242. doi:10.1021/bi9826299.

[86] P. Wadhwani, R.F. Epand, N. Heidenreich, J. Bürck, A.S. Ulrich, R.M. Epand, Membrane-active peptides and the clustering of anionic lipids, Biophys. J. 103 (2012) 265–274. doi:10.1016/j.bpj.2012.06.004.
[87] R.M. Epand, C. Walker, R.F. Epand, N.A. Magarvey, Molecular mechanisms of membrane targeting antibiotics, Biochim. Biophys. Acta BBA - Biomembr. 1858 (2016) 980–987. doi:10.1016/j.bbamem.2015.10.018.
[88] A. Arouri, M. Dathe, A. Blume, Peptide induced demixing in PG/PE lipid mixtures: a mechanism for the specificity of antimicrobial peptides towards bacterial membranes?, Biochim. Biophys. Acta. 1788 (2009) 650–659. doi:10.1016/j.bbamem.2008.11.022.
[89] K. Matsumoto, J. Kusaka, A. Nishibori, H. Hara, Lipid domains in bacterial membranes, Mol. Microbiol. 61 (2006) 1110–1117. doi:10.1111/j.1365-2958.2006.05317.x.
[90] K. Fosgerau, T. Hoffmann, Peptide therapeutics: current status and future directions, Drug Discov. Today. 20 (2015) 122–128. doi:10.1016/j.drudis.2014.10.003.
[91] K.E. Greber, M. Dawgul, Antimicrobial Peptides Under Clinical Trials, Curr. Top. Med. Chem. 17 (2017) 620–628.
[92] C.G. Starr, W.C. Wimley, Antimicrobial peptides are degraded by the cytosolic proteases of human erythrocytes, Biochim. Biophys. Acta BBA - Biomembr. 1859 (2017) 2319–2326. doi:10.1016/j.bbamem.2017.09.008.
[93] R. Oliva, M. Chino, K. Pane, V. Pistorio, A. De Santis, E. Pizzo, G. D'Errico, V. Pavone, A. Lombardi, P. Del Vecchio, E. Notomista, F. Nastri, L. Petraccone, Exploring the role of unnatural amino acids in antimicrobial peptides, Sci. Rep. 8 (2018) 8888. doi:10.1038/s41598-018-27231-5.
[94] A.K. Marr, W.J. Gooderham, R.E. Hancock, Antibacterial peptides for therapeutic use: obstacles and realistic outlook, Curr. Opin. Pharmacol. 6 (2006) 468–472. doi:10.1016/j.coph.2006.04.006.
[95] D.J. Craik, D.P. Fairlie, S. Liras, D. Price, The future of peptide-based drugs, Chem. Biol. Drug Des. 81 (2013) 136–147. doi:10.1111/cbdd.12055.
[96] B.A. Lipsky, K.J. Holroyd, M. Zasloff, Topical versus systemic antimicrobial therapy for treating mildly infected diabetic foot ulcers: a randomized, controlled, double-blinded, multicenter trial of pexiganan cream, Clin. Infect. Dis. Off. Publ. Infect. Dis. Soc. Am. 47 (2008) 1537–1545. doi:10.1086/593185.
[97] M.N. Melo, D. Dugourd, M.A.R.B. Castanho, Omiganan pentahydrochloride in the front line of clinical applications of antimicrobial peptides, Recent Patents Anti-Infect. Drug Disc. 1 (2006) 201–207.
[98] D.M. Rothstein, P. Spacciapoli, L.T. Tran, T. Xu, F.D. Roberts, M. Dalla Serra, D.K. Buxton, F.G. Oppenheim, P. Friden, Anticandida activity is retained in P-113, a 12-amino-acid fragment of histatin 5, Antimicrob. Agents Chemother. 45 (2001) 1367–1373. doi:10.1128/AAC.45.5.1367-1373.2001.

[99] W. Stillwell, An introduction to biological membranes: from bilayers to rafts, Elsevier/Academic Press, London ; Waltham, MA, 2013.
[100] N.A. Campbell, Biology, 2005.
[101] S.J. Singer, G.L. Nicolson, The fluid mosaic model of the structure of cell membranes, Science. 175 (1972) 720–731.
[102] F.M. Goñi, The basic structure and dynamics of cell membranes: An update of the Singer–Nicolson model, Biochim. Biophys. Acta BBA - Biomembr. 1838 (2014) 1467–1476. doi:10.1016/j.bbamem.2014.01.006.
[103] H. Watson, Biological membranes, Essays Biochem. 59 (2015) 43–69. doi:10.1042/bse0590043.
[104] M. Ikeda, A. Kihara, Y. Igarashi, Lipid Asymmetry of the Eukaryotic Plasma Membrane: Functions and Related Enzymes, Biol. Pharm. Bull. 29 (2006) 1542–1546. doi:10.1248/bpb.29.1542.
[105] K. Simons, E. Ikonen, Functional rafts in cell membranes, Nature. 387 (1997) 569–572. doi:10.1038/42408.
[106] S.A. Baldwin, ed., Membrane transport: a practical approach, Oxford University Press, Oxford ; New York, 2000.
[107] S. -i. Hakomori, The glycosynapse, Proc. Natl. Acad. Sci. 99 (2002) 225–232. doi:10.1073/pnas.012540899.
[108] G. van Meer, A.I.P.M. de Kroon, Lipid map of the mammalian cell, J. Cell Sci. 124 (2011) 5–8. doi:10.1242/jcs.071233.
[109] Y.L. Baburina, A.E. Gordeeva, D.A. Moshkov, O.V. Krestinina, A.A. Azarashvili, I.V. Odinokova, T.S. Azarashvili, Interaction of myelin basic protein and 2′,3′-cyclic nucleotide phosphodiesterase with mitochondria, Biochem. Mosc. 79 (2014) 555–565. doi:10.1134/S0006297914060091.
[110] R.F. Epand, P.B. Savage, R.M. Epand, Bacterial lipid composition and the antimicrobial efficacy of cationic steroid compounds (Ceragenins), Biochim. Biophys. Acta BBA - Biomembr. 1768 (2007) 2500–2509. doi:10.1016/j.bbamem.2007.05.023.
[111] M. Kates, J.-Y. Syz, D. Gosser, T.H. Haines, pH-dissociation characteristics of cardiolipin and its 2′-deoxy analogue, Lipids. 28 (1993) 877–882. doi:10.1007/BF02537494.
[112] G.L. Nicolson, The Fluid—Mosaic Model of Membrane Structure: Still relevant to understanding the structure, function and dynamics of biological membranes after more than 40years, Biochim. Biophys. Acta BBA - Biomembr. 1838 (2014) 1451–1466. doi:10.1016/j.bbamem.2013.10.019.
[113] I. Vivanco, C.L. Sawyers, The phosphatidylinositol 3-Kinase–AKT pathway in human cancer, Nat. Rev. Cancer. 2 (2002) 489–501. doi:10.1038/nrc839.
[114] S. Furse, Is phosphatidylglycerol essential for terrestrial life?, J. Chem. Biol. 10 (2017) 1–9. doi:10.1007/s12154-016-0159-3.
[115] W. Zhao, T. Róg, A.A. Gurtovenko, I. Vattulainen, M. Karttunen, Role of phosphatidylglycerols in the stability of bacterial membranes, Biochimie. 90 (2008) 930–938. doi:10.1016/j.biochi.2008.02.025.

[116] E. Mileykovskaya, W. Dowhan, Cardiolipin membrane domains in prokaryotes and eukaryotes, Biochim. Biophys. Acta BBA - Biomembr. 1788 (2009) 2084–2091. doi:10.1016/j.bbamem.2009.04.003.
[117] B. Ramstedt, J.P. Slotte, Membrane properties of sphingomyelins, FEBS Lett. 531 (2002) 33–37.
[118] A.B. García-Arribas, A. Alonso, F.M. Goñi, Cholesterol interactions with ceramide and sphingomyelin, Chem. Phys. Lipids. 199 (2016) 26–34. doi:10.1016/j.chemphyslip.2016.04.002.
[119] J.R. Silvius, Role of cholesterol in lipid raft formation: lessons from lipid model systems, Biochim. Biophys. Acta. 1610 (2003) 174–183.
[120] D. Brown, Structure and function of membrane rafts, Int. J. Med. Microbiol. IJMM. 291 (2002) 433–437.
[121] P.H. Lopez, R.L. Schnaar, Gangliosides in cell recognition and membrane protein regulation, Curr. Opin. Struct. Biol. 19 (2009) 549–557. doi:10.1016/j.sbi.2009.06.001.
[122] E.J. Dufourc, Sterols and membrane dynamics, J. Chem. Biol. 1 (2008) 63–77. doi:10.1007/s12154-008-0010-6.
[123] J.M. Sanderson, Peptide–lipid interactions: insights and perspectives, Org Biomol Chem. 3 (2005) 201–212. doi:10.1039/B415499A.
[124] J.M. Boggs, Myelin basic protein: a multifunctional protein, Cell. Mol. Life Sci. 63 (2006) 1945–1961. doi:10.1007/s00018-006-6094-7.
[125] E.A. Garber, E. Margoliash, Interaction of cytochrome c with cytochrome c oxidase: an understanding of the high- to low-affinity transition, Biochim. Biophys. Acta. 1015 (1990) 279–287.
[126] M.R.R. de Planque, B.B. Bonev, J.A.A. Demmers, D.V. Greathouse, R.E. Koeppe, F. Separovic, A. Watts, J.A. Killian, Interfacial Anchor Properties of Tryptophan Residues in Transmembrane Peptides Can Dominate over Hydrophobic Matching Effects in Peptide−Lipid Interactions †, Biochemistry. 42 (2003) 5341–5348. doi:10.1021/bi027000r.
[127] K.S. Mineev, E.V. Bocharov, P.E. Volynsky, M.V. Goncharuk, E.N. Tkach, Y.S. Ermolyuk, A.A. Schulga, V.V. Chupin, I.V. Maslennikov, R.G. Efremov, A.S. Arseniev, Dimeric structure of the transmembrane domain of glycophorin a in lipidic and detergent environments, Acta Naturae. 3 (2011) 90–98.
[128] A. Ishchenko, L. Peng, E. Zinovev, A. Vlasov, S.C. Lee, A. Kuklin, A. Mishin, V. Borshchevskiy, Q. Zhang, V. Cherezov, Chemically Stable Lipids for Membrane Protein Crystallization, Cryst. Growth Des. 17 (2017) 3502–3511. doi:10.1021/acs.cgd.7b00458.
[129] K. Zeth, K. Diederichs, W. Welte, H. Engelhardt, Crystal structure of Omp32, the anion-selective porin from Comamonas acidovorans, in complex with a periplasmic peptide at 2.1 A resolution, Struct. Lond. Engl. 1993. 8 (2000) 981–992.

[130] N.G. Bednarska, B.W. Wren, S.J. Willcocks, The importance of the glycosylation of antimicrobial peptides: natural and synthetic approaches, Drug Discov. Today. 22 (2017) 919–926. doi:10.1016/j.drudis.2017.02.001.
[131] K. Brandenburg, O. Holst, Glycolipids: Distribution and Biological Function, in: John Wiley & Sons Ltd (Ed.), ELS, John Wiley & Sons, Ltd, Chichester, UK, 2015: pp. 1–10. doi:10.1002/9780470015902.a0001427.pub3.
[132] R.V. Serrato, Lipopolysaccharides in diazotrophic bacteria, Front. Cell. Infect. Microbiol. 4 (2014). doi:10.3389/fcimb.2014.00119.
[133] G. van Meer, D.R. Voelker, G.W. Feigenson, Membrane lipids: where they are and how they behave, Nat. Rev. Mol. Cell Biol. 9 (2008) 112–124. doi:10.1038/nrm2330.
[134] H.I. Ingólfsson, M.N. Melo, F.J. van Eerden, C. Arnarez, C.A. Lopez, T.A. Wassenaar, X. Periole, A.H. de Vries, D.P. Tieleman, S.J. Marrink, Lipid Organization of the Plasma Membrane, J. Am. Chem. Soc. 136 (2014) 14554–14559. doi:10.1021/ja507832e.
[135] I.M. López-Lara, O. Geiger, Bacterial lipid diversity, Biochim. Biophys. Acta BBA - Mol. Cell Biol. Lipids. 1862 (2017) 1287–1299. doi:10.1016/j.bbalip.2016.10.007.
[136] C. Sohlenkamp, O. Geiger, Bacterial membrane lipids: diversity in structures and pathways, FEMS Microbiol. Rev. 40 (2016) 133–159. doi:10.1093/femsre/fuv008.
[137] J. Parker, Bacteria, in: Encycl. Genet., Elsevier, 2001: pp. 146–151. doi:10.1006/rwgn.2001.0102.
[138] N. Malanovic, K. Lohner, Gram-positive bacterial cell envelopes: The impact on the activity of antimicrobial peptides, Biochim. Biophys. Acta BBA - Biomembr. 1858 (2016) 936–946. doi:10.1016/j.bbamem.2015.11.004.
[139] C. Tanford, The hydrophobic effect: formation of micelles and biological membranes, 2d ed, Wiley, New York, 1980.
[140] D. Marsh, Thermodynamics of Phospholipid Self-Assembly, Biophys. J. 102 (2012) 1079–1087. doi:10.1016/j.bpj.2012.01.049.
[141] G. Tresset, The multiple faces of self-assembled lipidic systems, PMC Biophys. 2 (2009) 3. doi:10.1186/1757-5036-2-3.
[142] D. Marsh, CRC handbook of lipid bilayers, CRC Press, Boca Raton, Fla, 1990.
[143] P.R. Cullis, B. de Kruijff, Lipid polymorphism and the functional roles of lipids in biological membranes, Biochim. Biophys. Acta. 559 (1979) 399–420.
[144] J. Jouhet, Importance of the hexagonal lipid phase in biological membrane organization, Front. Plant Sci. 4 (2013). doi:10.3389/fpls.2013.00494.
[145] D.P. Siegel, M.M. Kozlov, The Gaussian Curvature Elastic Modulus of N-Monomethylated Dioleoylphosphatidylethanolamine: Relevance to Membrane Fusion and Lipid Phase Behavior, Biophys. J. 87 (2004) 366–374. doi:10.1529/biophysj.104.040782.

[146] J.M. Seddon, J. Robins, T. Gulik-Krzywicki, H. Delacroix, Inverse micellar phases of phospholipids and glycolipids, Phys. Chem. Chem. Phys. 2 (2000) 4485–4493. doi:10.1039/b004916f.
[147] B. Tenchov, R. Koynova, Cubic phases in membrane lipids, Eur. Biophys. J. 41 (2012) 841–850. doi:10.1007/s00249-012-0819-3.
[148] P. Khakbaz, J.B. Klauda, Investigation of phase transitions of saturated phosphocholine lipid bilayers via molecular dynamics simulations, Biochim. Biophys. Acta BBA - Biomembr. 1860 (2018) 1489–1501. doi:10.1016/j.bbamem.2018.04.014.
[149] J.H. Ipsen, G. Karlström, O.G. Mouritsen, H. Wennerström, M.J. Zuckermann, Phase equilibria in the phosphatidylcholine-cholesterol system, Biochim. Biophys. Acta. 905 (1987) 162–172.
[150] J.V. Busto, A.B. García-Arribas, J. Sot, A. Torrecillas, J.C. Gómez-Fernández, F.M. Goñi, A. Alonso, Lamellar gel (lβ) phases of ternary lipid composition containing ceramide and cholesterol, Biophys. J. 106 (2014) 621–630. doi:10.1016/j.bpj.2013.12.021.
[151] M.G.K. Benesch, D.A. Mannock, R.N.A.H. Lewis, R.N. McElhaney, A Calorimetric and Spectroscopic Comparison of the Effects of Lathosterol and Cholesterol on the Thermotropic Phase Behavior and Organization of Dipalmitoylphosphatidylcholine Bilayer Membranes, Biochemistry. 50 (2011) 9982–9997. doi:10.1021/bi200721j.
[152] R. Koynova, M. Caffrey, Phases and phase transitions of the phosphatidylcholines, Biochim. Biophys. Acta. 1376 (1998) 91–145.
[153] C. Huang, S. Li, Calorimetric and molecular mechanics studies of the thermotropic phase behavior of membrane phospholipids, Biochim. Biophys. Acta. 1422 (1999) 273–307.
[154] N.V. Bhagavan, C.-E. Ha, Lipids I, in: Essent. Med. Biochem., Elsevier, 2015: pp. 269–297. doi:10.1016/B978-0-12-416687-5.00016-6.
[155] R. Koynova, M. Caffrey, Phases and phase transitions of the hydrated phosphatidylethanolamines, Chem. Phys. Lipids. 69 (1994) 1–34.
[156] R.N.A.H. Lewis, R.N. McElhaney, The physicochemical properties of cardiolipin bilayers and cardiolipin-containing lipid membranes, Biochim. Biophys. Acta BBA - Biomembr. 1788 (2009) 2069–2079. doi:10.1016/j.bbamem.2009.03.014.
[157] R. Mendelsohn, J.W. Brauner, A. Gericke, External Infrared Reflection Absorption Spectrometry of Monolayer Films at the Air-Water Interface, Annu. Rev. Phys. Chem. 46 (1995) 305–334. doi:10.1146/annurev.pc.46.100195.001513.
[158] T.C. Wong, Micelles and Bicelles as Membrane Mimics for NuclearMagnetic Resonance Studies of Peptides and Proteins, Encycl. Surf. Colloid Sci. (2006).

[159] V. Kiessling, S.-T. Yang, L.K. Tamm, Supported Lipid Bilayers as Models for Studying Membrane Domains, in: Curr. Top. Membr., Elsevier, 2015: pp. 1–23. doi:10.1016/bs.ctm.2015.03.001.
[160] A. Akbarzadeh, R. Rezaei-Sadabady, S. Davaran, S.W. Joo, N. Zarghami, Y. Hanifehpour, M. Samiei, M. Kouhi, K. Nejati-Koshki, Liposome: classification, preparation, and applications, Nanoscale Res. Lett. 8 (2013) 102. doi:10.1186/1556-276X-8-102.
[161] A.D. Bangham, R.W. Horne, NEGATIVE STAINING OF PHOSPHOLIPIDS AND THEIR STRUCTURAL MODIFICATION BY SURFACE-ACTIVE AGENTS AS OBSERVED IN THE ELECTRON MICROSCOPE, J. Mol. Biol. 8 (1964) 660–668.
[162] M. Alavi, N. Karimi, M. Safaei, Application of Various Types of Liposomes in Drug Delivery Systems, Adv. Pharm. Bull. 7 (2017) 3–9. doi:10.15171/apb.2017.002.
[163] B. Mui, L. Chow, M.J. Hope, Extrusion Technique to Generate Liposomes of Defined Size, in: Methods Enzymol., Elsevier, 2003: pp. 3–14. doi:10.1016/S0076-6879(03)67001-1.
[164] T.J. Politano, V.E. Froude, B. Jing, Y. Zhu, AC-electric field dependent electroformation of giant lipid vesicles, Colloids Surf. B Biointerfaces. 79 (2010) 75–82. doi:10.1016/j.colsurfb.2010.03.032.
[165] B. Mishra, S. Reiling, D. Zarena, G. Wang, Host defense antimicrobial peptides as antibiotics: design and application strategies, Curr. Opin. Chem. Biol. 38 (2017) 87–96. doi:10.1016/j.cbpa.2017.03.014.
[166] B.E. Haug, M.L. Skar, J.S. Svendsen, Bulky aromatic amino acids increase the antibacterial activity of 15-residue bovine lactoferricin derivatives, J. Pept. Sci. 7 (2001) 425–432. doi:10.1002/psc.338.
[167] H.-Y. Yu, Y.-A. Chen, B.-S. Yip, S.-Y. Wang, H.-J. Wei, Y.-H. Chih, K.-H. Chen, J.-W. Cheng, Role of β-naphthylalanine end-tags in the enhancement of antiendotoxin activities: Solution structure of the antimicrobial peptide S1-Nal-Nal in complex with lipopolysaccharide, Biochim. Biophys. Acta BBA - Biomembr. 1859 (2017) 1114–1123. doi:10.1016/j.bbamem.2017.03.007.
[168] B.O. Schroeder, Z. Wu, S. Nuding, S. Groscurth, M. Marcinowski, J. Beisner, J. Buchner, M. Schaller, E.F. Stange, J. Wehkamp, Reduction of disulphide bonds unmasks potent antimicrobial activity of human β-defensin 1, Nature. 469 (2011) 419–423. doi:10.1038/nature09674.
[169] I. Wiegand, K. Hilpert, R.E.W. Hancock, Agar and broth dilution methods to determine the minimal inhibitory concentration (MIC) of antimicrobial substances, Nat. Protoc. 3 (2008) 163–175. doi:10.1038/nprot.2007.521.
[170] K. Pane, L. Durante, E. Pizzo, M. Varcamonti, A. Zanfardino, V. Sgambati, A. Di Maro, A. Carpentieri, V. Izzo, A. Di Donato, V. Cafaro, E. Notomista, Rational Design of a Carrier Protein for the Production of Recombinant Toxic Peptides in Escherichia coli, PLOS ONE. 11 (2016) e0146552. doi:10.1371/journal.pone.0146552.

[171] K. Pane, V. Sgambati, A. Zanfardino, G. Smaldone, V. Cafaro, T. Angrisano, E. Pedone, S. Di Gaetano, D. Capasso, E.F. Haney, V. Izzo, M. Varcamonti, E. Notomista, R.E.W. Hancock, A. Di Donato, E. Pizzo, A new cryptic cationic antimicrobial peptide from human apolipoprotein E with antibacterial activity and immunomodulatory effects on human cells, FEBS J. 283 (2016) 2115–2131. doi:10.1111/febs.13725.
[172] P. Boukamp, S. Popp, S. Altmeyer, A. Hülsen, C. Fasching, T. Cremer, N.E. Fusenig, Sustained nontumorigenic phenotype correlates with a largely stable chromosome content during long-term culture of the human keratinocyte line HaCaT, Genes. Chromosomes Cancer. 19 (1997) 201–214.
[173] S.M. Kelly, T.J. Jess, N.C. Price, How to study proteins by circular dichroism, Biochim. Biophys. Acta BBA - Proteins Proteomics. 1751 (2005) 119–139. doi:10.1016/j.bbapap.2005.06.005.
[174] R.L. Biltonen, D. Lichtenberg, The use of differential scanning calorimetry as a tool to characterize liposome preparations, Chem. Phys. Lipids. 64 (1993) 129–142. doi:10.1016/0009-3084(93)90062-8.
[175] J.R. Lakowicz, ed., Principles of Fluorescence Spectroscopy, Springer US, Boston, MA, 2006. doi:10.1007/978-0-387-46312-4.
[176] B. Valeur, Molecular fluorescence: principles and applications, Wiley-VCH, Weinheim ; New York, 2002.
[177] M. van de Weert, L. Stella, Fluorescence quenching and ligand binding: A critical discussion of a popular methodology, J. Mol. Struct. 998 (2011) 144–150. doi:10.1016/j.molstruc.2011.05.023.
[178] G. Kasetty, P. Papareddy, M. Kalle, V. Rydengård, M. Mörgelin, B. Albiger, M. Malmsten, A. Schmidtchen, Structure-Activity Studies and Therapeutic Potential of Host Defense Peptides of Human Thrombin, Antimicrob. Agents Chemother. 55 (2011) 2880–2890. doi:10.1128/AAC.01515-10.
[179] N. Molchanova, P.R. Hansen, P. Damborg, H.M. Nielsen, H. Franzyk, Lysine-Based α-Peptide/β-Peptoid Peptidomimetics: Influence of Hydrophobicity, Fluorination, and Distribution of Cationic Charge on Antimicrobial Activity and Cytotoxicity, ChemMedChem. 12 (2017) 312–318. doi:10.1002/cmdc.201600553.
[180] R. Woody, Contributions of tryptophan side chains to the far-ultraviolet circular dichroism of proteins, Eur. Biophys. J. 23 (1994) 253–262. doi:10.1007/BF00213575.
[181] C. Krittanai, W.C. Johnson, Correcting the Circular Dichroism Spectra of Peptides for Contributions of Absorbing Side Chains, Anal. Biochem. 253 (1997) 57–64. doi:10.1006/abio.1997.2366.
[182] I.B. Grishina, R.W. Woody, Contributions of tryptophan side chains to the circular dichroism of globular proteins: exciton couplets and coupled oscillators, Faraday Discuss. 99 (1994) 245. doi:10.1039/fd9949900245.
[183] M. Dathe, H. Nikolenko, J. Klose, M. Bienert, Cyclization Increases the Antimicrobial Activity and Selectivity of Arginine- and Tryptophan-

Containing Hexapeptides †, Biochemistry. 43 (2004) 9140–9150. doi:10.1021/bi035948v.
[184] E. Pizzo, R. Oliva, R. Morra, A. Bosso, S. Ragucci, L. Petraccone, P. Del Vecchio, A. Di Maro, Binding of a type 1 RIP and of its chimeric variant to phospholipid bilayers: evidence for a link between cytotoxicity and protein/membrane interactions, Biochim. Biophys. Acta BBA - Biomembr. 1859 (2017) 2106–2112. doi:10.1016/j.bbamem.2017.08.004.
[185] O. Cañadas, C. Casals, Differential Scanning Calorimetry of Protein–Lipid Interactions, in: J.H. Kleinschmidt (Ed.), Lipid-Protein Interact., Humana Press, Totowa, NJ, 2013: pp. 55–71. doi:10.1007/978-1-62703-275-9_4.
[186] L.M.S. Loura, R.F.M. de Almeida, A. Coutinho, M. Prieto, Interaction of peptides with binary phospholipid membranes: application of fluorescence methodologies, Chem. Phys. Lipids. 122 (2003) 77–96.
[187] V. Tiriveedhi, P. Butko, A Fluorescence Spectroscopy Study on the Interactions of the TAT-PTD Peptide with Model Lipid Membranes, Biochemistry. 46 (2007) 3888–3895. doi:10.1021/bi602527t.
[188] R.M. Epand, Detecting the presence of membrane domains using DSC, Biophys. Chem. 126 (2007) 197–200. doi:10.1016/j.bpc.2006.05.008.
[189] T. Wiedmann, A. Salmon, V. Wong, Phase behavior of mixtures of DPPC and POPG, Biochim. Biophys. Acta. 1167 (1993) 114–120.
[190] G.A. Caputo, E. London, Cumulative Effects of Amino Acid Substitutions and Hydrophobic Mismatch upon the Transmembrane Stability and Conformation of Hydrophobic α-Helices †, Biochemistry. 42 (2003) 3275–3285. doi:10.1021/bi026697d.
[191] S. Sachdeva, Peptides as 'Drugs': The Journey so Far, Int. J. Pept. Res. Ther. 23 (2017) 49–60. doi:10.1007/s10989-016-9534-8.
[192] A. Di Grazia, F. Cappiello, H. Cohen, B. Casciaro, V. Luca, A. Pini, Y.P. Di, Y. Shai, M.L. Mangoni, d-Amino acids incorporation in the frog skin-derived peptide esculentin-1a(1-21)NH2 is beneficial for its multiple functions, Amino Acids. 47 (2015) 2505–2519. doi:10.1007/s00726-015-2041-y.
[193] K. Matsuzaki, Control of cell selectivity of antimicrobial peptides, Biochim. Biophys. Acta BBA - Biomembr. 1788 (2009) 1687–1692. doi:10.1016/j.bbamem.2008.09.013.
[194] N. Asthana, S.P. Yadav, J.K. Ghosh, Dissection of Antibacterial and Toxic Activity of Melittin: A LEUCINE ZIPPER MOTIF PLAYS A CRUCIAL ROLE IN DETERMINING ITS HEMOLYTIC ACTIVITY BUT NOT ANTIBACTERIAL ACTIVITY, J. Biol. Chem. 279 (2004) 55042–55050. doi:10.1074/jbc.M408881200.
[195] R. Saravanan, A. Bhunia, S. Bhattacharjya, Micelle-bound structures and dynamics of the hinge deleted analog of melittin and its diastereomer: Implications in cell selective lysis by d-amino acid containing antimicrobial peptides, Biochim. Biophys. Acta BBA - Biomembr. 1798 (2010) 128–139. doi:10.1016/j.bbamem.2009.07.014.

[196] A. Ramamoorthy, S. Thennarasu, D.-K. Lee, A. Tan, L. Maloy, Solid-State NMR Investigation of the Membrane-Disrupting Mechanism of Antimicrobial Peptides MSI-78 and MSI-594 Derived from Magainin 2 and Melittin, Biophys. J. 91 (2006) 206–216. doi:10.1529/biophysj.105.073890.

[197] A. Kumar, M. Mahajan, B. Awasthi, A. Tandon, M.K. Harioudh, S. Shree, P. Singh, P.K. Shukla, R. Ramachandran, K. Mitra, S. Bhattacharjya, J.K. Ghosh, Piscidin-1-analogs with double L- and D-lysine residues exhibited different conformations in lipopolysaccharide but comparable anti-endotoxin activities, Sci. Rep. 7 (2017). doi:10.1038/srep39925.

[198] L. Lombardi, M.I. Stellato, R. Oliva, A. Falanga, M. Galdiero, L. Petraccone, G. D'Errico, A. De Santis, S. Galdiero, P. Del Vecchio, Antimicrobial peptides at work: interaction of myxinidin and its mutant WMR with lipid bilayers mimicking the P. aeruginosa and E. coli membranes, Sci. Rep. 7 (2017) 44425. doi:10.1038/srep44425.

[199] M. Fernández-Reyes, D. Díaz, B.G. de la Torre, A. Cabrales-Rico, M. Vallès-Miret, J. Jiménez-Barbero, D. Andreu, L. Rivas, Lysine N^{ε} -Trimethylation, a Tool for Improving the Selectivity of Antimicrobial Peptides, J. Med. Chem. 53 (2010) 5587–5596. doi:10.1021/jm100261r.

[200] A.L. den Hertog, J. van Marle, E.C.I. Veerman, M. Valentijn-Benz, K. Nazmi, H. Kalay, C.H. Grün, W. van't Hof, J.G.M. Bolscher, A.V. Nieuw Amerongen, The human cathelicidin peptide LL-37 and truncated variants induce segregation of lipids and proteins in the plasma membrane of Candida albicans, Biol. Chem. 387 (2006). doi:10.1515/BC.2006.187.

[201] H.W. Huang, Action of antimicrobial peptides: two-state model, Biochemistry. 39 (2000) 8347–8352.

[202] G.A. Woolley, A. Dunn, B.A. Wallace, Gramicidin-lipid interactions induce specific tryptophan side-chain conformations, Biochem. Soc. Trans. 20 (1992) 864–867.

[203] A.S. Ladokhin, M.E. Selsted, S.H. White, CD Spectra of Indolicidin Antimicrobial Peptides Suggest Turns, Not Polyproline Helix †, Biochemistry. 38 (1999) 12313–12319. doi:10.1021/bi9907936.

[204] E.J. Prenner, R.N.A.H. Lewis, L.H. Kondejewski, R.S. Hodges, R.N. McElhaney, Differential scanning calorimetric study of the effect of the antimicrobial peptide gramicidin S on the thermotropic phase behavior of phosphatidylcholine, phosphatidylethanolamine and phosphatidylglycerol lipid bilayer membranes, Biochim. Biophys. Acta BBA - Biomembr. 1417 (1999) 211–223. doi:10.1016/S0005-2736(99)00004-8.

[205] R. Oliva, P. Del Vecchio, M.I. Stellato, A.M. D'Ursi, G. D'Errico, L. Paduano, L. Petraccone, A thermodynamic signature of lipid segregation in biomembranes induced by a short peptide derived from glycoprotein gp36 of feline immunodeficiency virus, Biochim. Biophys. Acta BBA - Biomembr. 1848 (2015) 510–517. doi:10.1016/j.bbamem.2014.10.017.

[206] P. Joanne, C. Galanth, N. Goasdoué, P. Nicolas, S. Sagan, S. Lavielle, G. Chassaing, C. El Amri, I.D. Alves, Lipid reorganization induced by membrane-active peptides probed using differential scanning calorimetry, Biochim. Biophys. Acta BBA - Biomembr. 1788 (2009) 1772–1781. doi:10.1016/j.bbamem.2009.05.001.
[207] R.N.A.H. Lewis, Y.-P. Zhang, R.N. McElhaney, Calorimetric and spectroscopic studies of the phase behavior and organization of lipid bilayer model membranes composed of binary mixtures of dimyristoylphosphatidylcholine and dimyristoylphosphatidylglycerol, Biochim. Biophys. Acta BBA - Biomembr. 1668 (2005) 203–214. doi:10.1016/j.bbamem.2004.12.007.
[208] K.E. Van Holde, W.C. Johnson, P.S. Ho, Principles of physical biochemistry, 2nd ed, Pearson/Prentice Hall, Upper Saddle River, N.J, 2006.
[209] R.F. Epand, W.L. Maloy, A. Ramamoorthy, R.M. Epand, Probing the "Charge Cluster Mechanism" in Amphipathic Helical Cationic Antimicrobial Peptides, Biochemistry. 49 (2010) 4076–4084. doi:10.1021/bi100378m.
[210] I. Hurjui, A. Neamtu, D.O. Dorohoi, Computational and spectral studies of 1,6-diphenyl-1,3,5-hexatriene (DPH) multicomponent solutions, Spectrochim. Acta. A. Mol. Biomol. Spectrosc. 115 (2013) 382–387. doi:10.1016/j.saa.2013.06.017.
[211] G. Bocchinfuso, S. Bobone, C. Mazzuca, A. Palleschi, L. Stella, Fluorescence spectroscopy and molecular dynamics simulations in studies on the mechanism of membrane destabilization by antimicrobial peptides, Cell. Mol. Life Sci. 68 (2011) 2281–2301. doi:10.1007/s00018-011-0719-1.
[212] H. Zhao, P. Lappalainen, A simple guide to biochemical approaches for analyzing protein–lipid interactions, Mol. Biol. Cell. 23 (2012) 2823–2830. doi:10.1091/mbc.e11-07-0645.
[213] F. Moro, F.M. Goñi, M.A. Urbaneja, Fluorescence quenching at interfaces and the permeation of acrylamide and iodide across phospholipid bilayers, FEBS Lett. 330 (1993) 129–132.
[214] X.-C. Fei, C. Song, H.-W. Gao, Transmembrane transports of acrylamide and bisphenol A and effects on development of zebrafish (Danio rerio), J. Hazard. Mater. 184 (2010) 81–88. doi:10.1016/j.jhazmat.2010.08.007.
[215] K. Lohner, New strategies for novel antibiotics: peptides targeting bacterial cell membranes, Gen. Physiol. Biophys. 28 (2009) 105–116.
[216] A.C. Figueiredo, C.C. Clement, S. Zakia, J. Gingold, M. Philipp, P.J.B. Pereira, Rational Design and Characterization of D-Phe-Pro-D-Arg-Derived Direct Thrombin Inhibitors, PLoS ONE. 7 (2012) e34354. doi:10.1371/journal.pone.0034354.
[217] J. Reed, T.A. Reed, A Set of Constructed Type Spectra for the Practical Estimation of Peptide Secondary Structure from Circular Dichroism, Anal. Biochem. 254 (1997) 36–40. doi:10.1006/abio.1997.2355.

[218] A.S. Ladokhin, S. Jayasinghe, S.H. White, How to Measure and Analyze Tryptophan Fluorescence in Membranes Properly, and Why Bother?, Anal. Biochem. 285 (2000) 235–245. doi:10.1006/abio.2000.4773.
[219] Z.J. Huang, R.P. Haugland, Partition coefficients of fluorescent probes with phospholipid membranes, Biochem. Biophys. Res. Commun. 181 (1991) 166–171.
[220] T. Parasassi, G. De Stasio, G. Ravagnan, R.M. Rusch, E. Gratton, Quantitation of lipid phases in phospholipid vesicles by the generalized polarization of Laurdan fluorescence, Biophys. J. 60 (1991) 179–189. doi:10.1016/S0006-3495(91)82041-0.
[221] M.I. Angelova, S. Soléau, P. Méléard, F. Faucon, P. Bothorel, Preparation of giant vesicles by external AC electric fields. Kinetics and applications, in: C. Helm, M. Lösche, H. Möhwald (Eds.), Trends Colloid Interface Sci. VI, Steinkopff, Darmstadt, 1992: pp. 127–131. doi:10.1007/BFb0116295.
[222] C.A. Schneider, W.S. Rasband, K.W. Eliceiri, NIH Image to ImageJ: 25 years of image analysis, Nat. Methods. 9 (2012) 671–675.
[223] H. Chakraborty, B.R. Lentz, A Simple Method for Correction of Circular Dichroism Spectra Obtained from Membrane-Containing Samples, Biochemistry. 51 (2012) 1005–1008. doi:10.1021/bi300025c.
[224] M.A. Amon, M. Ali, V. Bender, K. Hall, M.-I. Aguilar, J. Aldrich-Wright, N. Manolios, Kinetic and conformational properties of a novel T-cell antigen receptor transmembrane peptide in model membranes, J. Pept. Sci. 14 (2008) 714–724. doi:10.1002/psc.987.
[225] B.D. Fleming, K.M.W. Keough, Thermotropic mesomorphism in aqueous dispersions of 1-palmitoyl-2-oleoyl- and 1,2-dilauroyl-phosphatidylglycerols in the presence of excess Na^{+} or Ca^{2+}, Can. J. Biochem. Cell Biol. 61 (1983) 882–891. doi:10.1139/o83-113.
[226] T. Parasassi, E.K. Krasnowska, L. Bagatolli, E. Gratton, Laurdan and Prodan as Polarity-Sensitive Fluorescent Membrane Probes, J. Fluoresc. 8 (1998). doi:10.1023/A:102052871.
[227] O. Maniti, I. Alves, G. Trugnan, J. Ayala-Sanmartin, Distinct Behaviour of the Homeodomain Derived Cell Penetrating Peptide Penetratin in Interaction with Different Phospholipids, PLoS ONE. 5 (2010) e15819. doi:10.1371/journal.pone.0015819.
[228] M. Schmid, C. Wölk, J. Giselbrecht, K.L.A. Chan, R.D. Harvey, A combined FTIR and DSC study on the bilayer-stabilising effect of electrostatic interactions in ion paired lipids, Colloids Surf. B Biointerfaces. 169 (2018) 298–304. doi:10.1016/j.colsurfb.2018.05.031.
[229] V.B. Henriques, R. Germano, M.T. Lamy, M.N. Tamashiro, Phase Transitions and Spatially Ordered Counterion Association in Ionic-Lipid Membranes: Theory versus Experiment, Langmuir. 27 (2011) 13130–13143. doi:10.1021/la202302x.

[230] G. D'Errico, G. Vitiello, A.M. D'Ursi, D. Marsh, Interaction of short modified peptides deriving from glycoprotein gp36 of feline immunodeficiency virus with phospholipid membranes, Eur. Biophys. J. 38 (2009) 873–882. doi:10.1007/s00249-009-0454-9.

[231] N. Phambu, B. Almarwani, A. Alwadai, E.N. Phambu, N. Faciane, C. Marion, A. Sunda-Meya, Calorimetric and Spectroscopic Studies of the Effects of the Cell Penetrating Peptide Pep-1 and the Antimicrobial Peptide Combi-2 on Vesicles Mimicking *Escherichia coli* Membrane, Langmuir. 33 (2017) 12908–12915. doi:10.1021/acs.langmuir.7b01910.

[232] J.E. Shaw, R.F. Epand, J.C.Y. Hsu, G.C.H. Mo, R.M. Epand, C.M. Yip, Cationic peptide-induced remodelling of model membranes: Direct visualization by in situ atomic force microscopy, J. Struct. Biol. 162 (2008) 121–138. doi:10.1016/j.jsb.2007.11.003.

[233] A. Marquette, B. Lorber, B. Bechinger, Reversible Liposome Association Induced by LAH4: A Peptide with Potent Antimicrobial and Nucleic Acid Transfection Activities, Biophys. J. 98 (2010) 2544–2553. doi:10.1016/j.bpj.2010.02.042.

[234] M. Deleu, J.-M. Crowet, M.N. Nasir, L. Lins, Complementary biophysical tools to investigate lipid specificity in the interaction between bioactive molecules and the plasma membrane: A review, Biochim. Biophys. Acta BBA - Biomembr. 1838 (2014) 3171–3190. doi:10.1016/j.bbamem.2014.08.023.

[235] Y. Huang, L. He, G. Li, N. Zhai, H. Jiang, Y. Chen, Role of helicity of α-helical antimicrobial peptides to improve specificity, Protein Cell. 5 (2014) 631–642. doi:10.1007/s13238-014-0061-0.

[236] I. Zelezetsky, A. Tossi, Alpha-helical antimicrobial peptides—Using a sequence template to guide structure–activity relationship studies, Biochim. Biophys. Acta BBA - Biomembr. 1758 (2006) 1436–1449. doi:10.1016/j.bbamem.2006.03.021.

[237] R.F. Epand, W.L. Maloy, A. Ramamoorthy, R.M. Epand, Probing the "Charge Cluster Mechanism" in Amphipathic Helical Cationic Antimicrobial Peptides, Biochemistry. 49 (2010) 4076–4084. doi:10.1021/bi100378m.

[238] Y. Lv, J. Wang, H. Gao, Z. Wang, N. Dong, Q. Ma, A. Shan, Antimicrobial Properties and Membrane-Active Mechanism of a Potential α-Helical Antimicrobial Derived from Cathelicidin PMAP-36, PLoS ONE. 9 (2014) e86364. doi:10.1371/journal.pone.0086364.

[239] A. Bhunia, H. Mohanram, P.N. Domadia, J. Torres, S. Bhattacharjya, Designed β-Boomerang Antiendotoxic and Antimicrobial Peptides: STRUCTURES AND ACTIVITIES IN LIPOPOLYSACCHARIDE, J. Biol. Chem. 284 (2009) 21991–22004. doi:10.1074/jbc.M109.013573.

[240] A. Sivertsen, J. Isaksson, H.-K.S. Leiros, J. Svenson, J.-S. Svendsen, B. Brandsdal, Synthetic cationic antimicrobial peptides bind with their hydrophobic parts to drug site II of human serum albumin, BMC Struct. Biol. 14 (2014) 4. doi:10.1186/1472-6807-14-4.

[241] V.J. Stella, Q. He, Cyclodextrins, Toxicol. Pathol. 36 (2008) 30–42. doi:10.1177/0192623307310945.
[242] G. Astray, C. Gonzalez-Barreiro, J.C. Mejuto, R. Rial-Otero, J. Simal-Gándara, A review on the use of cyclodextrins in foods, Food Hydrocoll. 23 (2009) 1631–1640. doi:10.1016/j.foodhyd.2009.01.001.
[243] P. Jansook, N. Ogawa, T. Loftsson, Cyclodextrins: structure, physicochemical properties and pharmaceutical applications, Int. J. Pharm. 535 (2018) 272–284. doi:10.1016/j.ijpharm.2017.11.018.
[244] S.S. Jambhekar, P. Breen, Cyclodextrins in pharmaceutical formulations I: structure and physicochemical properties, formation of complexes, and types of complex, Drug Discov. Today. 21 (2016) 356–362. doi:10.1016/j.drudis.2015.11.017.
[245] T. Irie, Cyclodextrins in peptide and protein delivery, Adv. Drug Deliv. Rev. 36 (1999) 101–123. doi:10.1016/S0169-409X(98)00057-X.
[246] M.E. Davis, M.E. Brewster, Cyclodextrin-based pharmaceutics: past, present and future, Nat. Rev. Drug Discov. 3 (2004) 1023–1035. doi:10.1038/nrd1576.
[247] M.E. Brewster, T. Loftsson, Cyclodextrins as pharmaceutical solubilizers, Adv. Drug Deliv. Rev. 59 (2007) 645–666. doi:10.1016/j.addr.2007.05.012.
[248] M.M.B. Ribeiro, H.G. Franquelim, M.A.R.B. Castanho, A.S. Veiga, Molecular interaction studies of peptides using steady-state fluorescence intensity. Static (de)quenching revisited, J. Pept. Sci. 14 (2008) 401–406. doi:10.1002/psc.939.
[249] C.R. Cantor, P.R. Schimmel, The behavior of biological macromolecules, W. H. Freeman, San Francisco, 1980.
[250] L.D. Hansen, G.W. Fellingham, D.J. Russell, Simultaneous determination of equilibrium constants and enthalpy changes by titration calorimetry: Methods, instruments, and uncertainties, Anal. Biochem. 409 (2011) 220–229. doi:10.1016/j.ab.2010.11.002.
[251] R.J. Falconer, Applications of isothermal titration calorimetry - the research and technical developments from 2011 to 2015: Review of Isothermal Titration Calorimetry from 2011 to 2015, J. Mol. Recognit. 29 (2016) 504–515. doi:10.1002/jmr.2550.
[252] M. Niccoli, R. Oliva, G. Castronuovo, Cyclodextrin–protein interaction as inhibiting factor against aggregation: A calorimetric study at 298 K, J. Therm. Anal. Calorim. 127 (2017) 1491–1499. doi:10.1007/s10973-016-5736-8.
[253] J.-F. Li, J.-X. Zhang, Z.-G. Wang, Y.-J. Yao, X. Han, Y.-L. Zhao, J.-P. Liu, S.-Q. Zhang, Identification of a cyclodextrin inclusion complex of antimicrobial peptide CM4 and its antimicrobial activity, Food Chem. 221 (2017) 296–301. doi:10.1016/j.foodchem.2016.10.040.
[254] Captisol, (n.d.). https://www.captisol.com/ (accessed October 17, 2018).
[255] M.V. Rekharsky, Y. Inoue, Complexation Thermodynamics of Cyclodextrins, Chem. Rev. 98 (1998) 1875–1918.

[256] M.T. Sikder, M.M. Rahman, M. Jakariya, T. Hosokawa, M. Kurasaki, T. Saito, Remediation of water pollution with native cyclodextrins and modified cyclodextrins: A comparative overview and perspectives, Chem. Eng. J. 355 (2019) 920–941. doi:10.1016/j.cej.2018.08.218.
[257] A.R. Hedges, Industrial Applications of Cyclodextrins, Chem. Rev. 98 (1998) 2035–2044.

List of Publications

1. **R. Oliva**, P. Del Vecchio, A. Grimaldi, E. Notomista, V. Cafaro, K. Pane, V. Schuabb, R. Winter, L. Petraccone, *Membrane disintegration by the antimicrobial peptide (P)GKY20: lipid segregation, domain formation, budding and micellization,* Physical Chemistry Chemical Physics, under revision
2. S. Cozzolino, **R. Oliva**, G. Graziano, P. Del Vecchio, *Counteraction of denaturant-induced protein unfolding is a general property of stabilizing agents,* Physical Chemistry Chemical Physics, 20 (2018) 29389-29398 (doi: 10.1039/C8CP04421J).
3. S. Patra, V. Schuabb, I. Kiesel, J. M. Knop, **R. Oliva**, R. Winter, *Exploring the effects of cosolutes and crowding on the volumetric and kinetic profile of the conformational dynamics of a poly dA loop DNA hairpin: a single-molecule FRET study,* Nucleic Acids Research, gky1122, 2018 (doi: 10.1093/nar/gky1122)
4. M. Siepi[1], **R. Oliva[1],** L. Petraccone, P. Del Vecchio, E. Ricca, R. Isticato, M. Lanzilli, O. Maglio, A. Lombardi, L. Leone, E. Notomista, G. Donadio, *Fluorescent peptide dH3w: a sensor for environmental monitoring of mercury (II),* PLoS ONE 13(10): e0204164 (doi: 10.1371/ journal.pone.0204164). [1]These authors have contributed equally to this work.
5. V. Elia, **R. Oliva**, E. Napoli, R. Germano, G. Pinto, L. Lista, M. Niccoli, D. Toso, G. Vitiello, M. Trifuoggi, A. Giarra, T. A. Yinnon, *Experimental study of physicochemical changes in water by iterative contact with hydrophilic polymers: a comparison between Cellulose and Nafion,* Journal of Molecular Liquids, 268 (2018) 598-609 (doi: 10.1016/j.molliq.2018.07.045).
6. **R. Oliva**, M. Chino, K. Pane, V. Pistorio, A. De Santis, E. Pizzo, G. D'Errico, V. Pavone, A. Lombardi, P. Del Vecchio, E. Notomista, F. Nastri, L. Petraccone, *Exploring the role of unnatural amino acids in antimicrobial peptides,* Scientific Reports, 2018, 8 (doi: 10.1038/s41598-018-27231-5).
7. M. Vigorita, S. Cozzolino, **R. Oliva**, G. Graziano, P. Del Vecchio, *Counteraction ability of TMAO toward different denaturing agents*, Biopolymers, 2018 e23104 (doi: 10.1002/bip.23104).
8. V. Elia, T. A. Yinnon, **R. Oliva**, E. Napoli, R. Germano, F. Bobba, A. Amoresano, *DNA and the chiral water superstructure,* Journal of Molecular Liquids, 248 (2017) 1028-1029 (doi: 10.1016/j.molliq.2017.10.140).
9. E. Pizzo[1], **R. Oliva[1]**, R. Morra, A. Bosso, S. Ragucci, L. Petraccone, P. Del Vecchio, A. Di Maro, *Binding of a type 1 RIP and of its chimeric variant to phospholipid bilayers: evidence for a link between cytotoxicity and protein/membrane interactions,* Biochimica et Biophysica Acta, 1859 (2017)

2106-2112 (doi: 10.1016/j.bbamem.2017.08.004) [1]These authors have contributed equally to this work.

10. L. Lombardi, M. I. Stellato, **R. Oliva**, A. Falanga, M. Galdiero, L. Petraccone, G. D'Errico, A. De Santis, S. Galdiero, P. Del Vecchio, *Antimicrobial peptides at work: interaction of myxinidin and its mutant WMR with lipid bilayers mimicking the P. aeruginosa and E.coli membranes*, Scientific Reports, 2017, 7 (doi: 10.1038/srep44425).
11. G. Donadio, R. Di Martino, **R. Oliva**, L. Petraccone, P. Del Vecchio, E. Ricca, R. Isticato, A. Di Donato, E. Notomista, *A new peptide-based fluorescent probe selective for zinc (II) and copper (II),* Journal of Material Chemistry B, 2016, 4, 6979-6988 (doi: 10.1039/C6TB00671J).
12. M. Niccoli, **R. Oliva,** G. Castronuovo, *Cyclodextrin-protein interaction as inhibiting factor against aggregation. A calorimetric study at 298 K,* Journal of Thermal Analysis and Calorimetry, 126 (2017) 1491-1499 (doi: 10.1007/s10973-016-5736-8).
13. M. Ricci, **R. Oliva**, P. Del Vecchio, M. Paolantoni, A. Morresi, P. Sassi, *DMSO-induced perturbation of thermotropic properties of cholesterol-containing DPPC liposomes,* Biochimica et Biophysica Acta, 1858 (2016) 3024-3031 (doi:10.1016/j.bbamem.2016.09.012).
14. **R. Oliva**, A. Emendato, G. Vitiello, A. De Santis, M. Grimaldi, A.M. D'Ursi, E. Busi, P. Del Vecchio, L. Petraccone, G. D'Errico, *On the microscopic and mesoscopic perturbations of lipid bilayers upon interaction with the MPER domain of the HIV glycoprotein gp41,* Biochimica et Biophysica Acta 1858 (2016) 1904-1913 (doi: 10.1016/j.bbamem.2016.05.007).
15. **R. Oliva**, P. Del Vecchio, M. I. Stellato, A. M. D'Ursi, G. D'Errico, L. Paduano, L. Petraccone, *A thermodynamic signature of lipid segregation in biomembranes induced by a short peptide derived from glycoprotein gp36 of feline immunodeficiency virus*, Biochimica et Biophysica Acta 1848 (2015) 510–517 (doi: 10.1016/j.bbamem.2014.10.017).

Congress/Summer Schools/Attended Courses/Awards

Attended Courses for PhD Students at the Department of Chemical Sciences of University Federico II of Naples

1. Title: "*The techniques of solid-liquid extraction used in the preparation of the sample for chemical analysis and production of extracts for industrial uses*". Professor Daniele Naviglio.
2. Title: "*Biophysics of Nucleic Acids*". Professor Luigi Petraccone.
3. Title: "*Recombinant Production of Natural and Mutant Proteins*". Professor Angela Duilio.
4. Title: "*Advanced Mass Spectrometry Course*". Professor Piero Pucci.
5. Title: "*Persistent organic pollutants (POPs)*". Dr Anna Andolfi.

Attended Seminars at the Department of Chemical Sciences of University Federico II of Naples

1. Title: "*Computational Chemistry Beyond Molecules*". Dr Alessio Petrone.
2. Title: "*Functionalized and Artificial Enzymes: New Bio-inspired Catalysts*". Dr Thierry Tron.
3. Title: "*Biopesticides which Target Voltage-gated Ion Channles: Efficacy and Biosefety*". Professor Angharad M. R. Gatehouse.
4. Title: "*Multimodal Approaches for Preclinical Molecular Imaging*". Dr Luca Menichetti and Dr Mario Chiariello.
5. Title: "*The Chemistry: a Diamond*". Dr Mario Marzullo.
6. Title: "*New Directions in the Field of Energy Electrochemical Accumulators*". Dr Claudio Gerbaldi.
7. Title: "*Paleoproteomics: the State of the Art on Ancient Proteins in Art and Archeology*". Professor Enrico Cappellini.
8. Title: "*Metalloprotein Mimics by Design: Strategies and Applications*". Professor Angelina Lombardi.
9. Title: "*Antibacterial and Immunomodulatory Activity of the Host Defense Peptide CATH-2*". Dr Edwin J. A. Veldhuizen.
10. Title: "*Structural Bioinformatics: a Window to Observe New Aspects of Protein Behaviors*". Professor Neri Niccolai.
11. Title: "*A Life of Magical Spinning*". Professor Nigel J. Clayden.

Congress/Workshops/Summer Schools

1. **5-6 June 2018**: 2nd National Congress of the Italian Peptide Society (ItPS), Naples, Italy. **Oral Contribution**: P. Del Vecchio, E. Notomista, V. Cafaro, K. Pane, A. Grimaldi, V. Schuabb, R. Winter, L. Petraccone and **R. Oliva**, Title: "*The mechanism of action of the GKY20 antimicrobial peptide*".
2. **17-21 February 2018**: 62nd Annual Meeting of Biophysical Society, San Francisco, USA. **Oral Contribution**: S. Patra, V. Schuabb, **R. Oliva** and R. Winter. Title: "*Effect of Pressure on the Conformational Landscape of a Large Loop DNA Hairpin in the Presence of Salts and Osmolytes*".
3. **18-20 October 2017**: Applied Nanotechnology and Nanoscience International Conference 2017 (ANNIC 2017), Rome, Italy. **Poster Presentation**: G. Donadio, **R. Oliva**, M. Siepi, P. Del Vecchio, L. Petraccone, E. Ricca, R. Isticato, M. Lanzilli, E. Notomista, Title: "*A new peptide-based fluorescent probe selective for mercury(II)*".
4. **20-24 September 2017**: 13th Mediterranean Conference on Calorimetry and Thermal Analysis (MEDICTA 2017), Loano (SV), Italy. **Poster Presentation**: L. Petraccone, **R. Oliva**, A. Grimaldi, P. Del Vecchio, V. Cafaro, K. Pane, E. Notomista, Title: "*Calorimetric Study of the interaction of an antimicrobial peptide with membrane models*".
5. **10-14 September 2017**: National Congress of the Italian Chemical Society (SCI), Peastum (Salerno), Italy. **Oral Contribution**: **R. Oliva**, A. Grimaldi, P. Del Vecchio, V. Cafaro, K. Pane, E. Notomista, L. Petraccone, Title: "*Biophysical studies of membrane perturbation induced by the antimicrobial peptide GKY20*".
6. **24-26 May 2017**: Summer School "First National School of Chemical Sensors" organized by the Italian Chemical Society (SCI) – Interdivisional Group of Sensors. Department of Chemical Sciences, University of Naples "Federico II", Naples – Italy.
7. **29 November 2016**: Invited Speaker at the Department of Chemistry, Biology and Biotechnology, University of Perugia, Italy. Seminar Title: "*Physical-chemical studies on the interaction between antimicrobial peptides and model bio-membranes*" (Host: Dr. Paola Sassi).
8. **22-23 November 2016**: Light Sheet Fluorescence Microscopy Workshop, Department of Biology, Complesso Universitario di Monte Sant'Angelo, University of Naples "Federico II", Naples, Italy.
9. **25-28 September 2016**: XXXVIII National Congress on Calorimetry, Thermal Analysis and Applied Thermodynamics, Ischia, Italy. **Oral**

Contribution: **R. Oliva**, L. Lombardi, M. I. Stellato, A. Falanga, M. Galdiero, L. Petraccone, G. D'Errico, S. Galdiero, P. Del Vecchio, Title: "*Calorimetric and spectroscopic studies of the interaction of antimicrobial peptides with model bio-membranes*".

10. **20-23 September 2016**: XLIV Congress of the Physical Chemistry Division of the Italian Chemical Society, University of Naples "Federico II", Naples, Italy. **Oral Contribution**: **R. Oliva**, Title: "*Physical-chemical studies on the interaction between antimicrobial peptides and model bio-membranes*". **Poster Presentation**: **R. Oliva**, M. Ricci, P. Del Vecchio, L. Petraccone, M. Paolantoni, A. Morresi, P. Sassi, Title: "*The effect of DMSO on the thermotropic properties of cholesterol-containing DPPC liposomes*". **Poster Presentation**: **R. Oliva**, G. Donadio, R. Di Martino, L. Petraccone, P. Del Vecchio, E. Ricca, R. Isticato, A. Di Donato, E. Notomista, Title: "*Physico-chemical characterization of a peptide-based fluorescent probe selective for zinc(II) and copper(II)*".
11. **4-6 July 2016**: Summer School "Advanced Applications of Fluorescence Techniques" organized by the Fluorescence Foundation and Institute of Food Science CNR Avellino - Italy.
12. **23-25 June 2016**: 15th Naples Workshop on Bioactive Peptides, Centro Congressi "Federico II", Naples, Italy. **Poster Presentation**: **R. Oliva**, L. Lombardi, M. I. Stellato, A. Falanga, M. Galdiero, L. Petraccone, G. D'Errico, S. Galdiero, P. Del Vecchio, Title: "*Effect of lipid composition and peptide sequence on the interaction between myxinidin and model membranes*".

Awards

1. **23 September 2016**: PCCP (Physical Chemistry Chemical Physics, Royal Society of Chemistry) Poster Prize at the Congress of the Physical Chemistry Division of the Italian Chemical Society.

2. **15 July 2016**: Young Scientists Award at the XXXVIII National Congress on Calorimetry, Thermal Analysis and Applied Thermodynamics.

Additional Information

1. **5 July-17 December 2017**: Visiting PhD student at the Faculty of Chemistry and Biological Chemistry, Technical University Dortmund, Germany (Host: Prof. Dr. Roland Winter). Scientific Activity: i) Application of Atomic Force Microscopy (AFM), Steady-State Fluorescence Spectroscopy and Confocal

Fluorescence Microscopy to the interaction of antimicrobial peptides with model membrane systems; ii) Fluorescence spectroscopy studies of the effects of high pressure and cosolutes on the conformational behavior of DNA hairpin.

2. **October 2016-June 2017**: Scholarship for the support to lectures and numerical exercises for the course of Mathematics and Statistics (Prof. R. Trombetti), Bachelor's Degree in Biotechnology, University of Naples "Federico II", Italy.